MPHIL

Optimising Output Characteristics of (edgeemitting) Light Emitting Diodes (eeLEDs)

Chen, Xizi

Award date:
2009

Awarding institution:
University of Bath

Optimising Output Characteristics
of
(edge-emitting) Light Emitting Diodes (ee-LEDs)

Submitted by

Xizi Chen

For the degree of Master of Philosophy

The University of Bath

Department of Electronic and Electrical Engineering

December 2009

Abstract

Stripe contact (edge-emitting) LEDs have been found to be suitable for many applications in present day optical/photonics devices and systems. Polarised light (i.e., light with dominantly a single polarisation direction) is required for various applications. Semiconductor LASERs generate polarized light but such sources may not be suitable due to other reasons such as the 'speckle' effect that occurs due to the highly coherent LASER light; also, if the source is to be part of a monolithically integrated optical circuit it will be expensive to produce the two reflective planes needed for the LASER to operate. Unlike semiconductor Lasers, however, stripe-contact edge-emitting LEDs in bulk active layer semiconductor material tend to produce nearly unpolarised light. LED sources but with polarised output are attractive for various applications such as in Optical Coherence Tomography (OCT).

The objective of this project is to design a simple, inexpensive device structure to achieve polarisation enhanced output by using stripe-contact edge-emitting LEDs in bulk active layer semiconductor material, with multilayer, Double-Heterostructure (DH), as commonly used for semiconductor Lasers and LEDs. As is well known light in the material is primarily generated by spontaneous emission. If the material is 'pumped' sufficiently then there will be net stimulated emission which corresponds to having optical gain; in that case the spontaneously emitted light will experience optical emission as it progresses through the material resulting in Amplified Spontaneous Emission (ASE). In this condition of operation the ee-LED is often referred to as the Superluminescent LED (SLED). It is also well known that in bulk active layer semiconductors spontaneous emission occurs uniformly in all polarisations and that the material gain is also polarisation independent. Hence the generated ASE is equally distributed in TE & TM polarisations. The challenge, therefore, is to find a scheme which that would generate dominantly TE or dominantly

TM ASE, and yet be easy to fabricate.

Rays and Rate Equations analysis is used to model the device. A computationally efficient model for stripe contact semiconductor optical devices is designed and used to obtain design guidelines for the “V”-geometry device, which is taking benefits and advantages to design a polarisation-selective ee-LED device. Simulation results from the model are shown.

Acknowledgments

I am deeply indebted to Dr J Sarma for introducing the research project during these years, and for his enlightening quality teaching and unlimited suggestions. This work could never been possible without his help.

Many thanks also to Dr F Causa for helping discussions and support.

I would like to specially thank to Dr A Tarlis and Dr F.K. Lau. Dr A Tarlis instructed me on the basic theory background and experience on the set-up of the experiment was extremely helpful. With his patience and earnest teaching, my confidence had built up. Dr F.K. Lau gave me a very important support on the MATLAB programming, and guided me through all the difficulties.

Finally, deep thanks to Miss L Ma who is my research group mate and my forever best friend. She is always there to support and help me throughout the ups and downs; share tears and happiness with me all the way. I am so lucky to have such amazing best friend in my life.

Contents

List of Figures

List of Tables

List of Symbols

A	Area; cross section area
A_0	Material constant (1.5×10^{-18} cm^{-3})
B_r	Bi-modular Recombination Constant (cm s^{-1})
c	Speed of light in vacuum (2.998×10^{10} cm s^{-1})
d	Thickness of device active layer (μm)
E	Energy
E_g	Band-gap energy of Gallium Arsenide (1.43eV)
f	Frequency (Hz)
g	Gain coefficients (cm^{-1})
h	Planck's constant (6.626×10^{-34} Js)
I	Injection Current (A)
J_0	Injection Current density (A/cm^2)
k	Boltzmann constant (1.382×10^{-34} JK^{-1})
L	Stripe length (μm)
$n_{1,2}$	Refractive index for medium1 and 2
n_{ff}	Effective refractive index for that mode
N	Carrier density (cm^{-3})
N_d	Doping density in active layer (cm^{-3})
N_0	Initial carrier density (cm^{-3})
N_{tr}	Transparency carrier density (1.55×10^{18} cm^{-3})
$P, P_{e,h}$	Forward travelling photon density (cm^{-3}), for transverse electric and magnetic field modes, respectively

$P_{0,L}, P_{0e,0h}$	Forward travelling photon density at z=0,L, for transverse electric and magnetic field modes, respectively
q	Electron charge (1.602×10^{-19} C)
$Q, Q_{e,h}$	Reverses travelling photon density (cm^{-3}), for transverse electric and magnetic field modes, respectively
$Q_{0,L}, Q_{0e,0h}$	Reverse travelling photon density at z=0,L, for transverse electric and magnetic field modes, respectively
$R_m, R_{me,h}$	Mirror/coupling reflectivity, for Transverse Electric and Transverse Magnetic field modes,, respectively
TE	Transverse Electric field modes
TM	Transverse Magnetic field modes
w	Stripe width (μm)
$\Gamma_{e,h}$	Confinement factor for Transverse Electric or Transverse Magnetic field modes
$\delta, \delta_{f,r}$	The fraction of spontaneous emission, in the forward and reverse direction
η	Refractive index of medium
ϕ_i	Incidence angle
ϕ_B	The Brewster angle
λ	Emission wavelength (cm)
λ_0	Vacuum wavelength (cm)
μ_0	Magnetic permeability of vacuum ($4\pi\times10^{-7}$ Hm^{-1})
τ_{sp}	Average time for an electron-hole pair recombination by spontaneous emission (s^{-1})
$\varepsilon_{1,2}$	Effective relative permittivity for mediums 1 and 2
ε_{ff}	Effective relative permittivity
v	Velocity of light in the medium (cm s^{-1})
ω	Angular frequency (radian s^{-1})

List of Abbreviations

L-I	Light-Current
DH	Double Heterostructure
ee-LED	Edge-Emitting Light Emitting Diode
ee-s-LED	Superluminescent Edge-Emitting Light Emitting Diode
GaAs	Gallium Arsenide
GaAlAs	Gallium Aluminium Arsenide
s-LED	Superluminescent Light Emitting Diode

Chapter 1

Introduction

1.1 Introduction

Optical sources are now used in a wide range of applications such as in Optical Coherence Tomography (OCT) technology, [1-2], OCT in medicine and biology, [3], in fiber gyroscopes, [4], and, of course, is used for optical communication applications, [5-7]. Semiconductor optical devices are perhaps, by far, in most common use these days.

A general introduction to semiconductor optical sources is given in Sec.1.2. Sec.1.3 presents a basic description of superluminescent Light Emitting Diodes (s-LEDs) and their diverse applications. Finally, a layout of the thesis is given in Sec.1.4.

1.2 Semiconductor Optical Sources

The semiconductor optical source is often considered to be the active component in an optical fiber communication system. Its fundamental function is to convert electrical energy in the form of a current into optical energy (Light) in an efficient manner, which allows the light output to be effectively launched or coupled into an optical fiber, [8]. Although gas and solid-state coherent optical sources were developed initially, the advent of semiconductor optical devices has truly heralded in optoelectronics/photonics with optical communication arguably providing the jewel in

the crown. The main reason why semiconductor-optoelectronics is proving to be successful is because it provides for very much more robust compact, light-weight and efficient devices. There are two types of optical sources that provide the electrical-optical conversion: in a semiconductor, Light Amplification by Stimulated Emission of Radiation (LASER), and Light Emitting Diode (LED). There are two types of LEDs: surface-emitting LED and edge-emitting LED (ee-LED). When an ee-LED operates at high Injection Currents the quasi-coherent optical power output from the LED can approach that of the coherent output from injection lasers; this is the case called superluminescent-LED (ee-s-LED). Typically, laser diodes produce highly polarised coherent optical output power. By contrast, in general, LEDs produce incoherent and unpolarised optical output. .

Today, LEDs are everywhere, in many shapes and forms, and cover a wide range of applications from indicator lights and solid-state lighting, [9], to optical coherence tomography in biology, medicine and, increasingly, applications in cosmetics. The need for LEDs is growing rapidly because of their particular attractive characteristics; e.g., the high coherence output of laser diodes leading to undesirable speckle patterns in many applications is avoided when illuminated with LEDs that have incoherent output. However, there are applications where, e.g., the highly polarised light from laser diodes is required but this feature is not usually available with bulk-semiconductor material LED sources. Although quantum-well material inherently has highly polarisation selective gain which can be used to produce polarisation enhanced LEDs, from the viewpoint of cost and higher optical power requirements the bulk material has advantages. In this context the main focus in this project is to investigate simple, practical designs for bulk-semiconductor ee-s-LEDs which will produce highly polarised optical outputs.

1.3 Superluminescent Diodes

The details of a ee-s-LED will be discussed later on in this thesis but it is informative to mention here that the device is almost the same in structure to a stripe contact edge-emitting Laser-diode, Fig.1.1. The main difference is that in the LED the stripe, injection contact is made only over a part of the length of the semiconductor chip, so that the remaining length of the semiconductor is 'un-pumped' and is therefore highly absorbent to the light that is generated in the pumped (optical gain) region and propagates into the unpumped region; the essential point being that the light in the LED effectively 'sees' only one, the front, reflective facet of the chip. As will be discussed in detail later, if even one of the facet reflectivities of a region with optical gain is (ideally) zero then the lasing condition cannot happen. However, if the pumped region of the LED is long and the device is pumped in to a level of high optical gain then the output characteristics of the LED begins to increasingly approach that of the ee-Laser diode. A schematic of the essential multi-layer structure of a present-day ee-LED is shown in Fig.1.2.

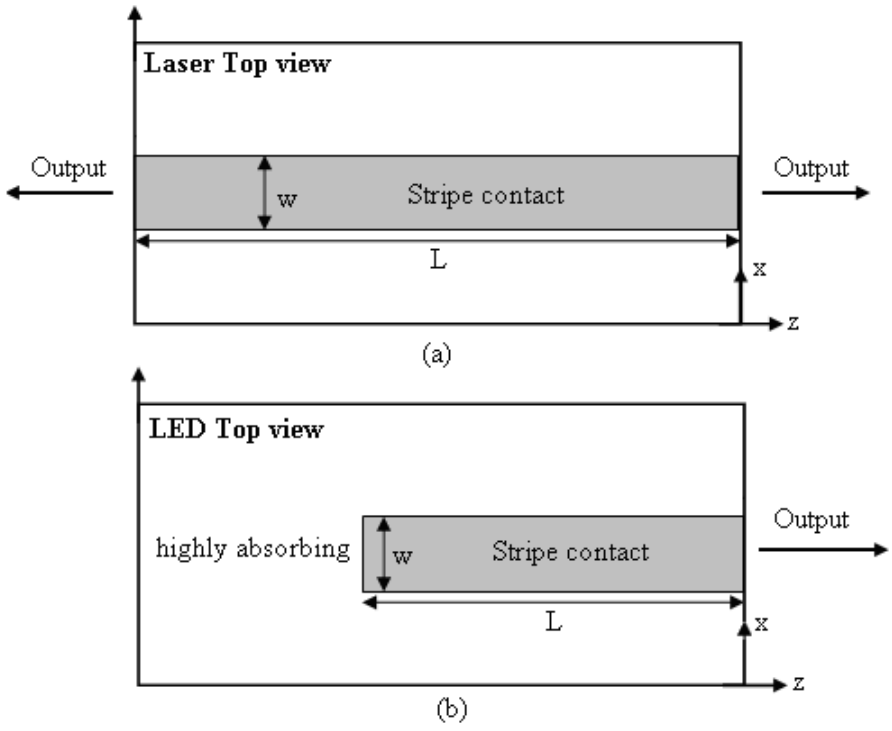

Figure 1.1 Top view device structure difference for Laser and LED; w is stripe width and L is stripe length

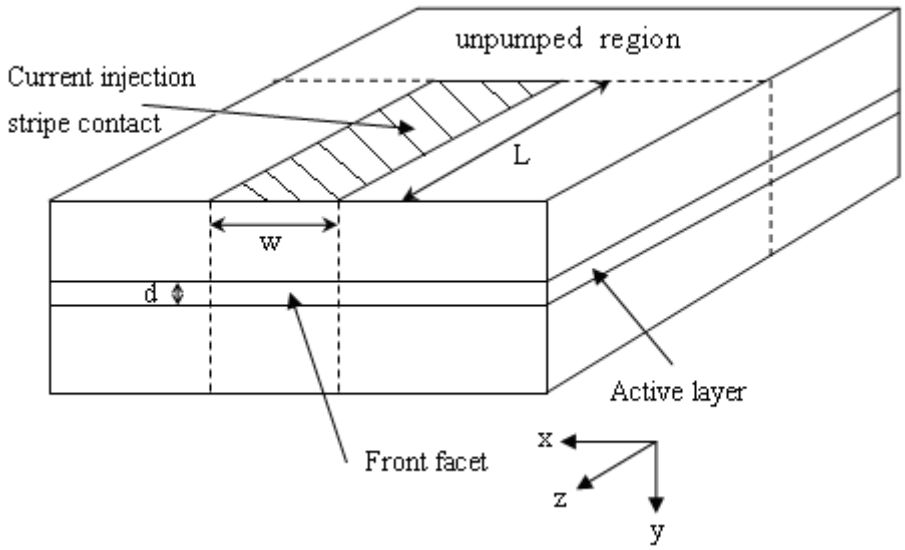

Figure 1.2 Schematic diagram of a typical structure of an edge-emitting superluminescent diode; w is stripe width and L is stripe length and d is the active layer thickness

For example, superluminescent diodes are now used extensively for optical coherence tomography to do medical tissue imaging, [10], related to skin diagnostics and cosmetics measurement, [11]; in fibre optic gyroscopes, [12]. Further, polarisation-sensitive OCT, [13], is used in sensor systems, such as in aircraft maintenance to detect discontinuities on aircraft structure, components and installed engine, [14]. A massive effort is presently under way to replace all traditional lighting with LEDs, [15]; also LED illumination in space applications has been widely applied in the past few years, [16].

Reliability, efficiency, low heat output and low cost has attracted the use of LEDs as the optical source in an increasing number of areas. As mentioned above, one of the LED applications is to use on cosmetics measurement, which is to control the quality of those cosmetics that require techniques that depend on more than just ordinary reflectance, like lip sticks, foundation creams, shampoo and nail polish. The traditional colour-measuring devices (colorimeters and spectrophotometers) are designed to come into contact with the sample, but products such as lip sticks are non-drying, sticky or translucent, [11]. Therefore, X-Rite Ltd. of Grandville, Mich., have designed a more cost-effective solution with built-in light sources which

illuminate the sample, and detectors measure the intensity of reflected light at various wavelengths, [11]. Another company, Moritex Corp. of Tokyo, which has been making instruments for studying the appearance and condition of human skin and hair, has developed a product called i-Scope, which use a white LED light source to show the condition of the hair and scalp to provide detailed analysis of hair cuticles and keratin cells, [11].

1.4 Thesis Layout

This thesis describes the development and study of polarisation-selective edge-emitting light emitting diodes (ee-LEDs). All the ee-LEDs optimised throughout the research work is bulk material active layer semiconductor device. In Chapter-2 a description of basic principles of interaction of light, optical emissions from semiconductor (e.g. band structure, *p-n* junction and DH structure) and optical gain follow by an introduction of general relevant electromagnetic theories including Maxwell's equations, wave equations and wave reflection and transmission. Importantly, in this chapter we have made a clear definition of polarisations for general plane wave polarisation and polarisations in slab dielectric waveguide, to avoid further confusion. We have also given a brief introduction of the Snell's and the Fresnel's equations with a more detailed discussion of the Brewster angle in this section, where the Brewster angle plays a key factor throughout the project.

Chapter-3 contains a study of ee-LEDs with stripe contact perpendicular to the front facet. A general introduction of the multi-layer structure is given in Sec.3.1, followed by detailed discussion of the Rate Equation. Special attention is given to the approximation of the $N = \bar{N}$ constant, where $\bar{N}$ is a weighted average constant carrier density. This $\bar{N}$ approximation enabled a simple mathematical method to

solve the Rays and Rate Equation, as $\bar{N}$ will be the only unknown variable in the Rate Equations. A self iterative model has been built to determine the value of $\bar{N}$. Simulation result presented the tests that have been verified whether the self iterative model is working reasonable.

In Chapter-4, the approximate analysis of the "V"-shaped stripe (V-stripe) ee-LED is introduced and the V-stripe is designed to achieve single polarised output. The "V"-geometric design has utilised the phenomenon of the Brewster angle, to develop a simple polarisation-selective ee-LED device. The computational model built for the approximate analysis of the V-stripe is described and examined. The development of the V-stripe is an improvement/optimisation from the angled stripe. Because for the angled stripe, the transmitted signal at stripe angle being equal to the Brewster angle is not purely single/TM polarisation, thus it is not good enough for some applications that only want a single polarisation signal; and also the reflected signal from the angled stripe is directly reflected into the absorbing/"umpumped" region, hence it is essential to have a second stripe to maintain/generate the reflected signal.

A refined analysis of the V-stripe is explained in Chapter-5, which is a modified and improved model to the approximate analysis of the V-stripe model from Chapter-4. In the refined model we have added the affect of angular distribution of intensities on top of the approximate analysis. A computational model has also been built and examined. This model provides a more realistic simulation of the "V"-geometric polarisation-selective stripe. Finally, the simulation results for the optimised polarisation-selective bulk material active layer semiconductor ee-LED will be presented.

Finally, conclusions that have been drawn from the research work are presented in Chapter-6, along with suggestion for future work.

References 1

[1] A.G. Podoleanu, J. A. Rogers and D.A. Jackson, **'OCT en-face Images from the Retina with Adjustable Depth resolution in Real Time'**, IEEE J. Sel. Top. Quantum Electron. 5, pp. 1176-1184, 1999

[2] F. Causa, J. Sarma, 'Realistic Model for the Output Bean Profile of Stripe and Tapered Superluminescent Light-Emitting Diodes', Applied Optics, Vol. 42, No. 21, pp. 4341-4348, July 2003

[3] J.M. Schmitt, **'Optical Coherence Tomography (OCT): A Review'**, IEEE Selected Topics in Quantum Electronics, Vol. 5, No. 4, pp. 1205-1215, 1999

[4] W.K. Burns, C-L. Chen, and R.P. Moeller, **'Fiber-optics Gyroscopes with Broadband Sources'**, J. Lightwave Technol, LT-1, pp. 98-105, 1983

[5] S.S. Wagner and T.E. Chapuran, **'Broadband Hight-density WDM Transmittion Using Superluminescent Diodes'**, Electron. Letter. 26, pp. 696-697, 1990

[6] T. Yamatoya, S. Mori, F. Koyama and K. Iga, **'Hight-power GaInAsP/InP Strained Quantum Well Superluminescent Diode with Tapered Active Region'**, Jpn. J. Applied Physics. 28. pp. 5121-5122, 1999

[7] Y. Kashima, A. Maroba and H. Takano, **'Linear InGaAsP Edge-Emitting LEDs for Single-mode Fiber Communications'**, J. Lightwave Technol, 12, pp. 1650-1655, 1992

[8] J.M. Senior, '**Optical Fiber Communications Principles and Practice'**, Second Edition, Prentice Hall Europe, 1985, 1992

[9] I. Moreno and C.C. Sun, **'Modeling the radiation pattern of LEDs'**, Optics Express 1808, Vol. 16, No.3, 4 February 2008

[10] D. Huang, **'Optical Coherence Tomography'**, Science, Vol.254, pp.1178-1181, 1987

[11] C. Connolly, **'Photonic Instrumentation Aids Cosmetic Measurements'**, Photonics Spectra, pp.80-86, July 2005

[12] W.K. Burns, C L. Chen, R P. Moeller, **'Fibre Optic Gyroscopes with Broad-Band Sources'**, Journal of Lightwave Technology, Vol. LT-1, pp.98-105, 1983

[13] D. Stifter[1], A.D. Sanchis Dufau[1], E. Breuer[1], K. Wiesauer[1], P. Burgholzer[1], O. Hoglinger[1], E. Gotzinger[2], M. Pircher[2], C.K. Hitzenberger[2], **'Polarisation-Sensitive Optical Coherence Tomography for Material Characterisation and Testing'**, [1]*Upper Austrian Research GmbH, Linz, Austria*; [2]*Department of medical Physics, Medical University of Vienna, Vienna, Austria*, Insight: Non-Destructive Testing & Condition Monitoring; Vol. 47 Issue 4, pp.209-212, April 2005

[14] M.U. Khan, **'Applications of Optical Device during Maintenance of Aircraft'**, *Biman Bangladesh Airlines, Dhaka, Bangladesh*, 16th WCNDT - World Conference on NDT, 2004

[15] N.B. Soni, *Member IEEE, Certified Energy Auditor* and P. Devendra, *Miste*, **'The Transition to LED Illumination: a case study on energy conservation'**, Journal of Theoretical and Applied Information Technology, Vol.4, NO.11, pp.1083-1087

[16] W. Lu, T. Zhang, S.M. He, B. Zhang, N. Li and S.S. Liu, **'Light-Emitting Diodes for Space Applications'**, Editorial Manager ™ for Optical and Quantum Electronics, OQEL1002, 2009

Chapter 2:

Basic Principles

2.1 Introduction

The chapter contains the basic principles relevant to this project. First of all, it presents a discussion of the basic concepts of light (photon) emission and absorption in Sec.2.2, and then it presents the explanation of the structure of optical source semiconductor and its characteristics in Sec.2.4. This is followed by a general introduction of relevant simple electromagnetic (EM), such as optical fields and EM wave in Sec.2.5, and most importantly in Sec.2.6, we will explain wave reflection and transmission, especially the definition of polarisations. We have clearly defined the polarisation in general plane waves and in slab dielectric waveguide, to avoid confusion. In between the explanation for polarisations in plane wave and in slab dielectric waveguide, we also discuss the characteristics of the Brewster angle and its advantage to this project design. Finally in the last section, we will introduce the confinement factor, which is considered as a fraction of the optical field.

2.2 Absorption and Emission of Radiation

The interaction of light with matter takes place in discrete packets of energy or quanta, called photons, [1]. From Quantum Mechanics considerations Max Planck established that light at a particular wavelength, λ_0 (or f) (λ_0 is the vacuum wavelength and f is frequency), can be considered as photons corresponding to energy $E = hf$, where

$h = 6.624 \times 10^{-27} (erg.s) = 6.624 \times 10^{-31} (Joules.s)$ is Planck's constant, [1].

The interaction of photons with a medium which is representable by a simple two level atomic system, [1], is shown in Fig.2.1. Such interactions are strictly analysed using quantum mechanics. However, as in classical mechanics, the concepts of momentum and energy conservation still apply.

A basic example of the application of the above momentum and energy conservation laws is presented here with reference to photon interaction with electrons in a simple two level atomic system, Fig.2.1, which represents the medium in this case.

To satisfy energy conservation, for absorption it therefore follows, that only photons of energy,

$$E = hf \geq (E_2 - E_1) \qquad (2.1)$$

will be absorbed in the medium; for photons with $E = hf < (E_2 - E_1)$, the medium will appears transparent. Similarly, an electron making a downward transition from energy level E_2 to energy level E_1 will emit a photon of frequency f, such that,

$$hf = E_2 - E_1 . \qquad (2.2)$$

In this example, it is assumed that the momentum of the electron is not changed when it moves from one energy level to the other. Since it is also known that a photon has negligible momentum, it follows that momentum conservation is satisfied in photon interaction with this medium.

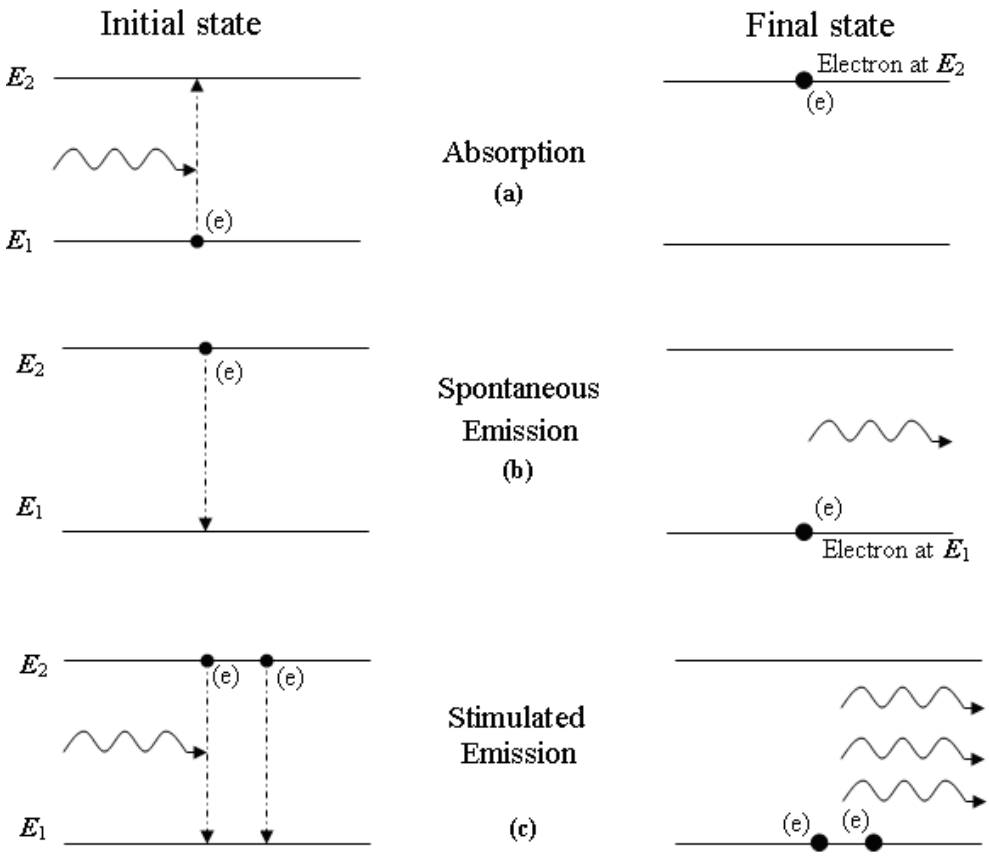

Figure 2.1 Energy state diagrams showing: (a) absorption; (b) spontaneous emission; (c) stimulated emission. The black dot indicates the state of the atom before and after a transition takes place

In the case of absorption, an incident photon of energy $hv = E_2 - E_1$ will produce an upward transition of the electron and the photon will be totally absorbed. The electron would initially be in the lower energy state E_1 as show in Fig.2.1(a) above.

Interestingly and very importantly, two kinds of emission processes are possible. The first, spontaneous emission, is the most commonly occurring, Fig.2.1(b); it occurs in the situation of an electron initially in the higher energy state E_2, spontaneously (randomly) falls to the lower energy level thereby emitting a corresponding photon. Such emissions from different atoms are about the same in wavelength (frequency), but they are in general otherwise incoherent. That is, they do not, in general, have the same phase, polarisation, and direction of propagation.

Stimulated emission is coherent emission where electrons located at the higher energy level E_2 makes a transition to the lower energy level E_1, Fig.2.1(c), are synchronized to the incident photon. The photons generated from such emission are coherent. They have the same wavelength, phase, polarisation and direction of propagation as the incident photon. If there are more photons emitted than the incident photon, there is optical gain.

2.3 Population Inversion

In the 2-level (gas) system, under the condition of particles in thermal equilibrium, which for gases is given by the Maxwell-Boltzmann distribution, the lower energy level E_1 of the two level atomic systems contains more atoms than the upper energy level E_2. This is the usual situation at room temperature, [1], Fig.2.2(a).

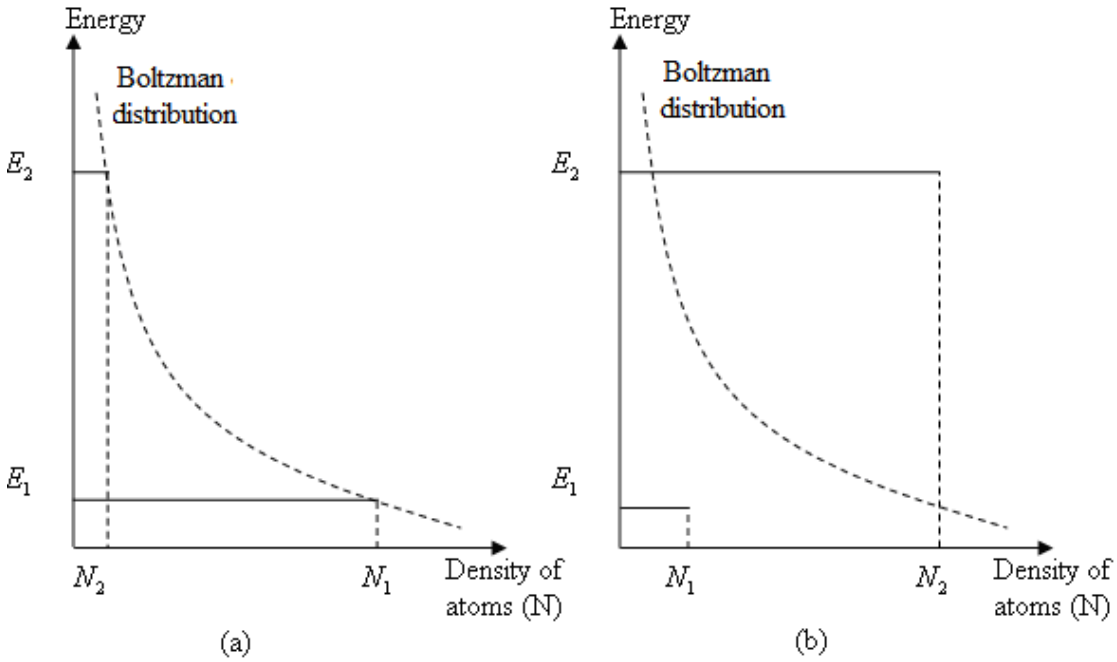

Figure 2.2 Populations in a two energy level system: a) Maxwell-Boltzmann distribution for a system in thermal equilibrium; b) a nonequilibrium distribution showing population inversion, [1]

Population inversion is the condition to create a nonequilibrium distribution of atoms such that the number of atoms in the upper energy level is greater than that in the lower energy level. Thus, the atoms must be excited into the upper energy level E_2 and hence obtain a nonequilibrium distribution, as illustrated in Fig.2.2(b); this process is achieved by optical "pumping" and is important to achieve optical gain.

2.4 Optical Emission from Semiconductor

2.4.1 Crystalline Semiconductor

Although gas and solid-state coherent optical sources were developed initially, the development of semiconductor optical devices has truly made a huge improvement in optoelectronics/photonics for optical communications. The main reason why semiconductor-optoelectronics is proving to be successful is because it provides for very much more robust, compact, light-weight and efficient devices.

Predominantly, the semiconductor material used for electronic devices are crystalline solids, [1]; it is well known that crystalline solids have a periodic lattice structure- the nuclei of the atoms of the media are periodically located and the outer shell electrons of the atoms are under the influence of all atoms; so, very large numbers of atoms are very close to each other. Electron orbits of one atom are strongly influenced by other atoms. Electrons must be considered quantum mechanically as waves and interaction of a large set of periodic atoms has to be included. Such analysis leads to a compact description of a crystalline solid in terms of energy bands and band-gaps.

2.4.2 Band Structure

For a crystalline semiconductor the valence band is the lower energy level and the conduction band is the higher energy level, shown in Fig.2.3,

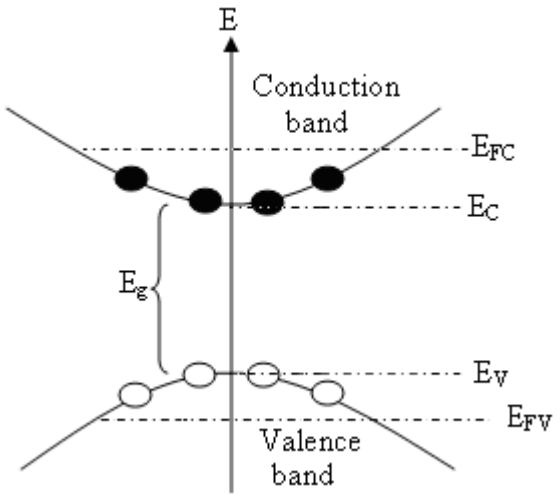

Figure 2.3 Energy band structure of intrinsic semiconductor, showing an equal number of electrons and holes in the conduction band and the valence band respectively

Electrons located in the valence band can be raised to the conduction band if sufficient energy is available. On the other hand, electrons initially located in the conduction band drop to the valence band by releasing the energy difference as an optical emission.

For the semiconductor, the pass-band implies that electrons can exist in valence and conduction band regions but they cannot exist in the band-gap region. There are two classes of semiconductor. One is where the minimum of the conduction band is directly above the maximum of the valence band and both conduction and valence band have the same k value (crystal momentum); this is called direct band-gap semiconductor, such as GaAs. Thus recombination is easily possible (Fig.2.4(a)). In the case of the minimum of the conduction band displaced from the maximum of the valence band, having different values of k, this is know as indirect band-gap semiconductor (Fig.2.4(b)), such as Si and Ge.

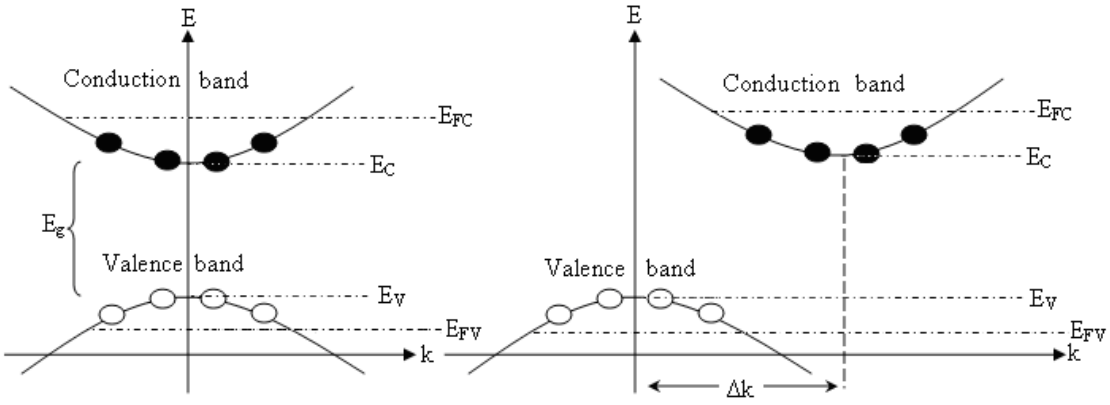

Figure 2.4 Energy momentum diagrams showing the types of transition: (a) Direct band gap semiconductor; (b) Indirect band gap semiconductor

E_{FC} and E_{FV} are the Fermi level for conduction band and valence band, that will be discussed in the following section. In order to produce electroluminescence it is necessary to select an appropriate semiconductor material. The most useful materials for this purpose are direct band-gap semiconductors, [2].

In direct band-gap semiconductors, when the electron-hole recombination process occurs, the momentum of the electron in the conduction band remains virtually constant and energy is released, which corresponds to the band-gap energy $E_g = E_c - E_v$ (where E_c represent the energy in conduction band and E_v represent the energy in valence band), may be emitted as light. Therefore the direct band-gap semiconductors are very suitable for optical devices. But in an indirect band-gap semiconductor, a photon has very small momentum, an incident photon of $hf \geq E_g$ will have a very small chance of being absorbed or emitted since the conservation of momentum could not be satisfied, that means the indirect band-gap semiconductors have poor optical interaction. Apart from the energy and momentum conservation requirements, upward (absorption) or downward (emission) transitions need two other obvious conditions to be satisfied. Namely a filled lower energy level (valence band) and a relatively empty upper energy level (conduction band) are needed for absorption to occur. Similarly, a filled conduction band and a relatively empty valence band are needed for emissi on to occur.

2.4.3 The *p-n* Junction

In order to allow consideration of semiconductor optical sources, a review some of the properties of semiconductor materials is necessary, especially with regard to the $p-n$ junction. A $p-n$ junction diode can be constructed as a homojunction in its simplest form, using an abrupt change between $P-$ and $n-type$ regions in a single piece of semiconductor [5], there are electrons in the $n-type$ material and holes in the $p-type$, Fig.2.5(a).

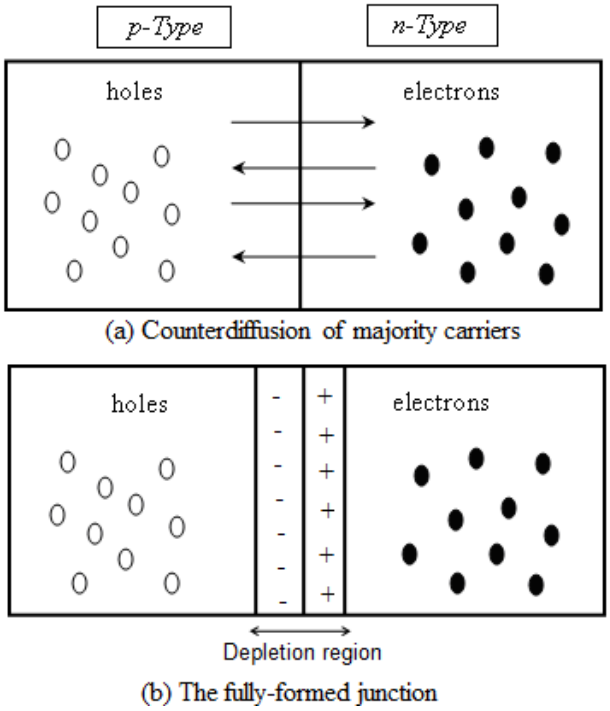

Figure 2.5 *p-n* junction formation

When the two pieces are brought into contact, electrons from the $n-region$ near the interface diffuse into the $p-side$, leaving behind a layer which is positively charged by the donors. Similarly, holes diffuse in the opposite direction, leaving behind a negatively charged layer stripped of holes. The resulting junction region then contains practically no mobile charge carriers, and the fixed charges of the dopant atoms create a potential barrier acting against a further flow of electrons and holes, known as the depletion region, Fig.2.5(b).

In practice, the dynamics of junction formation are irrelevant to the operation of the device [5], and the situation needed to be considered is $p-n$ junction in equilibrium. Fig.2.6 shows an energy band diagram for a $p-n$ junction in equilibrium, where the Fermi levels in the *p*-type and *n*-type sides are equal.

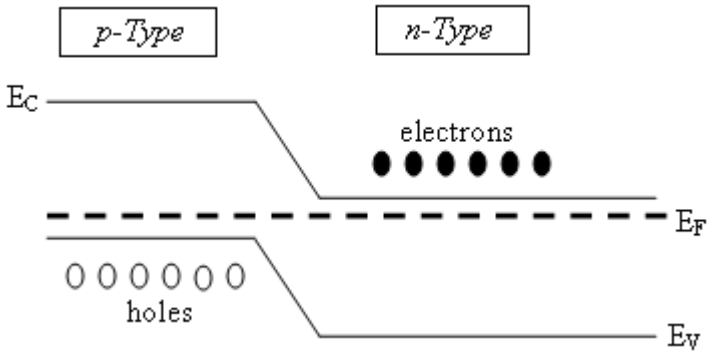

Figure 2.6 Schematic diagram of *p-n* junction in equilibrium

E_F is Fermi level and it is only a mathematical parameter but it gives an indication of the distribution of carriers within the material. When the Fermi level is in equilibrium, a barrier has formed to prevent electrons and holes from diffusing to the opposite type region.

Applied bias will allow electrons to diffuse, and be injected into the *p*-side. When the *n*-type side is more negative than the *p*-type side, it is known as the forward bias condition and if *n*-type side is more positive than the *p*-type side, it is the reverse bias condition. A forward biased $p-n$ junction allows electrons and holes across the junction to form inversion population in the depletion region, illustrated in Fig.2.7,

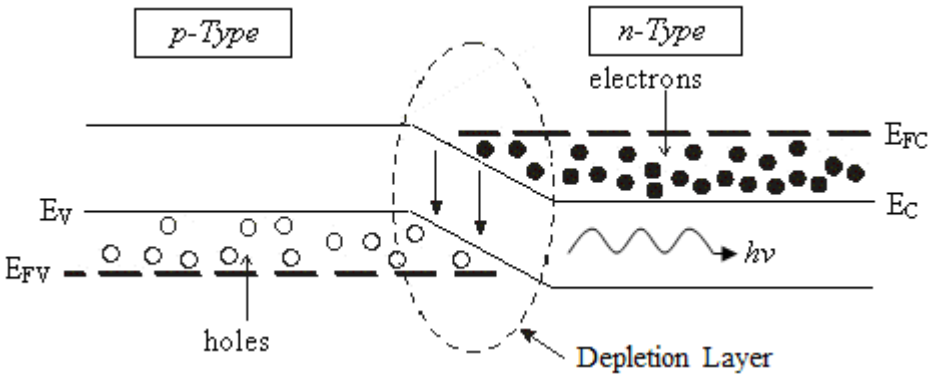

Figure 2.7 Schematic diagram of a forward bias p-n junction

E_{FC} is the Fermi level for electrons and E_{FV} is the Fermi level for holes. Inversion population could be achieved by optical pumping use (incoherent) optical signal with $hv > E_g$ to move electrons in large numbers into the conduction band. Forward biased $p-n$ junction is most common and conveniently establishes an inversion population density. Large doping densities are better for achieving inversion population, thus more light emission can be produced.

2.4.4 Double-Heterostructure Material

According to the definition, the simplest type of junction is a homojunction, where on either side of a junction they have the same material (same bandgap), and a junction between two different bandgap semiconductor is known as heterojunction. A semiconductor device structure that has junctions between different band-gap materials is called heterostructure device (HD), [2]. In a $p-n$ junction, although it can have electron injection and can produce light emission, but as the depletion layer is too thick, the corresponding carrier density is small, thus it is not efficient to generate light emission. In order to utilise the injection electrons, using a narrow depletion layer can have higher carrier density to enable a more effective recombination process. Also optical field confinement is desired to increase stimulated emission. To achieve a thinner effective depletion layer, which is usually called the active layer, the Double-Heterostructure (DH) material is used. DH structure has two sets of different band-gap materials; it forms a perfect thin active layer due to the different material fraction, hence can increase the intensity of the output light, illustrated in Fig.2.8.

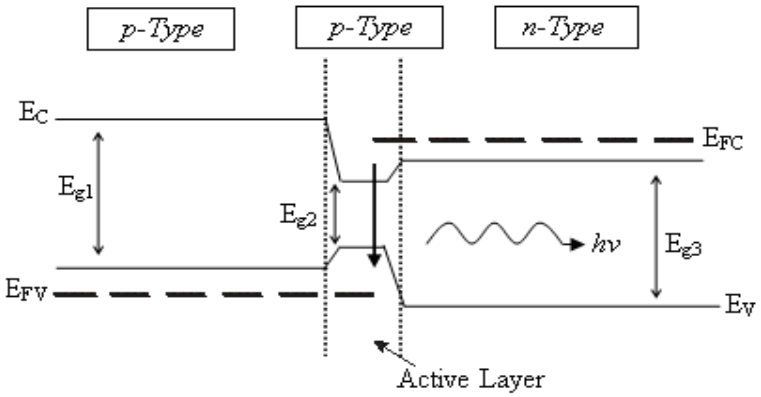

Figure 2.8 Energy band gap diagram of a forward biased double heterostructure material

$E_{g1,2,3}$ are different bandgaps, E_{FC} is the Fermi level for electrons and E_{FV} is the Fermi level for holes. The active layer is very thin, typically is about $0.2\mu m$, as the refractive index of a semiconductor material depends on its band-gap, the wider the band-gap semiconductor the lower the refractive index, fortunately the chemical element Al on both side of the active region appears to have produced a refractive index bump, which reflect both electrons and holes back into the active layer, also enabled room temperature continuous-wave (CW) operation. With such a thin active region in a DH structure material it is very effective interaction for carriers and photons, because it provides large carrier density, where the photon field is concentrated within the same region. Also optical field confinement is desired so an increase in optical energy density (to increase stimulated emission) can be achieved.

Most of the LEDs are fabricated with a double heterostructure, which when implemented means the resulting carrier and optical confinement reduce the Injection Currents and hence obtain higher efficiencies.

2.4.5 Optical Gain

In order to increase the optical energy, refer to Fig.2.9, the rate of electron transition will need to satisfy energy momentum conservation and also need to have the corresponding states occupied and vacant for the transitions to occur, especially the

downward transition, which produce spontaneous emission and stimulated emission. Optical gain depends on net stimulated emission, where

Net stimulated emission = Stimulation emission - Absorption

The details of calculating the rates of optical emission can be referred to as the occupation equation. So when net stimulation emission is greater then zero, it is possible to have optical gain, while spontaneous emission is always happening.

The optical gain in the material active layer represented as $g_{mat}(N,E)$ is the macroscopic representation of the net stimulated emission rate, produced by inversion population density, N. A very simplified linear approximation for material gain is,

$$g_{mat}(N,E) = A_0(E)\left[N - N_{tr}(E)\right] \qquad (2.3)$$

where E is the energy of photon, and $A_0(E)$, $N_{tr}(E)$ are values that locally best fit the actual gain curves, when $g_{mat} = 0$ at $N = N_{tr}$, the inversion population density for transparency.

A realistic optical (material) gain spectrum in a semiconductor is as shown in Fig.2.9, [3], [4]. In this thesis, the main interests are the peak values of gain since the calculations do not involve wavelength spectrum.

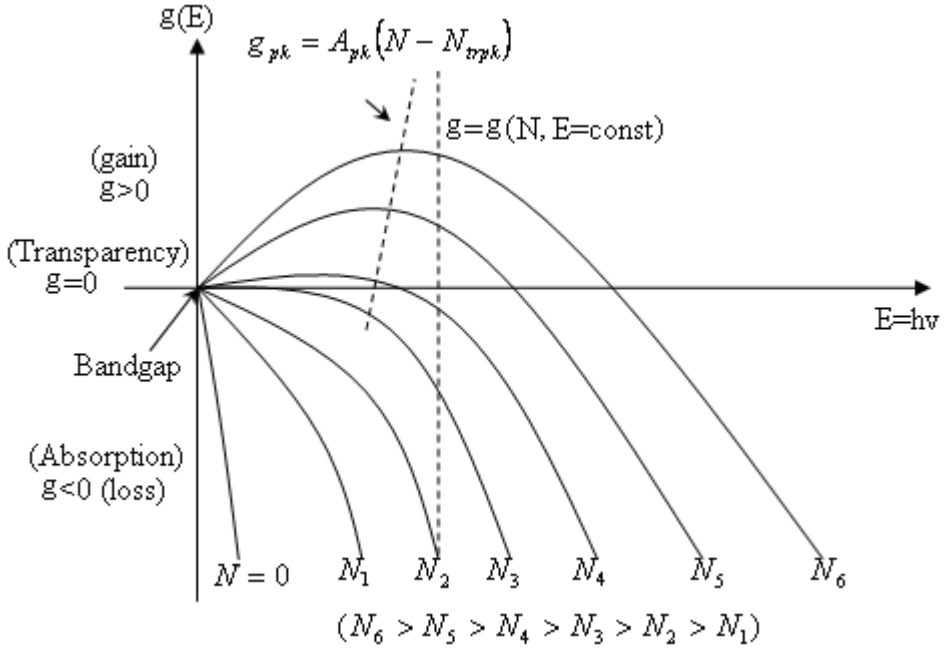

Figure 2.9 Optical gain spectrum in semiconductor

2.5 Optical Fields and Electromagnetic Waves

In classical theory, the laws of electricity and magnetism are described by Maxwell's equations, which in effect are a set of relations linking the values of a number of quantities that describe electric and magnetic fields, [5].

In general time dependent form, Maxwell's equations are:

$$\nabla \times \underline{\tilde{E}} = -\frac{\partial \underline{\tilde{B}}}{\partial t} \tag{2.4}$$

$$\nabla \times \underline{\tilde{H}} = \underline{\tilde{J}} + \frac{\partial \underline{\tilde{D}}}{\partial t} = \sigma \underline{\tilde{E}} + \frac{\partial \underline{\tilde{D}}}{\partial t} \tag{2.5}$$

$$\nabla \cdot \underline{\tilde{B}} = 0 \tag{2.6}$$

$$\nabla \cdot \underline{\tilde{D}} = \tilde{\rho} \tag{2.7}$$

∇ is a vector differential operator depending of the spatial co-ordinates, [6]; $\underline{\tilde{E}}$ and $\underline{\tilde{H}}$ are the electric and magnetic field vectors in time dependence respectively; $\underline{\tilde{D}}$ and $\underline{\tilde{B}}$ are the electric displacement and the magnetic flux vectors in time dependence respectively; where $\underline{D} = \varepsilon_0 \varepsilon \underline{E}$; $\underline{B} = \mu_0 \mu \underline{H}$; $\underline{\tilde{J}}$ is conduction current density (A / cm^2); charge density is $\rho\,(coulombs / cm^3); \varepsilon_0 = 8.8510^{-12}(F / m)$ is the permittivity of free space and ε is the relative permittivity of the medium; $\mu_0 = 4\pi 10^{-7}(henry / m)$ is the permeability of free space and μ is the relative permeability of the medium.

In a medium with constant real relative permittivity, ε, relative permeability μ, $\underline{\tilde{J}} = 0, \rho = 0$, and assuming harmonic time dependence ($e^{j\omega t}$), the Maxwell's equation become:

$$\nabla \cdot \underline{E} = 0 \tag{2.8}$$

$$\nabla \cdot \underline{H} = 0 \tag{2.9}$$

$$\nabla \times \underline{E} = -j\omega\mu_0\mu\underline{H} \tag{2.10}$$

$$\nabla \times \underline{H} = j\omega\varepsilon_0\varepsilon\underline{E} \tag{2.11}$$

where all fields have been represented as $\tilde{\underline{F}}(x,y,z,t) = \underline{F}(x,y,z)\exp(j\omega t)$, $\omega = \dfrac{2\pi c}{\lambda_0} = 2\pi v$ is the angular frequency; v is the signal frequency, and λ_0 is the vacuum wavelength.

The most basic but an important fundamental wave solution from Maxwell's equation corresponds to that of a Plane Wave (PW); a simple definition of an Electromagnetic plane wave ($EM-PW$) is one which has no field variation in the plane perpendicular to the direction of wave propagation. Specifically, assuming PW propagation along the $z-axis$ it follows that there is no variation along the $x-$ and $y-axis$, that is, $\partial_x \equiv 0$ and $\partial_y \equiv 0$ which implies that $F(x,y,z) = F(z)$.

For this simplified, special case, Maxwell's equations, Eq.(2.8)–(2.11), yield the one dimensional wave equation，

$$\frac{d^2F(z)}{dz^2} + k_0^2\mu\varepsilon F(z) = 0 \tag{2.12}$$

where $F(z)$ is any non-zero field component, $k_0^2 = \omega^2\varepsilon_0\mu_0$; $k_0 = \omega\sqrt{\varepsilon_0\mu_0} = \dfrac{2\pi}{\lambda_0}$, λ_0 is the vacuum wavelength and the velocity of light in vacuum is $c = \dfrac{1}{\sqrt{\mu_0\varepsilon_0}} = 3\times10^8(m/s)$ .The solution to Eq.(2.12) is,

$$\tilde{F}(z,t) = Ae^{j(\omega t - kz)} + Be^{j(\omega t + kz)} \qquad (2.13)$$

where $k^2 = k_0^2 \mu\varepsilon; k = k_0\sqrt{\mu\varepsilon}$.

If ω and k are positive then the first and second terms on the right hand side (RHS) of Eq.(2.13) represents forward and reverse travelling waves respectively where k corresponds to the *propagation constant* of the PW .

Phase velocity, $v_p = \frac{\omega}{k} = \frac{\omega}{k_0\sqrt{\mu\varepsilon}} = \frac{c}{\sqrt{\mu\varepsilon}}$, therefore

$$v_p = \frac{c}{n} \qquad (2.14)$$

where $n = \sqrt{\mu\varepsilon}$ is refractive index of material. For *non-magnetic* material, $\mu = 1$, then the refractive index,

$$n = \sqrt{\varepsilon} \qquad (2.15) \qquad \text{and} \qquad \frac{k}{k_0} = n = \sqrt{\varepsilon} \qquad (2.16)$$

where $\sqrt{\varepsilon}$ is the refractive index of the homogenous medium.

For this wave, Eq.(2.13), the use of Maxwell's equations yields $H_z = 0; E_z = 0$ which is an intrinsic property of PWs – that is, there are no field components in the direction of propagation. It also follows from Maxwell's equations that the electric and magnetic field components are orthogonal to one another. For the chosen co-ordinate system it is convenient and complete to consider two basic, independent configurations (polarizations), E_x with H_y and E_y with H_x and they are related, $E_x = ZH_y$ and $E_y = -ZH_x$, $Z = \frac{Z_0}{\sqrt{\varepsilon}}$, $Z_0 = \sqrt{\left(\frac{\mu_0}{\varepsilon_0}\right)}$, for $\mu = 1$.

2.6 Wave Reflection and Transmission

2.6.1 Plane Wave Polarisation

A Plane Wave (PW) in general is one which has no variation of any of its physical components in the plane transverse to the direction of propagation. If this special feature is applied to electro-magnetic (EM) PWs it follows from the theory (Maxwell's equations, see Sec.2.5) that there is no electric (E) or magnetic (H) field components in the direction of wave propagation. More formally, the PW is referred to as a Transverse Electro-Magnetic (TEM) wave - that is, a wave which has Non-Zero electric and magnetic field components only along axes transverse to the direction of propagation. The theory also establishes that the non-zero, transverse, E and H field components must be perpendicular to each other. It is further possible to show from the theory that, strictly speaking, EM PWs can exist only in a homogenous medium (in which the material properties have no spatial variation along the transverse axes).

Consider the rectangular co-ordinate system, x, y, z, Fig.2.10(a). In general a PW could propagate along any straight line in this 3-dimensional space. To be more specific, however, assume that the PW propagates along the z-axis; in that case the EM PW wave will have $E_z = H_z = 0$ with the non-zero field components in the $x - y$ plane. Thus, for example, there could be E_x with H_y or E_y with H_x, or any combination of these two basic sets which satisfy Maxwell's equations. Any other permissible non-zero field components associated with this PW can be decomposed in to these two basic sets. Similarly, if the PW propagates along the $x - axis$ then $E_x = H_x = 0$, and the non-zero fields will be in the $y - z$ plane. In electromagnetics the direction of the total electric field defines the polarization of the signal (wave). Thus, for the PW propagating along the $z - axis$, the two basic polarizations are linearly polarized along the *x*-axis and linearly polarized along the $y - axis$.

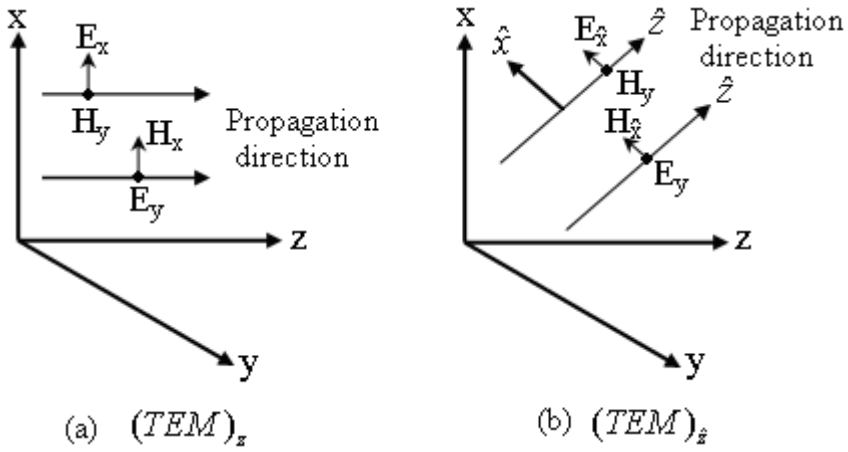

Figure 2.10 Rectangular co-ordinate system, x, y, z, where $\hat{x}, y, \hat{z}$ are the modified orthogonal co-ordinate system for *PWs* travel at some angle to the z-axis

If, however, the PW propagates along a line on the $x-z$ plane but at some angle to the $z-axis$, Fig.2.10(b), then, for ease of understanding, it is convenient to consider a modified orthogonal co-ordinate system, $\hat{x}, y, \hat{z}$, where, now, the wave propagates along the $\hat{z}-axis$. Then, from the properties of PWs presented above, it follows that $E_{\hat{z}} = H_{\hat{z}} = 0$ and the two basic sets of non-zero field components will be $E_{\hat{x}}$ with H_y or E_y with $H_{\hat{x}}$ (any other permissible non-zero field components for such a PW can be decomposed in to these two basic types). So, for this case the two basic categories are PWs linearly polarized along the $\hat{x}-axis$ and linearly polarized along the $y-axis$. Importantly note that a non-zero $E_{\hat{x}}$ can itself be decomposed in to E_x and E_z so that the PW linearly polarized along the $\hat{x}-axis$ will, in terms of the x, y, z, co-ordinate system, have E_x, H_y, E_z, as the non-zero components. Similarly, the PW polarized signal along the $y-axis$ will have H_x, E_y, H_z, as the non-zero field components. This form of notation of PW fields becomes more suitable for the analysis of reflection and refraction of EM fields from an abrupt, plane interface.

Consider, for example, an abrupt interface defined by the $x-y$ plane, $z=z_0$; that is, at least one or more of the electromagnetic properties (magnetic permeability – μ, electrical permittivity – ε, and electrical conductivity – σ) of the medium in the region $z<z_0$ are different from those in the region $z>z_0$. Further consider a PW propagating in the region $z<z_0$ along a straight line in the $x-y$ plane at an angle to $z-axis$, that is incident on the plane $z=z_0$, Fig 2.10.

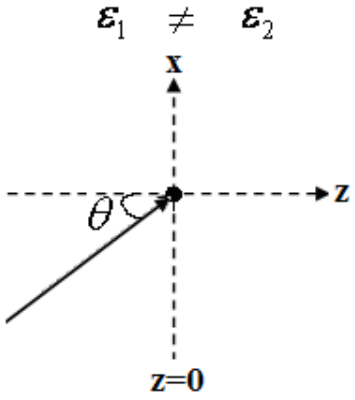

Figure 2.11 PW propagating in the *x-y* plane at an angle to *z-axis*

Following prevalent custom, the Plane of Incidence (PoI) is defined as that formed by the line perpendicular to the abrupt interface and the line of incidence. In this case, therefore, the PoI is the $x-z$ plane. This clearly defines a problem for the analysis of reflection and refraction of a EM PW from an abrupt interface. The Fresnel's equations pertinent to this analysis are shown in Sec.2.6.3, detailed discussions can be referred to reference, [6]; but here it is important to indicate the two primarily different cases that prevail.

The first case is when the electric field of the PW is perpendicular to the PoI and the second case is when the electric field is parallel to the PoI; that is, the incident PWs are characterized as being perpendicularly or parallel polarized (with respect to the PoI). In this particular example, therefore, perpendicular polarization corresponds to E_y as the only non-zero field component while for parallel polarization E_x and E_z are the non-zero electric field components. In the context

of reflection and refraction of *PWs* the most important point to note is that for:

a) Perpendicular polarization the non-zero electric field is totally tangential to the plane of the abrupt interface;

b) Parallel polarization a component of the non-zero electric field is normal (perpendicular) to the plane of the abrupt interface.

The importance of this categorization follows from the Fresnel equations analysis and is summarized here as case b) exhibits total transmission at the Brewster angle of incidence while case a) does not.

2.6.2 Snell's Law and Total Internal Reflection

To consider the propagation of light, where a plane wave travels at an angle to an abrupt interface, as shown in Fig.2.12.

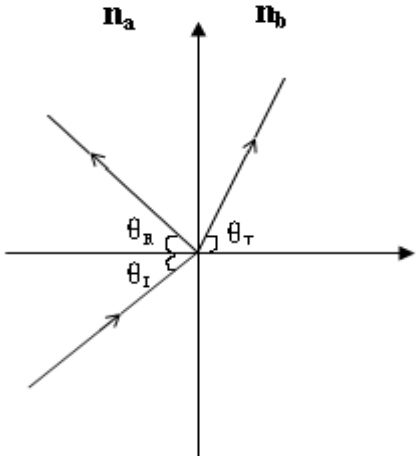

Figure 2.12 Plane wave travelling at an angle to an abrupt interface

where $\theta_I, \theta_R, \theta_T$ are incident angle, reflected angle and transmitted angle, respectively; n_a, n_b are refractive index for medium *a* and *b*.

Snell's law gives the relationship between angles of incidence and refraction for a wave impinging on an interface between two media with different indices of refraction, resulting in

$$n_a \sin\theta_I = n_b \sin\theta_T \qquad (2.17)$$

When $n_2 > n_1$ Total Internal Reflection (TIR) can occur, the transmitted angle is greater then the incident angle, when the refraction angle θ_t reaches $90°$, this is where total internal reflection occurs, which is given by

$$\sin_{TIR} = \frac{n_2}{n_1} \tag{2.18}$$

2.6.3 Brewster Angle

The behaviour of the electric and magnetic fields in between two media at a boundary can be governed by rules called boundary conditions, [2], which are obtained from Ampere's Law and Gauss's Law. The boundary condition indicates that the tangential electric (E) and magnetic (H) field component is continuous across the interface, also that the normal component of the magnetic flux density (B) and electric displacement vector (D) are continuous across the interface, which mans for a normal incident plane wave, the electric and magnetic fields are both always tangential to the boundary regardless of the wave polarisation.

Applying the boundary condition for the electromagnetic wave at $y = 0$, the reflected and transmitted waves can be found in terms of the incident wave. Consequently, the reflection and incident angle must equal, in order to satisfy the boundary condition, where $\theta_i = \theta_r$. Therefore by obeying Snell's Law $n_1 \sin\theta_i = n_2 \sin\theta_t$, the angle for incident and transmitted waves can be found. Subsequently, by using Fresnel's equation, a simple relationship between incident angle and media refractive index (n_1, n_2) can be found. The Fresnel reflection coefficient for perpendicular $(E_\perp)$ and parallel $(E_\parallel)$ polarisations are given by Eq.(2.19) and Eq.(2.20), [2],

$$r_{\perp} = \frac{\cos\theta_i - [n^2 - \sin^2\theta_i]^{1/2}}{\cos\theta_i + [n^2 - \sin^2\theta_i]^{1/2}} \tag{2.19}$$

$$r_{\parallel} = \frac{[n^2 - \sin^2\theta_i]^{1/2} - n^2\cos\theta_i}{[n^2 - \sin^2\theta_i]^{1/2} + n^2\cos\theta_i} \tag{2.20}$$

where $n = n_2 / n_1$, θ_i is the incident angle.

For $n_1 > n_2$, as the incident angle increases, reflectivity for parallel polarisation $(r_{\parallel})$ will eventually become zero at an angle called the Brewster angle, Fig.2.13 shows a typical Brewster angle curve by using the interface between the semiconductor gallium arsenide ($GaAs = n_1 = 3.6$) and air ($n_2 = 1$),:

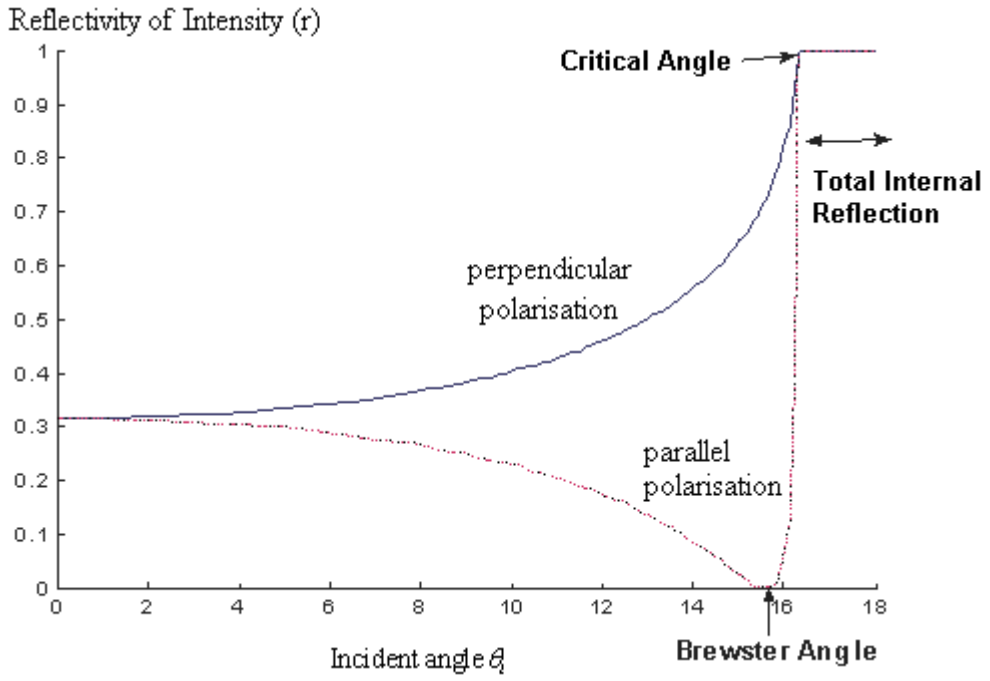

Figure 2.13 Reflectivities of a GaAs/air interface for two polarisations against incident angle θ_i

For parallel polarisation, the reflectivity first decreases slowly with angle of incidence to zero at the Brewster angle (15.5° for GaAs/air interface, [7]), and then the reflectivity increases dramatically to the critical angle (Total Internal Reflection, as defined by Snell's Law). For the perpendicular polarisation, the reflectivity increases

continuously with incident angle until it reaches the same angle of critical angle as for the parallel polarisation. The power reflection coefficient, reflectance (R) is calculate by $R_{\perp} = |r_{\perp}|^2$ and $R_{\parallel} = |r_{\parallel}|^2$. The Brewster angle from Eq.(2.20) is given by $\tan\theta_B = \frac{n_2}{n_1}$.

2.6.4 Optical confinement in DH semiconductor material

--- Slab Dielectric Waveguide

The DH material is used primarily for efficient (inversion population) carrier confinement in the 'active' (optical gain) region, core layer of the multilayer semiconductor material. But this also provides a very advantageous feature with respect to optical confinement since it turns out that the refractive index of the core layer is slightly larger than the adjacent, cladding layers. Hence, total internal reflection between the core and cladding layers is possible and this leads to the existence of optically confined bound modes corresponding to slab dielectric waveguides, [7]. The intention in this section is to provide a simple description of the slab-waveguide non-zero field components and their spatial distributions so that the relevant issues of reflection and refraction of waveguide fields at an abrupt interface can be presented, as has been done above for ideal PWs.

Referring to the Fig.2.14, the planes of the multi-layer material are perpendicular to the $y-axis$ and consider first that the signal propagation direction of the waveguide structure is along the longitudinal, $z-axis$. For this configuration there is no field variation along the $x-axis$; there is a confined (bound mode) field distribution along the $y-axis$ and a propagating field distribution along the $z-axis$, [6].

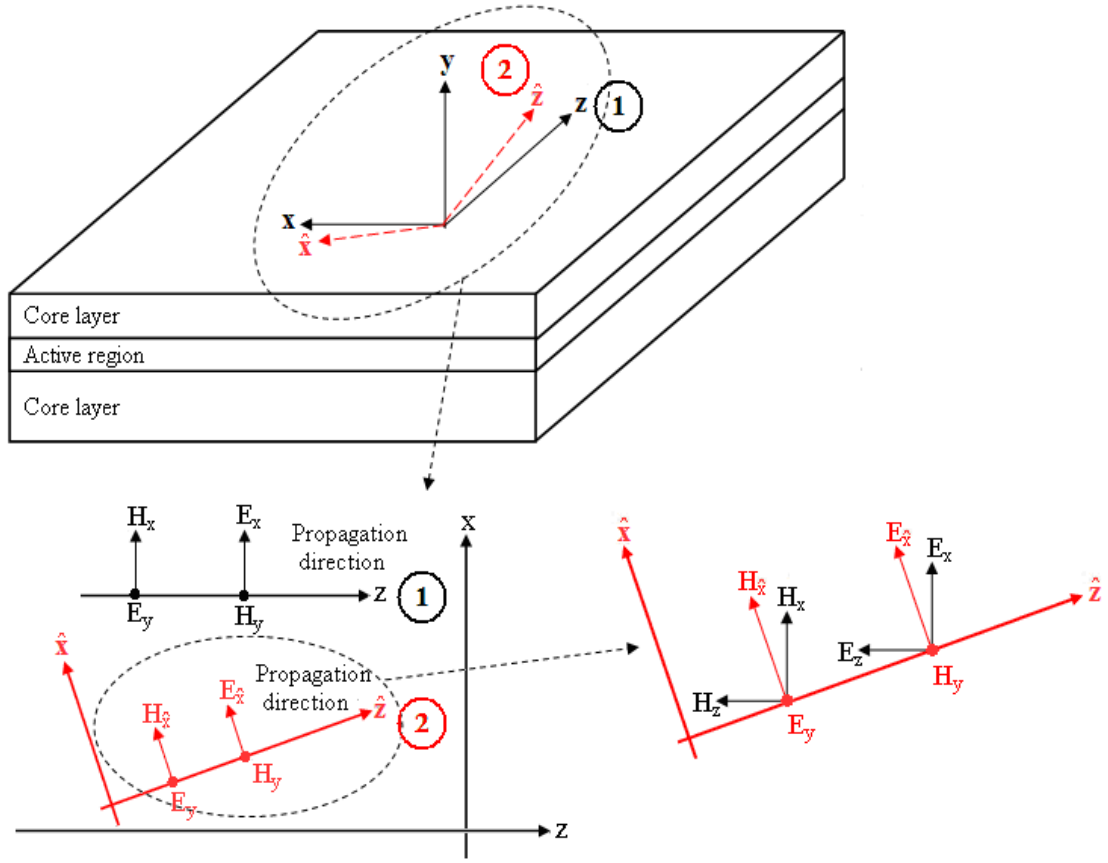

Figure 2.14 Schematic diagram analysing the wave propagating in DH semiconductor respectively to the *PW* propagating in *x-z* plane; where (1) represents *PW* propagating parallel to *z-axis* and (2) represents *PW* propagating at an angle to *z-axis*

Similarly to that with the case of the *PWs*, there are two basic, independent polarizations that can be supported. One is referred to as the Transverse Electric $(TE)_z$ and the other is Transverse Magnetic $(TM)_z$. As with *PWs* the notation indicates that for TE there is no electric field component along the propagation axis (z, in this case), so that $E_z = 0$; similarly for TM, $H_z = 0$. Proper analysis using Maxwell's equations (see Sec.2.5, and reference [7]), yields that the only non-zero field components for TE are E_x, H_y, H_z, while those for TM are H_x, E_y, E_z.

Further, it can be shown that for typical DH semiconductor materials the H_z and E_z components of the mode fields are much smaller than the two corresponding lateral (x) and transverse (y) components. Therefore, the TE polarization

approximates to parallel and the TM to perpendicular (to PoI) polarizations for PWs. There remains, however, the issue of field variation along the $y-axis$. A non-zero field component for a mode in a slab dielectric waveguide (refer to Fig.2.14) may be represented as,

$$F(x,y,z) = f(y)\exp(-j\beta z) \qquad (2.21)$$

where $f(y)$ is the mode-profile and β is the propagation constant of the mode, similar to the propagation constant k for the PW, Eq.2.13 .

Since $\mu = 1$, as for PWs, define,

$$\frac{\beta}{k_0} = n_{ff} = \sqrt{\varepsilon_{ff}} \qquad (2.22)$$

where ε_{ff} is the effective relative permittivity and n_{ff} is the effective refractive index for that mode. That is, this *mode in the multilayer media* may be viewed as a PW propagating in a *homogeneous media* of $\varepsilon = \varepsilon_{ff}$ and $n = n_{ff}$.

2.6.5 Confinement Factor

In the DH structure semiconductor material active layer the optical field propagates as a mode in a symmetric slab dielectric waveguide (Fig.2.15) with the fundamental (bound) mode field distribution along the vertical ($y-axis$) as shown. Note that the typical field distribution is not totally confined to the core but also spreads into the cladding layers. The confinement factor, Γ, is the fraction of the modal power in the active layer compared to the total power in the whole mode. Clearly, $0 < \Gamma < 1$. From modal theory it can be shown that at a given signal wavelength, $\Gamma = \Gamma(d, \Delta n)$, where d is the thickness of the core (active) layer and Δn is the refractive index step between the core and the cladding layers; Γ increases with increase in d and with increase in Δn.

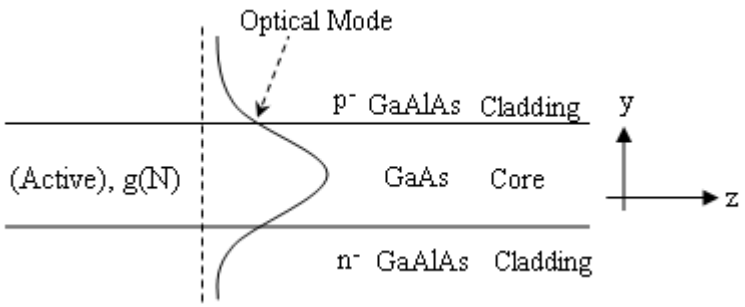

Figure 2.15 Optical field propagates as a mode in active layer

Since the inversion population (carrier) density, N, is confined to the active layer and produces the *material gain*, $g(N)$, it is clear that the mode does not experience the full material gain since only a fraction of the modal power is in the gain region.

From modal analysis it can be shown that to a very good approximation, [8],

$$g_{\mathrm{mod}al}(N) = \Gamma \cdot g(N) - (1-\Gamma)\left|\alpha_{fc}\right| \qquad (2.23)$$

Hence, the modal gain is less then the material gain not only since $\Gamma < 1$ but also due to free carrier absorption (α_{fc}) in the cladding layers. Typically, (α_{fc}) is quite small compared to $g(N)$ and so may be omitted in the first approximation.

The details of confinement factor calculation will not be discussed in this thesis. However, very importantly, it is noted that Γ has different values for TE and TM polarisation. In a bulk material active layer the material gain, $g(N)$, is almost the same for TE and TM polarisation, but the modal gain $(g_{\mathrm{mod}al})$ is different due to the difference in values for Γ_e and Γ_h. Therefore, the modal gain for TE polarisation is written as:

$$g_e(N) = \Gamma_e \cdot g(N) \qquad (2.24)$$

and for TM polarisation, modal gain is:

$$g_h(N) = \Gamma_h \cdot g(N) \qquad (2.25)$$

2.7 Summary

In this chapter, we have covered the background knowledge of this project. In Sec.2.1, we have explained the interaction of light, in this section we have presented the light generated process in a simple two level energy level system and follow by a discussion of population inversion is in Sec.2.3. In Sec.2.4 we have introduced the crystalline semiconductor (as this project is working on semiconductor ee-LEDs), the band structure (where for the purpose of producing electroluminescence, direct band-gap semiconductor material is preferred), the *p*-*n* junction and the DH structure, which enabled effective carrier recombination process. We have also discussed the optical gain (g), which is also known as the material gain.

Furthermore, later this project will involve wave analysis at the boundary. Therefore it is essential for us to introduce the simple relevant electromagnetic (Maxwell's equation, wave equations), which is in Sec.2.5. In Sec.2.6 is the introduction of plane wave reflection and transmission. In this section, we have explained the definition of the polarisation for plane waves, followed by a brief introduction of Snell's law, the Fresnel's law and the Brewster angle. Then we begin to explain the definition of the polarisation in the slab dielectric waveguide, and the section finished with an introduction of the confinement factor, which has different values for TE and TM polarisation (Γ_e, Γ_h) and hence leads to a difference in modal gain for the two polarisations (g_e, g_h).

References 2

[1] J.M. Senior, '**Optical Fiber Communications Principles and Practice'**, Second Edition, Prentice Hall Europe, 1985, 1992

[2] S.O. Kasap, **'Optoelectronics and Photonics Principles and Practice'**, First Edition, Prentice Hall Europe, 2001

[3] G.P. Agrawal, '**Fiber-Optic Communication Systems**', Third Edition, John Wiley & Sons Inc, 2002

[4] E. Kapon, **'Semiconductor Lasers I Fundamentals'**, Elsevier Science & Technology, Jan 1999

[5] R. Syms, J. Cozens, **'Optical Guided Waves and Devices'**, Imperial College London, McGraw-Hill Companies, September, 1992

[6] F.T. Ullaby, **'Electromagnetics for Engineer'**, International Edition, Pearson Education, c2005

[7] M.J. Adams, **'An Introduction to Optical Waveguides'**, Chichester: Wiley, 1981

[8] J. Wilson, **'Optoelectronics: An Introduction'**, Prentice Hall International Inc, 1983

Chapter 3:

Edge-Emitting Light Emitting Diodes (ee-LEDs) -- Stripe Perpendicular to the Front Facet

3.1 Introduction

The basic physics of optical absorption and emission in material media – in simple, two-level atomic systems and in crystalline semiconductors - was presented in Chapter-2. The use of $p-n$ junctions and the more sophisticated double-heterojunctions as the means of efficiently achieving current injected Population Inversion, and hence Optical Gain, were also presented in Chapter-2. The present Chapter-3 begins with an introduction to the multi-layer structures that are in practical use, Fig.3.1. Although various types of direct band-gap semiconductor materials are in use (depending on the optical wavelength of interest), to be specific, the Gallium Arsenide (GaAs) material system is referred to in this Chapter and assumed to be the material of interest throughout this thesis. The energy band-gap of GaAs is approximately $1.4eV$ and corresponds to an emission wavelength of $0.85\mu m$.

Referring to Fig.3.1, to begin with, there is the core layer, often referred to as the Active-layer, since that is where the inversion population is concentrated, the recombination and the optical emission occurs. This core layer is undoped-GaAs and is typically $0.2\mu m$ thick. The adjacent top and bottom (along $y-axis$) cladding layers are $P^{-}-doped$ and $n^{-}-doped$ GaAlAs and are each typically $1.0\mu m$ thick. The slightly larger band-gap of GaAlAs compared to GaAs provides the

injected carrier (electrons and holes) confinement in the active-layer. At the same time, the lower refractive index of the top and bottom cladding (GaAlAs) layers creates the 3-layer slab dielectric waveguide that efficiently confines the optical energy in the vertical ($y-axis$) direction while propagating along the longitudinal ($z-axis$) . These three layers can be considered to be the essential three layers of the double-heterostructure (DH) material needed for efficiently achieving optical gain. However, from the viewpoint of making practical electrical contacts and mechanical strength the heavily $n^{--}-doped$ bottom contact (substrate) layer – typically about $50\mu m$ thick – provides mechanical strength and allows the making of good ohmic metal contact. Similarly, the heavily $p^{++}-doped$ top contact layer which, however, typically needs to be very thin, $\sim 0.1\mu m$, to reduce current spreading, is sufficient to make the good ohmic metal contact at the top. The other advantage of this layer being very thin is that it reduces both electrical and thermal resistance and allows excellent heat conduction when the top-contact is also connected to the heat-sink. Note the very thin ($\sim 0.05\mu m$) insulating oxide layer that is deposited on the top $p^{++}-doped$ layer except for a window defining the narrow stripe width, w ($\sim 5-10\mu m$), and length, L ($\sim 300\mu m$). The metal is deposited on this top oxide layer so that there is a large area of metal ($1mm\times 1mm$, which is the typical size of the chip) that gives sufficient mechanical strength for wire bonds or a good heat-sink (when mounted $p-side$ down on to the heat sink fixture), while having a narrow current injection area (ohmic contact) defined by the stripe window in the oxide.

Although not fundamental to device operation, the narrow stripe width, w, the reduced current spreading, reduced electrical and thermal resistance and means of good heat conduction actually enable the realistic, robust and reliable operation of the present-day devices. The planar technology is very suitable for mass production and hence reduced costs.

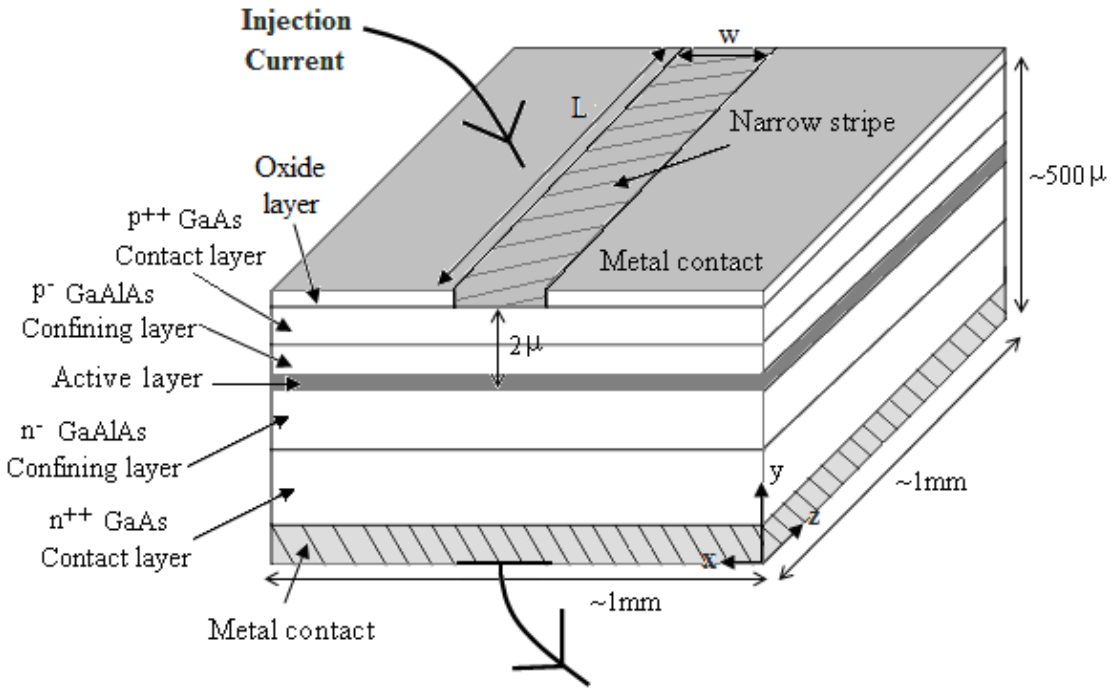

Figure 3.1 Schematic diagram of a DH structure LED device

It is most important to recognize that not only is there carrier confinement vertically (along $y-axis$) in the thin active layer because of the DH structure, the narrow stripe contact also provides carrier 'confinement' in the horizontal ($x-axis$) direction, even though current spreading and carrier diffusion lead to a somewhat wider carrier distribution in the active layer than the width of the stripe contact. (Note that the use of a thin $p^{++}-doped$ top contact layer reduces current spreading.) Because of these features even a small Injection Current ($\sim 50mA$) into the stripe contact produces a large Injection Current density leading to a large inversion population density and finally to a large optical gain in the small essential area of the active layer.

In this chapter, first we will introduce the use of Rate Equations in Sec.3.2; followed by the Rate Equation analysis of the simplest, stripe contact ee-LED. A computational model has been built to simulate the stripe contact light current characteristics; simulation results are showed in Sec.3.3.

3.2 Rate Equations

A description of the photon and inversion population densities in s-LEDs is presented in terms of what is referred to as the Rate Equation, [1]. The Rate Equations are essentially based on satisfying photon and carrier 'conservation' in the device and, as can be expected, it follows that the photon and carrier density distributions are interlinked (see below and Appendix-A). The empirical derivation of the Rate Equation is presented in some detail in Appendix-A. All the work presented in this thesis will be on Time Independent conditions hence only the time independent forms of the Rate Equation are used in this thesis. Solving the Rate Equation yield the required spatial variation of photons and the carriers for specified conditions, [2]. In this Chapter it is shown that convenient, simple yet quite satisfactory solutions to the Rate Equation can be obtained by starting with the assumption of a correspondingly constant carrier density. This procedure is used to obtain quite general expressions for the solutions to the Rate Equation that takes into consideration partial reflectivities and specified inputs at the two ends of a finite length of the optically active region, Fig.(3.2)

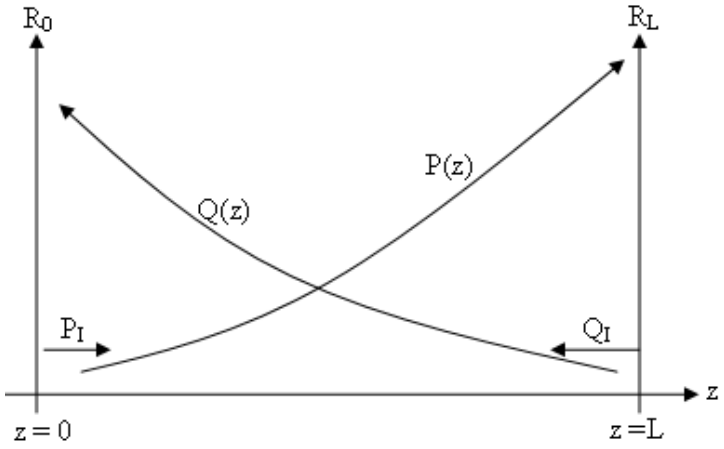

Figure 3.2 Schematic diagram of an optical cavity bound by parallel facets with reflectivity R_0 and R_L. *P(z), Q(z)* are the travelling direction of photon densities; P_I, Q_I are the external input sources.

$$\frac{dP(z)}{dz} = g(N)P(z) + \delta_f \frac{R_{sp}(N)}{v} \tag{3.1}$$

$$\frac{dQ(z)}{dz} = -g(N)Q(z) - \delta_r \frac{R_{sp}(N)}{v} \tag{3.2}$$

$$\frac{J_0}{qdv} = g(N)[P(z) + Q(z)] + \frac{R_{sp}(N)}{v} \tag{3.3}$$

$P(z)$ is the forward travelling photon density; $Q(z)$ is the reverse travelling photon density; $N(z)$ is the inversion population density; $g(N)$ is the material gain in units of length^{-1} and v is the velocity of photons in the medium; $R_{sp}(N)$ is the Spontaneous Recombination rate and δ_f, δ_r represent the fractions of spontaneous emission in the forward and reverse directions respectively.

In semiconductors, which is the media of interest in this project, Fig.3.1, it is most common to consider bi-molecular recombination so that

$$R_{sp}(N) = B_r(N + N_d)N \tag{3.4}$$

where N_d is the doping density in the semiconductor and B_r is the spontaneous recombination coefficient, [1]. The two extreme cases for Eq.(3.4) are

if $N << N_d$, then,

$$R_{sp}(N) \approx (B_r N_d)N = \frac{N}{\tau_{sp}} \tag{3.4a}$$

where $\tau_{sp} = 1/(B_r N_d)$, is referred to as the spontaneous lifetime;

if $N >> N_d$, then,

$$R_{sp}(N) \approx B_r N^2 \tag{3.4b}$$

In this thesis the fraction of spontaneous emission into the forward and reverse travelling photons, δ_f, δ_r, will be assumed to be constant (independent of z).

3.2.1 Use of The $N = \bar{N}$ Approximation

Although the Eq.(3.1)-(3.3) look simple, in general they actually represent a non-linear system (P, Q and N are interdependent), and even numerical solutions for the set of equations are not easy to obtain. But, although slightly approximate, a very much easier computation procedure is obtained by noting that if N is assumed constant, $N = \bar{N}$, then $g(N) = g(\bar{N}) = \bar{g}$, $R_{sp}(N) = R_{sp}(\bar{N}) = \bar{R}_{sp}$ are also constants. So, the formal solutions to Eq.(3.1), (3.2) are straightforward, Appendix-B-1, which give the formal expressions for $P(z;\bar{N})$ and $Q(z;\bar{N})$. Then using an integral of Eq.(3.3) over the finite length, $0 < z < L$, of the medium it is possible to obtain an analytic expression with $\bar{N}$ as the only parameter which is conveniently solved numerically, Appendix-B-1. It needs to be said that the $\bar{N}$ that is obtained from this computation is not the spatial average of the correct $N(z)$ over the length, L, of the optically active region, but a weighted-average which yields the most accurate values for the photon density distributions that can be obtained using a constant N. The flow chart for iteratively determining how this particular $\bar{N}$ is obtained is shown in Fig.3.3 in the following section.

3.2.2 The Flow Chart for Iteratively Determining $\bar{N}$

Eq.(3.3) is solved by using a numerical iteration scheme in which the carrier density $\bar{N}$ is kept constant at each iteration. By applying this technique, it is possible to find an analytic solution to Eq.(3.1) and (3.2). The iteration procedure is terminated when the $\bar{N}$ value satisfies Eq.(3.3). The figure below is the flowchart diagram of the model and analysis details of the model are discussed in the following section.

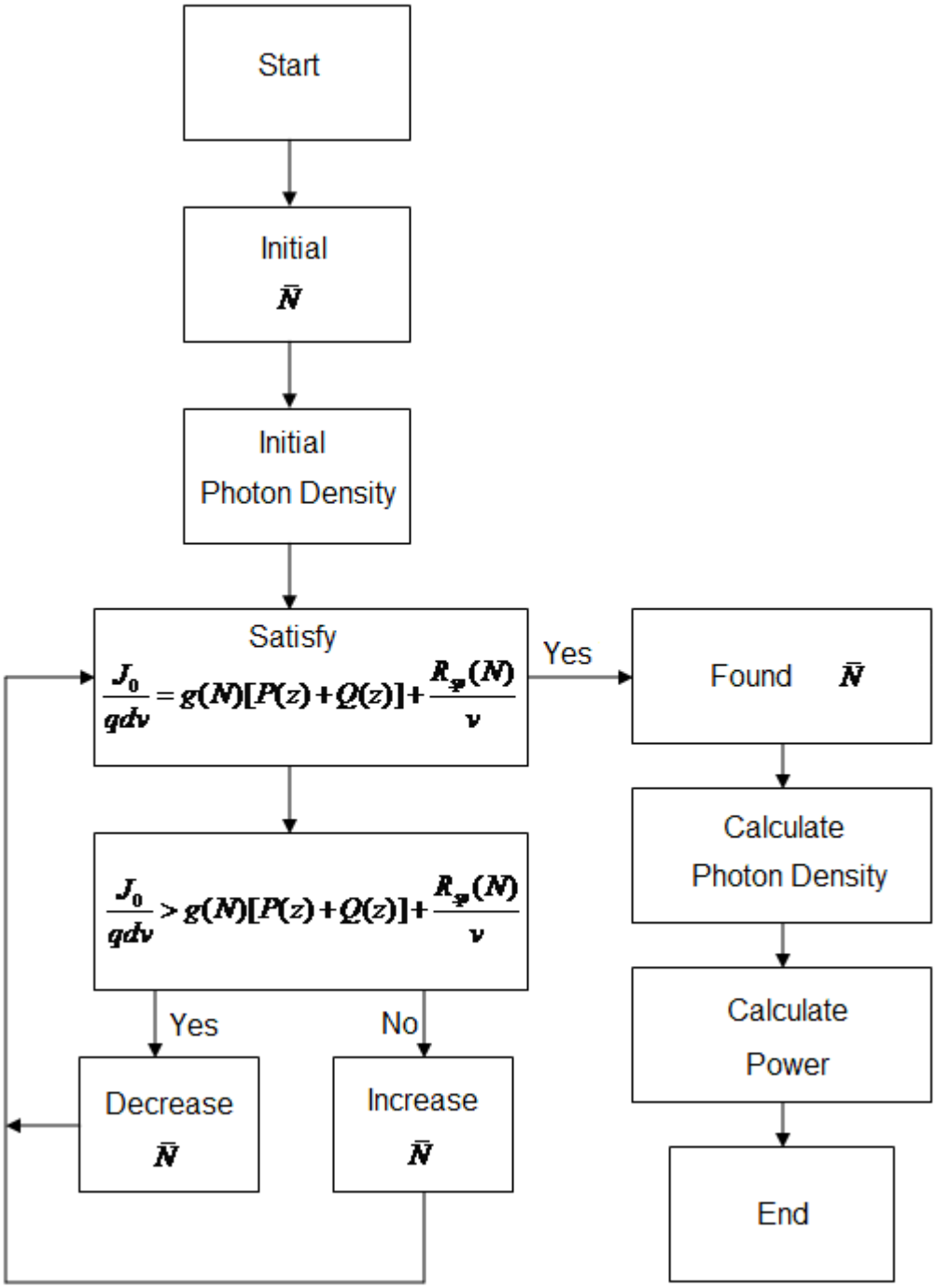

Figure 3.3 Flowchart diagram of the numerical iteration scheme for finding the weighted average carrier density value

3.2.3 Polarisation Decomposed Rate Equations

Since there is no significant wavelength dependency expected in the characteristics of the device that is studied in this project, the Rate Equation are not spectrally

decomposed. But the polarization of the optical waves play a crucial role in the operation of the device and so the Rate Equations are decomposed into the two orthogonal polarisations which are here loosely called TE (e) having field components, E_x, H_y and TM (h) having field components H_x, E_y, refer to Fig.2.13. Using the same photon and carrier 'conservation' requirements as applied in Appendix-A it follows that the polarization decomposed Rate Equation are

for TE polarized photons:

$$\frac{dP_e(z)}{dz} = \overline{g}_e(\overline{N})P_e(z) + \delta_f \frac{R_{sp}(\overline{N})}{v} \tag{3.5}$$

$$\frac{dQ_e(z)}{dz} = -\overline{g}_e(\overline{N})Q_e(z) + \delta_r \frac{R_{sp}(\overline{N})}{v} \tag{3.6}$$

for TM polarized photons:

$$\frac{dP_h(z)}{dz} = \overline{g}_h(\overline{N})P_h(z) + \delta_f \frac{R_{sp}(\overline{N})}{v} \tag{3.7}$$

$$\frac{dQ_h(z)}{dz} = -\overline{g}_h(\overline{N})Q_h(z) + \delta_r \frac{R_{sp}(\overline{N})}{v} \tag{3.8}$$

and for the carriers :

$$\frac{J}{qdv} = \overline{g}_e[P_e(\overline{N}) + Q_e(\overline{N})] + \overline{g}_h[P_h(\overline{N}) + Q_h(\overline{N})] + \frac{R_{sp}(\overline{N})}{v} \tag{3.9}$$

P_e, P_h represent the forward-travelling TE and TM polarized photon densities respectively and Q_e, Q_h represent the reverse travelling TE and TM polarized photons respectively; g_e, g_h are the optical gains for the TE and TM polarized photons; v is the velocity of light in the medium; δ_{fe}, δ_{fh} are the fractions of the total spontaneous emission in to the forward travelling TE and TM polarized photons respectively; similarly, δ_{re}, δ_{rh} for the reverse travelling photons. In this thesis it is assumed that $\delta_{fe} = \delta_{fh} = \frac{\delta_f}{2}$ and $\delta_{re} = \delta_{rh} = \frac{\delta_r}{2}$.

Note that the Eq.(3.4)-(3.8) are written in terms of constant $N = \bar{N}$ to enable a simple solution procedure (as discussed in the previous Section).

3.3 Stripe Contact ee-LED Model

The Rate Equations are used to estimate the photon density distributions in a stripe contact ee-LED. The active layer thickness, d, Fig.3.1, has already been specifically considered in obtaining the carrier Rate Equation Eq.(3.8). The other important parameter of the Rate Equation that is now specifically related to the ee-LED structure are the δ_f and δ_r. First of all, it is clear that $\delta_f = \delta_r = \delta$. From Appendix-A, $\delta_f = (\Delta\Omega)_f / 4\pi$, Eq.(A5); where

$$\Delta\Omega = \frac{dA}{R^2} \qquad (3.10)$$

Considering the fraction of spontaneous emission in the vertical angle, Fig.3.4

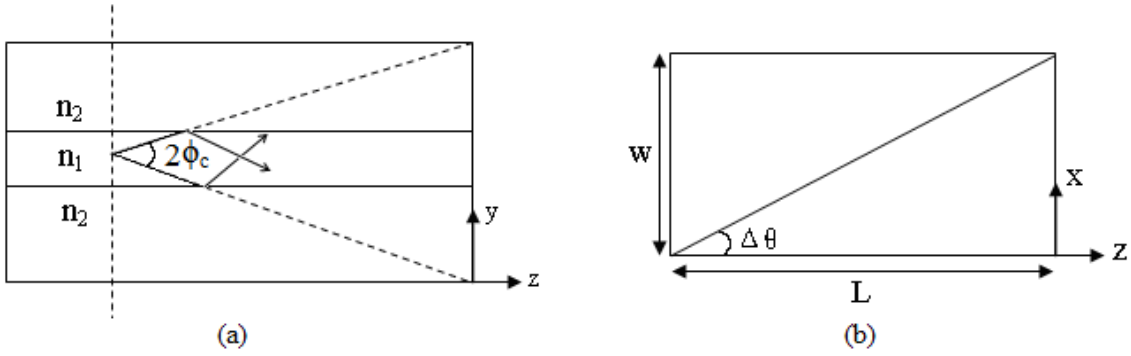

Figure 3.4 Fraction of spontaneous emission in the (a) vertical angle, (b) horizontal angle, where $2\phi_c$ is the critical angle of total internal reflection; $n_{1,2}$ are the refractive indices for different materials; Δθ is the horizontal angle; w, L are stripe width and length

Because of $dA = 2 \cdot R\Delta\theta \cdot R\Delta\phi_c$, hence Eq.(3.10) becomes,

$$\Delta\Omega = 2 \cdot \Delta\theta \cdot \Delta\phi_c \qquad (3.11)$$

$$\text{Where } \phi_c = \cos^{-1}\left(\frac{n_2}{n_1}\right) \qquad (3.12)$$

where $\Delta\theta$ is the horizontal angle and $\Delta\phi_c$ is the vertical angle, also it is the critical angle for total internal reflection, Fig.3.4, which can be calculated from Snell's Law.

Therefore, by submitting Eq.(3.12) into Eq.(3.11) and then submitted Eq.(3.11) into Eq.(A.5), the fraction of spontaneous emission becomes:

$$\delta = \frac{\cos^{-1}(n_2 / n_1) \times \Delta\theta}{2\pi} \qquad (3.13)$$

A basic structure of the LED device has been discussed earlier in this chapter. A typical top view of the ee-LED device is illustrated in Fig.3.5. In a bulk semiconductor material the spontaneous emission is uniformly distributed not only in spatial direction but also in the direction of polarisation. The material gain is not polarisation-selective and hence the generated amplification of spontaneous emission is equally distributed in the TE and TM polarizations. As defined in Chapter-2, Sec.2.6, with the electric field components perpendicular to the plane of incident (E_x, H_y) is the transverse electric (TE) polarisation and with the electric field components parallel to the plane of incident (H_x, E_y) is the transverse magnetic (TM) polarisation.

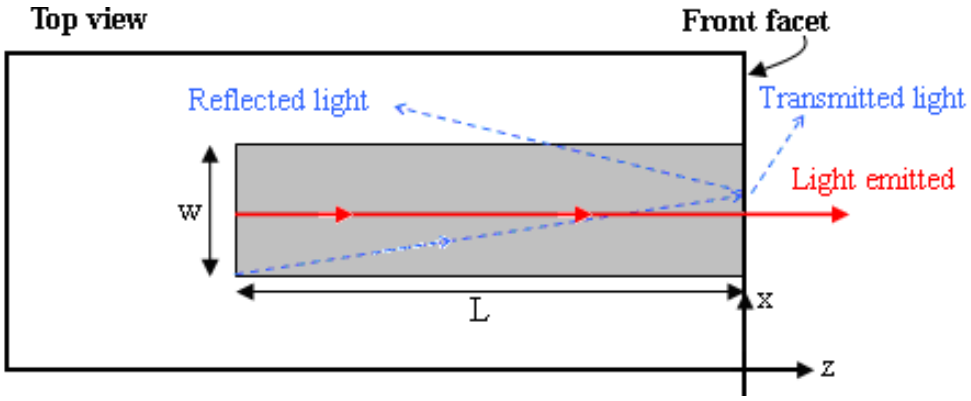

Figure 3.5 Top view of the stripe contact LED, where the dashed lines indicate rays we ignored in the approximate calculation

A computer model has been built to predict the light output characteristics from a single stripe contact ee-LED, where all light inside the stripe travel parallel to the stripe axis, and perpendicular to the front facet. In the following section, we will explain all the assumptions that we used in our computer model.

3.3.1 Stripe Contact Model Assumptions

In the analysis of a single stripe Rays and Rate Equation, we have assumed all rays travelling within the stripe are parallel to the stripe axis and perpendicular to the front facet. The reflectivity at $z = 0$ is almost equal to zero ($R_0 \approx 0$) for LED, so we use $R_0 = 0$, and R_L can be various from 0 to small amount. The carrier density we used in this model is the iterative numerical evaluation of the weighted average constant carrier density $\overline{N}$. The horizontal angle of the fraction of spontaneous emission is assumed to be $\Delta\theta = \frac{w}{L}$, as we used a simple trigonometric expression $\tan(\Delta\theta) = \frac{w}{L}$ to calculate the horizontal angle and because of rays travel parallel with in the stripe, so $\Delta\theta$ is very small, hence $\tan(\Delta\theta) \approx \Delta\theta$. Also because of when the stripe has gain, the photon from the rear of the stripe has the most effective impact to the output power, as from Rate Equation, $P_0 \simeq e^{\overline{g}L}$ (detail of fraction of spontaneous emission can be referred to Appendix-A), the approximation of horizontal angle is good enough for the calculation. Current density throughout the rectangular stripe contact region has been assumed to be constant and to remain constant throughout the different layers of the DH structure material.

3.3.2 Stripe Contact Model Simulation Results

By solving the photon density equations, the photon density can be derived at each point of the stripe, based on the stripe length and facet reflectivity. A number of tests have been simulated to study the L-I characteristics of the stripe contact ee-LED and the Degree of Polarisation (DOP, which will be explained below) to determine the effect of external input sources, facet reflectivity, and also the best stripe length (with respect to the Injection Current) to use in order to optimise a polarisation-selective output. The schematic diagram below explains the notation used in the following tests.

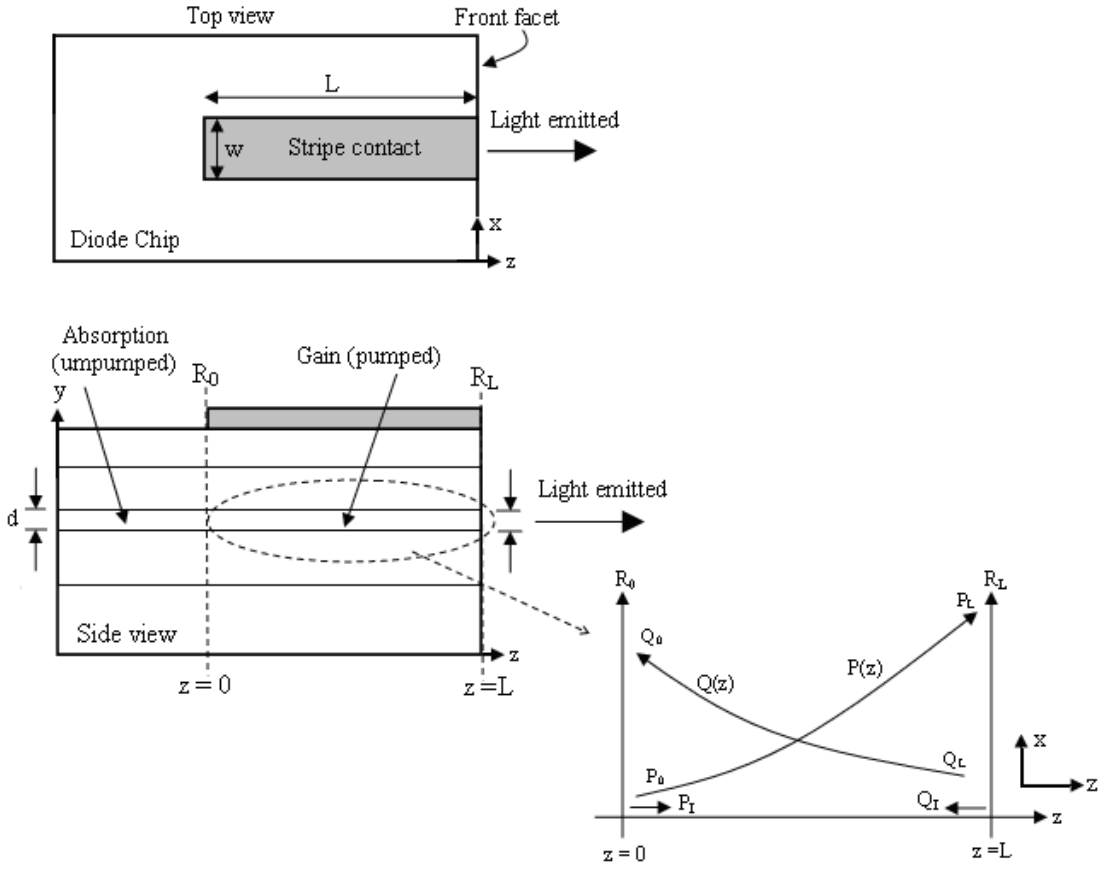

Figure 3.6 Schematic diagram of a stripe contact ee-LED from top view, side view and an enlarged top view picture of the photon density analysis schematic diagram for the single stripe contact, showing the notations used in this section

While the model was being built, it was been checked systematically, to make sure the model was built correctly and working properly. The first test is to compare the simulation and hand calculation result for the carrier density (N) before lasing without any external input signals (P_I, Q_I), to see if they matching. Secondly to test the P_I, Q_I effect by setting the fraction of spontaneous emission to be zero $\delta_f = 0$, an external input signal $P_I = 2 \times 10^{13} cm^{-3}$, the photon density at $z = L$ (P_L) will depend on P_I. There is also a need to test the output result to see if the TE and TM photon densities are correct. The difference between P_{Le} and P_{Lh} is mainly caused by the difference of the confinement factor for TE and TM (Γ_e, Γ_h). Therefore, the output

$\frac{P_{Le}}{P_{Lh}}$ ratio should be very close to $\frac{\Gamma_e}{\Gamma_h}$ ratio, because of $\frac{P_{Le}}{P_{Lh}} = e^{(\Gamma_e - \Gamma_h)\bar{g}L}$. So in the conditions of low gain and short device, these two ratios are comparable, and the compared result shows they are only 17% differences in ratio (1.16 for the ratio of output and 1.14 for the ratio of confinement factor).

Table.3.1 shows the parameters used in this stripe contact ee-LED model simulation.

Parameters	**Values**	**Parameters**	**Values**
Speed of light	$c = 3\times10^{10}\, cm/s$	Electron charge	$q = 1.602\times10-19 coul$
Refractive index in GaAs	$n_1 = 3.6$	Refractive index in AlGaAs	$n_2 = 3.36$
Wavelength	$\lambda = 850\times10^{-7}\, cm$	Planck's constant	$h = 6.626\times10^{-34}\, J/s$
Material gain coefficient	$A_0 = 1.5\times10^{-16}\, cm^2$	Transparency carrier density	$N_{tr} = 1.55\times10^{18}\, cm^{-3}$
Doping carrier density	$N_d = 1.7\times10^{17}\, cm^{-3}$	Bimolecular recombination constant	$B_r = 1\times10^{-10}\, cm^3/s$
Confinement factor TE	$\Gamma_e = 0.64$	Confinement factor TM	$\Gamma_h = 0.56$
Reflectivity at $z = 0$	$R_0 = 0$	Reflectivity at $z = L$	R_L various 0~0.3
External input (forward)	P_I various (see test condition)	External input (reverse)	Q_I various (see test condition)
Depth	$d = 0.15\mu m$	Width	$w = 10\mu m$
Length	L various (see test condition)		

Table 3.1 Parameters applied in the single stripe model

- **Degree of Polarisation (DOP)**

Degree of polarisation (DOP) is the ratio of the intensity of the polarised portion of the beam to its total intensity, both taken at the same point [4].

$$DOP = \frac{T_e - T_h}{T_e + T_h} \tag{3.14}$$

where T_e is TE polarisation and T_h is TM polarisation.

- **Test 1-1 L-I curve with No Reflectivity (at both ends)**

The first test is to simulate the light-current (L-I) characteristics for a single stripe contact ee-LED with the same Injection Current and different stripe lengths. The power output we simulated in this test is at $z = L$, Fig.3.6.

Parameters used:

I (A)	L (μm)	w (μm)	d (μm)	P_I, Q_I	R_0, R_L
0~0.16	400~1200	10	0.15	0	0

Table 3.2 Device relevant parameters used in Test 1-1

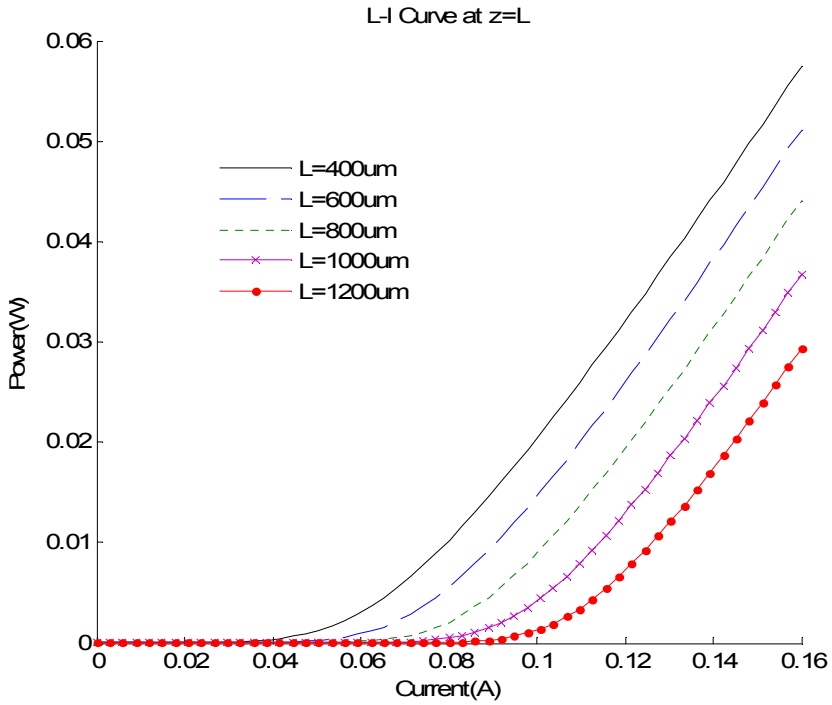

Figure 3.7 L-I curve of different stripe length and with the same current injection; where black line, *L=400μm*; blue dashed, *L=600μm*; green dotted, *L=800μm*; mauve crossed, *L=1000μm* and red circled, *L=1200μm*

Fig.3.7 shows that with the same Injection Current, I and the same stripe width, w; less power is being generated by using a longer length device; this is due to the stripe current density, J decreasing when the stripe length is increasing, as $J = \frac{I}{w \times L}$.

- **Test 1-2 L-I curve with Reflectivity (at one end)**

This test is to monitor the stripe L-I characteristic with the same Injection Current, and also with one-sided reflectivity. We used reflectivity at $R_L(z = L) = 0.3$, and $R_0(z = 0) = 0$. The other parameters are the same as we used in Test-1; the power output we simulated in this test is also at $z = L$, Fig.3.6.

Parameters used:

I (A)	L (μm)	w (μm)	d (μm)	P_I, Q_I	R_0, R_L
0~0.16	400~1200	10	0.15	0	$R_0 = 0, R_L = 0.3$

Table 3.3 Device relevant parameters used in Test 1-2

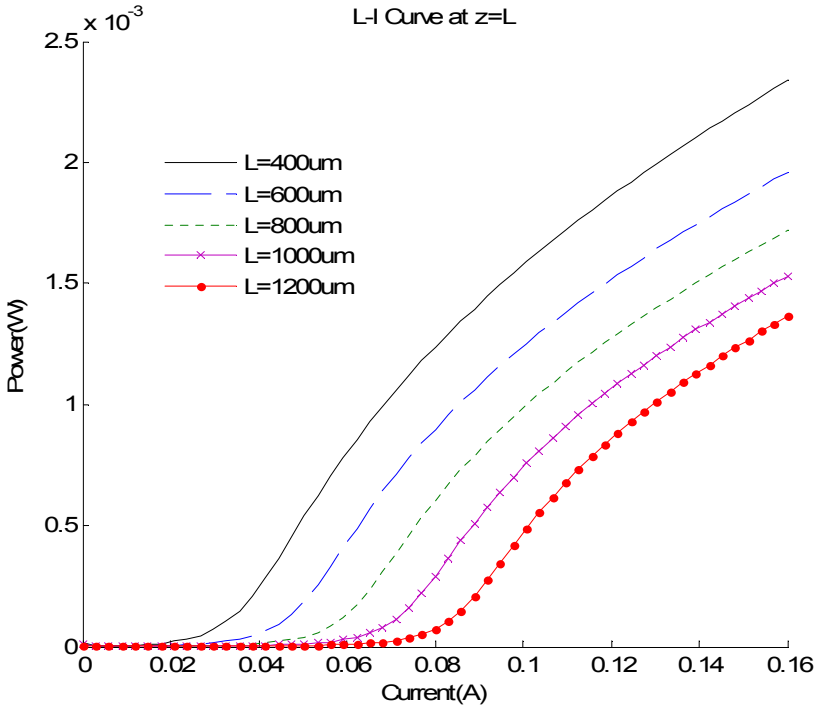

Figure 3.8 L-I curve for different stripe lengths at R_L=0.3; where black line, L=400μm; blue dashed, *L=600μm*; green dotted, *L=800μm*; mauve crossed, *L=1000μm* and red circled, *L=1200μm*

By comparing the results in Fig.3.7 and Fig.3.8, with $L = 400\mu m$ and $I = 0.06$; in Fig.3.8 ($R_L = 0.3$), the power output is ≈ 3.33 times less than the power output in Fig.3.7 ($R_L = 0$). This means with $R_L = 0.3$, Fig.3.8, $\approx 30\%$ of the generated light is being reflected and $\approx 70\%$ of the generated light is being transmitted out of the facet. As a result, Test.1 and Test.2 proved that the program is working reasonably with facet reflectivity.

- **Test 2 L-I curve Comparisons for Power Output at $z = 0$ and $z = L$**

The Rate Equation we used to calculate the forward and reverse photon density is symmetric (only the subscript notation is different). This test is designed to simulate and compare the power output at $z = 0$ and $z = L$, Fig.3.6, hence to prove the model is working reasonably well. The test is also extended to involve the external input source to the forward or reverse travelling photon (one-direction at a time), to give a firmer test result.

Parameters used:

I (A)	L (μm)	w (μm)	d (μm)
0~0.16	800	10	0.15

Table 3.4 Device relevant parameters used in Test 2

Test Conditions	Condition 1	Condition 2	Condition 3	Condition 4	Condition 5	Condition 6
R_L	0	0	0	0.3	0.3	0.3
$P_I(cm^{-3})$	0	1×10^{13}	0	0	1×10^{13}	0
$Q_I(cm^{-3})$	0	0	1×10^{13}	0	0	1×10^{13}

Table 3.5 Relevant parameters used in Test 2 for conditions 1to 6

Fig.3.9 is L-I curve at $z = L$, and Fig.3.10 is L-I curve at $z = 0$ for single stripe contact ee-LED.

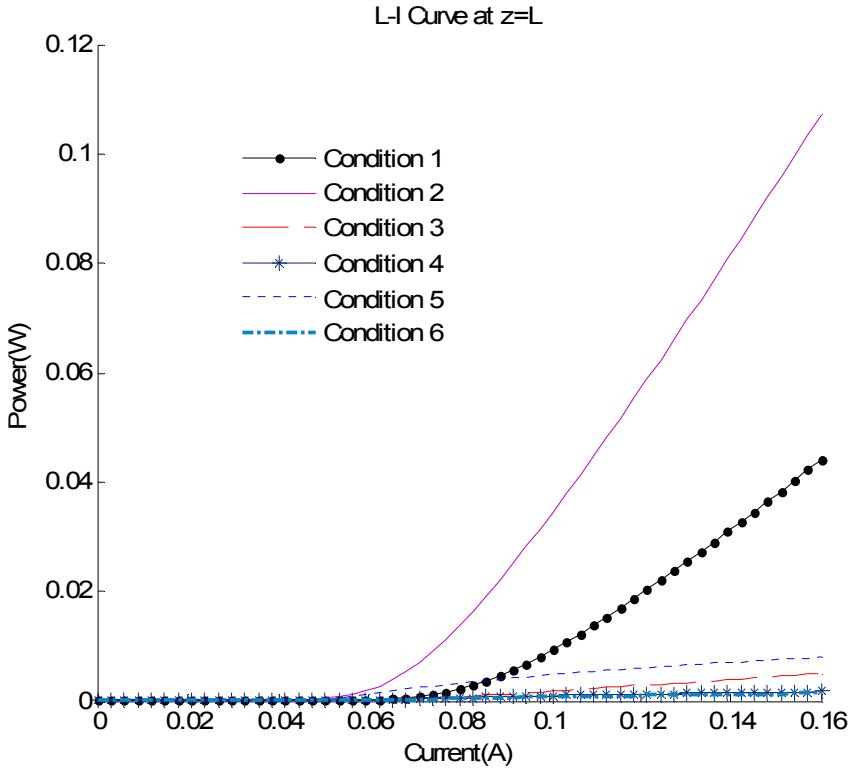

Figure 3.9 L-I curve at *z*=*L*, under the test conditions in Test 2; where black circled, condition 1; mauve line, condition 2; red dashed, condition 3; dark blue stared, condition 4; blue dotted, condition 5 and dotted dashed, condition 6

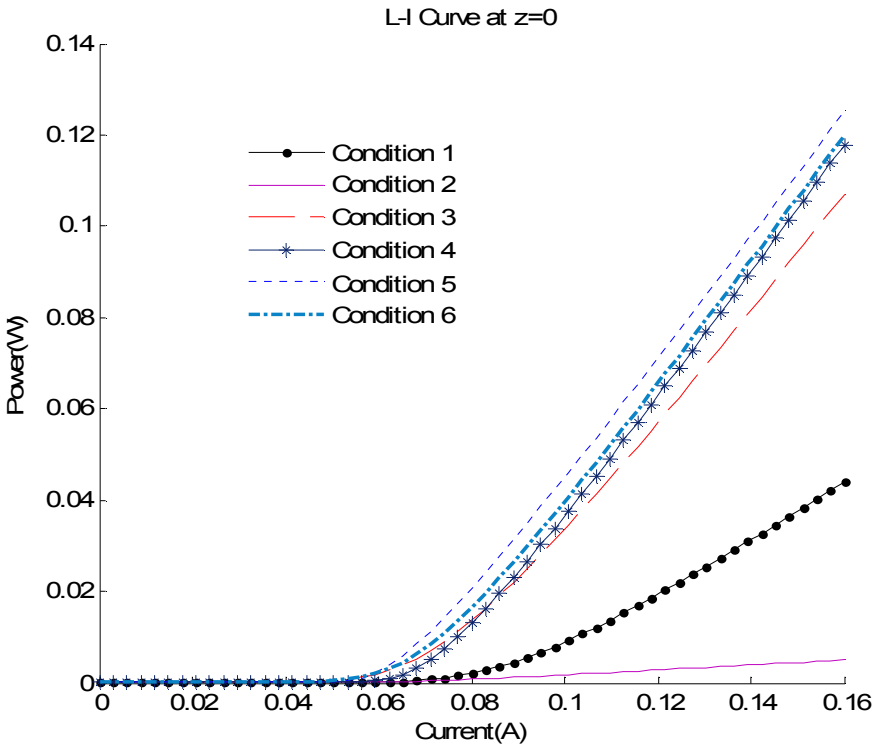

Figure 3.10 L-I curve at *z*=0, under the test conditions in Test 2; the line indications are the same as in Fig.3.9

Comparing the two figures above, under condition 1 (no external input and no facet reflectivity), the output powers are the same at $z = 0$ and $z = L$. Under the condition 2 ($P_I = 1 \times 10^{13} cm^{-3}$), the power at $z = L$ is higher than the power at $z = 0$, this is due to the external input source to the forward travelling photon, and vice versa for the condition 3. From the simulation result, it has proved that the forward and reverse Photon Rate Equations we used in the model are symmetric. For the condition 4 ($R_L = 0.3$), the power at $z = 0$ is ≈ 30 times higher than the power at $z = L$. This is due to, at $z = L$, $\approx 30\%$ of the forward travelling signal has been reflected and acts as an internal input source to the reverse travelling signal, which gets amplified as it travels along the stripe. For the conditions 5 and 6, the results are symmetric at $z = 0$ and $z = L$, due to P_I (condition 5) and Q_I (condition 6) being the same. In Fig.3.10 the result for condition 4 and 6 are almost equal, because of Q_I does not affect the result at $z = L$ significantly.

- **Test 3 The L-I curve With Polarisations**

Fig.3.11 is a typical L-I curve with TE and TM polarisation. The difference between these two polarisations purely depends on the confinement factor difference.

Parameters used:

I (A)	L (μm)	w (μm)	d (μm)	Γ_e	Γ_h
0~0.16	800	10	Γ_h	0.64	0.56

Table 3.6 Device relevant parameters used in Test 3

where Γ_e, Γ_h are the confinement factors for TE and TM polarisation; $P_I = Q_I = 0$ and $R_0 = R_L = 0$.

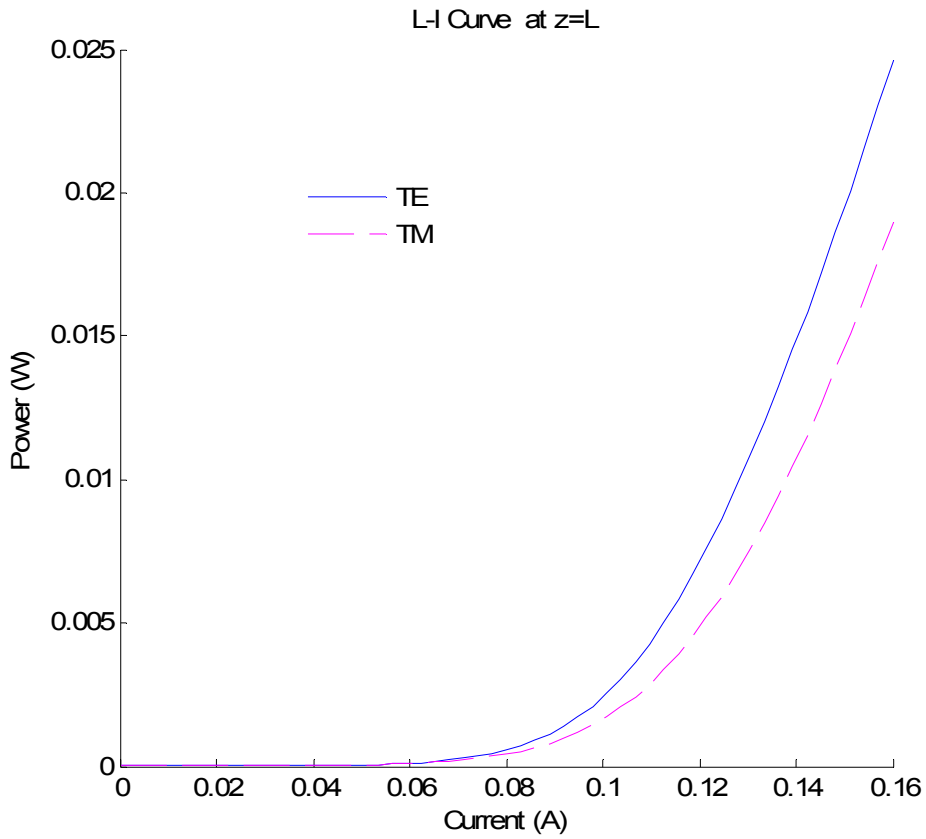

Figure 3.11 L-I curve with polarisation for single stripe; where blue line, TE polarisation and mauve dashed, TM polarisation.

This is the typical light-power output (L-I) curve for a superluminescent ee-LED device, where $\frac{P_{Le}}{P_{Lh}} \approx \frac{\Gamma_e}{\Gamma_h}$.

- **Test 4-1 DOP Vs Injection Current**

In order of predict the characteristics of the intensity of the radiation with TE and TM polarisation for the single stripe contact ee-LED, the aim of the test is to compare the DOP with different stripe lengths corresponding to the same range of current, and without any external input source.

Parameters used:

$I\,(A)$	L (μm)	w (μm)	d (μm)	Γ_e	Γ_h
0~0.16	400~1200	10	Γ_h	0.64	0.56

Table 3.7 Device relevant parameters used in Test 4-1

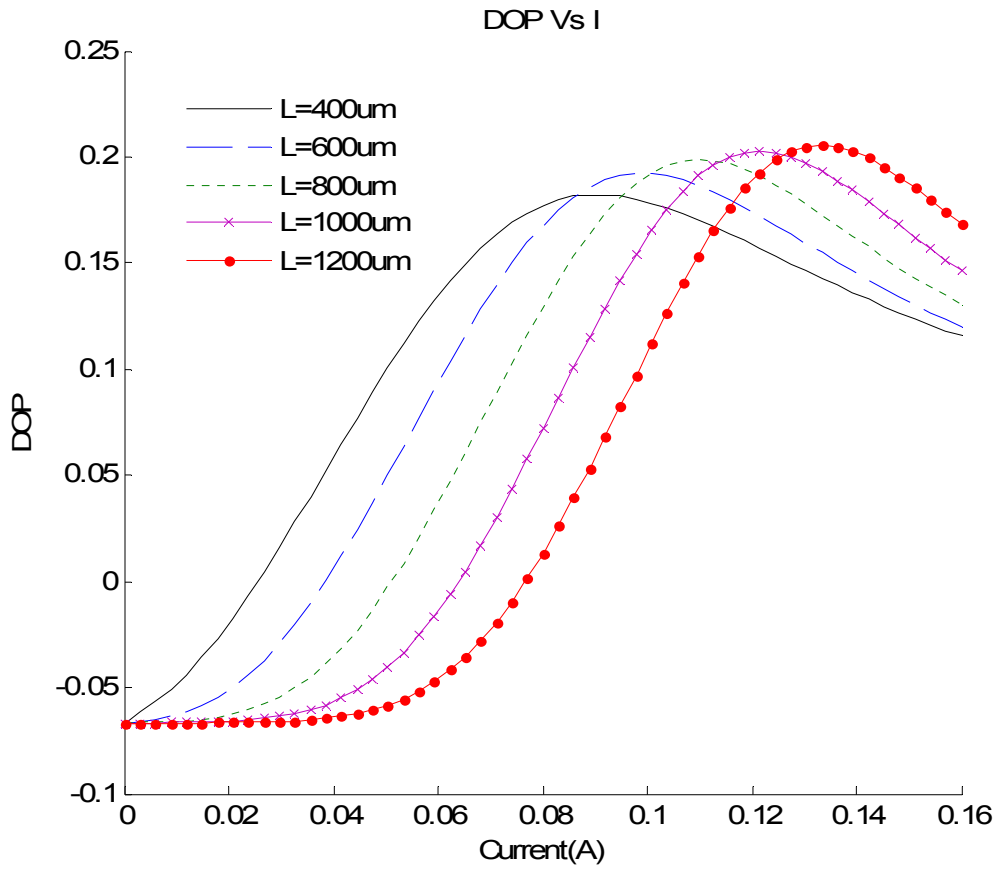

Figure 3.12 Degree of Polarisation against Injection Current with different stripe length; where black line, *L=400μm*; blue dashed, *L=600μm*; green dotted, *L=800μm*; mauve crossed, *L=1000μm* and red circled, *L=1200μm*

The result in Fig.3.12 shows that with the same Injection Current into different lengths of the stripe, the peak of the DOP curve shifts towards higher current injection and the shape of the curve remains the same. DOP increases slightly as stripe length increases, when $L = 400\mu m$, the corresponding $DOP_{peak} = 0.18$; and when $L = 1200\mu m$, the corresponding $DOP_{peak} = 0.20$. The change in peak of DOP is so small and can be ignored, which means the increase of stripe length does not have an impact on the peak value of DOP for a parallel stripe contact. Also note that the starting point of the curve gets lower as the stripe length is increasing, this is due to the low starting current lead to a small or even negative gain. For better comparison of the DOP for different stripe lengths, we used DOP against current density in the following test.

- **Test 4-2 DOP Vs Current Density**

This second test is to compare the DOP with different length of the stripe corresponding to the same range of current density, without any external input source.

Parameters used:

$J\ (A/cm^{-2})$	L (μm)	w (μm)	d (μm)	Γ_e	Γ_h
0~1700	400~1200	10	Γ_h	0.64	0.56

Table 3.8 Device relevant parameters used in Test 4-2

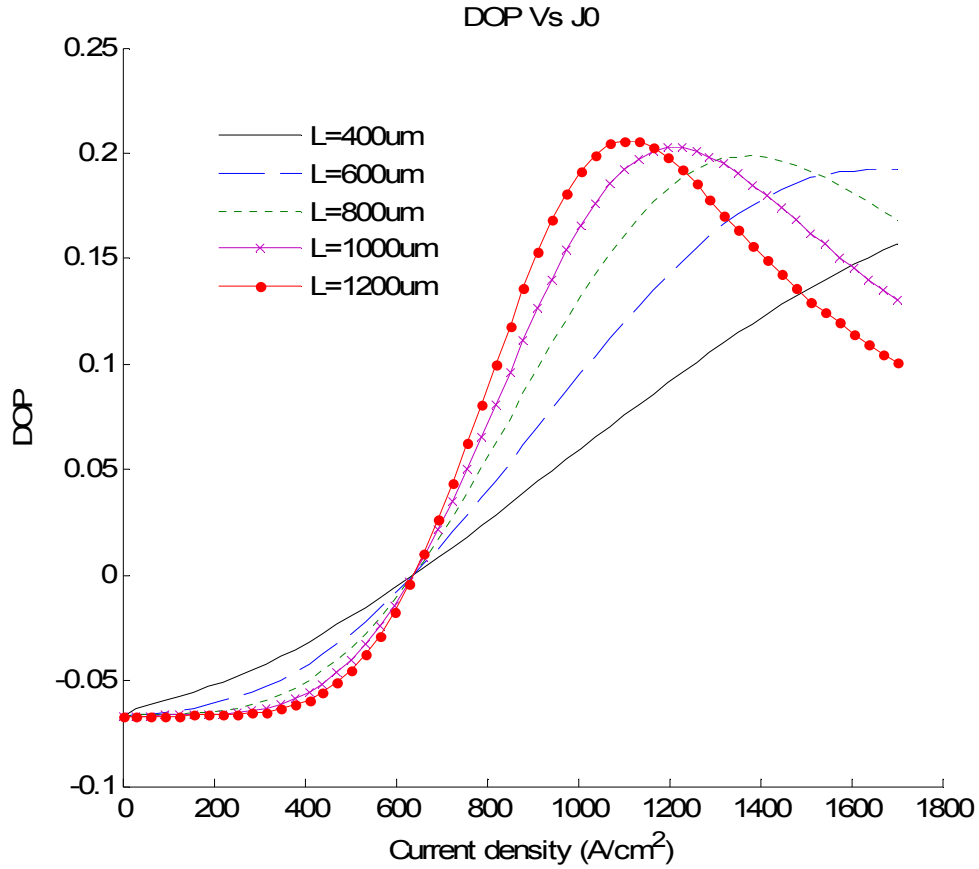

Figure 3.13 Degree of polarisation against current density with different stripe lengths; where black line, *L=400μm*; blue dashed, *L=600μm*; green dotted, *L=800μm*; mauve crossed, *L=1000μm* and red circled, *L=1200μm*

Fig.3.13 shows that when external input $P_I = Q_I = 0$ and reflectivity $R_0 = R_L = 0$. At current density $J = 700A/cm^{-2}$, optical gain, $g_e = 7.2cm^{-1}$ and $g_h = 6.3cm^{-1}$; at $J = 1700A/cm^{-2}$, $g_e = 92.7cm^{-1}$ and $g_h = 82.8cm^{-1}$. The value of DOP is zero, while $J = 650A/cm^2$, which means the optical gain is at zero. When current density

increases above $650A/cm^2$, the longer the stripe length, the sharper the DOP curve becomes. At stripe length $L=800\mu m$ the peak value of DOP is at current density $J=1400A/cm^2$, which means, at this point TE and TM polarisation have the largest difference.. For $L=1000\mu m$ the peak value of DOP is at $J=1200A/cm^2$ and for $L=1200\mu m$ the peak value of DOP is at $J=1100A/cm^2$, this curve is a lot sharper than $L=800\mu m$. However, it does not mean the required stripe length and the corresponding current density are promotional in order to achieve peak value of DOP. It is not, as our test result shows at $L=1000\mu m$ the corresponding current needed to get the peak value of DOP is $1200A/cm^2$, but if we want to reduce the current density to $1000A/cm^2$, the corresponding stripe length required is $1600\mu m$. From the test result, the best suitable stripe length for single stripe contact to reach the needed separation of the two polarisations is at $L=1000\mu m$.

3.4 Summary

This chapter began with a general introduction of DH structure material, followed by an explanation of the Photon Rate Equations in Sec.3.2, which is used in the formulation of the computer model for ee-LED. A mathematic simplification of $N(z)$, which is the approximation of weighted average constant $\overline{N}$ is introduced in Sec.3.2.1. By using the $N=\overline{N}$ approximation the equations are simplified very significantly and yield analytic expressions. Simulation results are presented in Sec.3.3, the computer model has predicted the L-I characteristic and DOP of a single stripe contact ee-LED, with TE and TM polarisations where the intensity difference between the two polarisations is due to the confinement factor.

References 3

[1] H. Kressel and J.K. Butler, **'Semiconductor lasers and heterojunction LEDs'**, Academic Press, 1997

[2] J. Wilson and J.F.B. Hawkes, **'Optoelectronics An Introduction'**, Second Edition, 1989

[3] T. Kambayashi and J. Sarma, **'Spontaneous Emission Noise Distribution from a Gain-Guide Multimode Waveguide'**, IEEE J. Quantum Electron. QE-19, 1084-1091, 1983

[4] A. Al-Qasismi, O. Korotkova, D. James, E. Wolf, **'Definition of the degree of polarisation of a light beam'**, Optics Letters, Vol. 32, No. 9, pp.1015-1016, 1st May 2007

Chapter 4:

V-Stripe Edge-Emitting Light Emitting Diodes (ee-LEDs) – Approximate Analysis

4.1 Introduction

The formulation and a model of ee-LEDs based on the approximation that accounts for those photons that travel only along (or within a very small angle to) the longitudinal axis of the device and which itself is perpendicular to the front facet, is presented in Chapter-3. Moving along a step, Chapter-4 is devoted to applying the same restricted paraxial formulation to first model stripe contact ee-LEDs with the stripe axis at an angle to the front facet, [1], [2], Fig.4.1(a); the study is next directed to model V-stripe devices with the apex of the "V" at the front facet, Fig. 4.1(b).

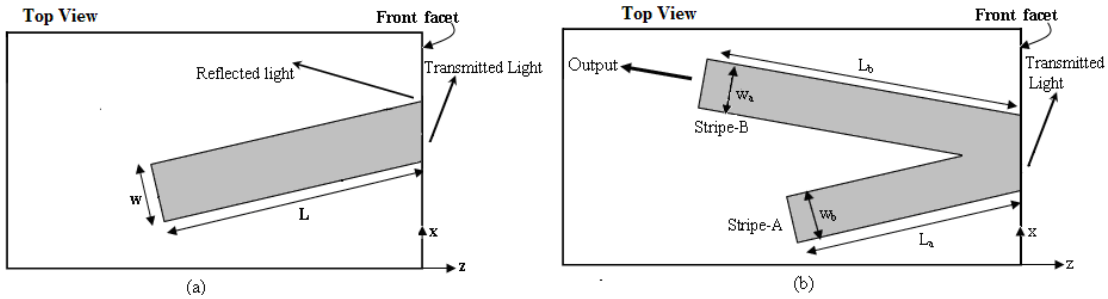

Figure 4.1 Top view of a stripe contact ee-LED; (a) angled stripe and (b) V-stripe; stripe width, w; stripe length, L; subscript a and b represent stripe-A and –B, respectively

As mentioned in Chapter-3, since these devices are assumed to have bulk material active layer the spontaneous emission can be considered to emit uniformly in all directions and polarisations. Hence, in the multilayer slab dielectric waveguide structure of the device the TE(e) and TM(h) polarised modes are excited equally. The optical gains of plane waves propagating in the bulk material – *Material gain* - for the different polarisations are also equal. However, as described in Chapter-2, here also

remember that in the multilayer structure of the device there is modal propagation and the (vertical, y-axis) confinement factors of the modes of the two, TE(e) and TM(h), polarisations are different which leads to different *Modal gains* (Chapter-2, Sec.2.6.5). Due to the different modal gains the two polarisations achieve different intensities further along the length of the device. However, the difference in confinement factors, and hence the difference in modal gains between the two polarisations is typically not large and so, as seen in Chapter-3, the difference between the 'output' intensities of the two polarisations is typically not large (unless a long stripe is used, which then requires lots of current) – that is, a large DOP is practically not able to be achieved by just utilising the differences in the TE/TM confinement factors (modal gains).

The details are presented later in this chapter but the objective is to obtain a LED source but with a much enhanced polarised light output by utilizing the well known properties of the reflection of electromagnetic (optical) plane waves from an abrupt interface between two homogenous dielectrics, refer to Fig.4.2. Fig.4.2 is the Brewster angle characteristic for a GaAs/air interface, where the refractive indices are, $GaAs = n_1 = 3.6$ and air $n_2 = 1$.

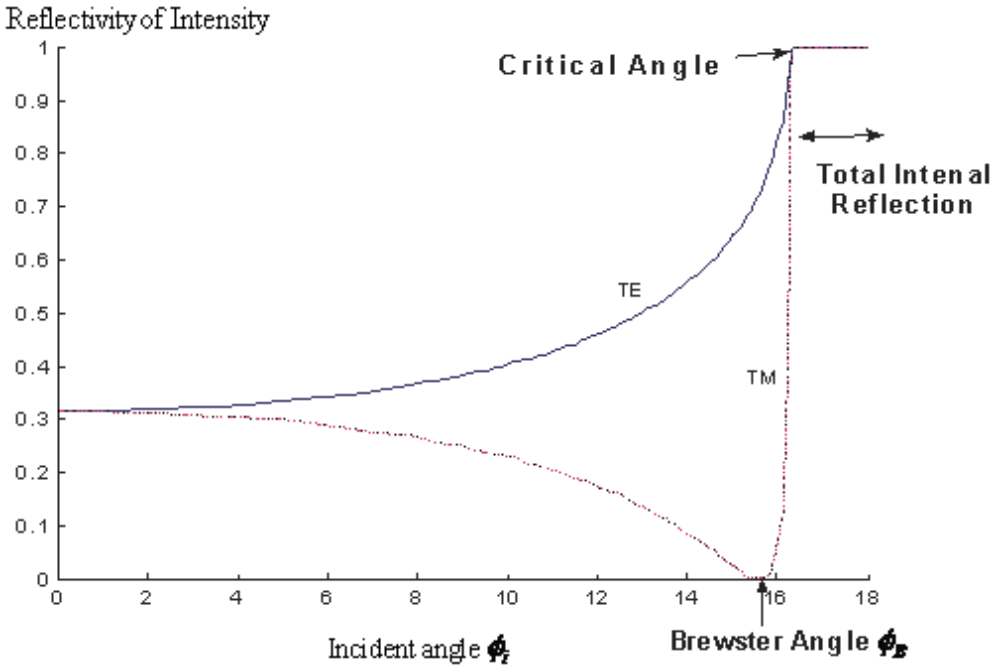

Figure 4.2 Reflectivity against incident angle Φ_i of a GaAs/air interface for two polarisations, where the Brewster angle occurs, [5]

Note that the facet of the LED chip is just such an abrupt interface between the semiconductor material and air. It has previously been discussed, Chapter-2, Sec.2.6.2, that the vertical ($y-axis$) multilayer structure and the corresponding modes can be treated as an optical plane wave but in a homogenous dielectric with an effective electrical permittivity (refractive index, n) so that the properties of optical plane wave reflections at an abrupt interface between two homogenous dielectrics can still be applied, Fig.2.11.

The striking feature to note about the optical reflectivities at an abrupt facet of plane waves is the dramatic difference between the two polarisations, Fig.4.2. For TE polarisation the reflectivity increases monotonically with the angle of incidence until the reflectivity becomes unity at the incidence angle corresponding to that of Total Internal Reflection as defined by Snell's Law. However, for TM polarisation, the behaviour is remarkably different – the reflectivity first decreases with angle of incidence until it becomes zero (unity transmission) at the Brewster angle, but then the reflectivity increases and becomes unity at the same angle of Total Internal Reflection as for the TE polarisation. *It is the phenomenon of Brewster angle that is proposed here to be utilised as the mechanism to design a bulk material LED with a highly enhanced polarised optical source.*

There is a number of assumptions we used in the approximation analysis, the most important assumptions are, the constant weighted average $\overline{N}_a$ and $\overline{N}_b$ for stripe-A and –B, respectively and all rays travelling inside the device are plane wave and parallel to the stripe axis ($x-axis$), full assumptions are detailed in Sec.4.4.1.

4.2 Angle Stripe ee-LED

It was decided to proceed with the analysis in stages so that the properties of each stage can be tested and 'understood' before analysing the complete V-shaped device. So, the single stripe at an angle to the facet, Fig.4.3, is considered first.

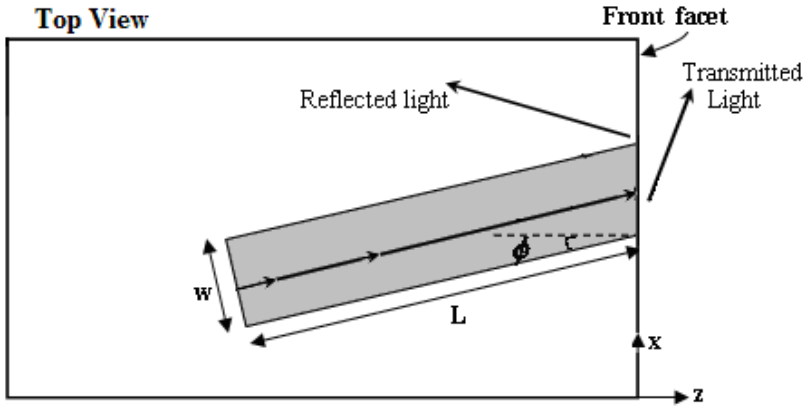

Figure 4.3 Top view of an angled stripe contact ee-LED, [3], [4]; stripe: width, w; length, L; facet plane, z = const

In this section it is discussed and shown that although this single angled stripe can provide some polarisation (selection) enhancement, it is not large and not convenient to use. From Chapter-3 it is understood that when there is optical gain then it is reasonable to consider only the light propagating parallel to and inside the region of the stripe for a preliminary, approximate description of operation. Both polarisations, (e) and (h), of light will be spontaneously emitted, and will propagate experiencing corresponding modal gains along the length of the stripe. This, in general, could generate some difference in the optical intensities of the two polarisations along the length, depending on the difference between the confinement factors of the two polarisations for that particular multi-layer structure; but that can typically be quite small and for the present we even assume that they are equal. However, at the facet the two polarisations can experience very different reflectivities particularly if the stripe is positioned close to or at an angle $\phi = \phi_B$, Brewster angle, Fig.4.3. For the typical (semiconductor) dielectric/air interface, for light of one polarisation the reflectivity of TE polarisation is ≈ 0.7 while for TM polarisation it is almost zero. So, in the air the TM polarised light will have a larger intensity compared to that TE

polarised by approximately a factor of $\frac{1.0}{0.3} \simeq 3.33$, which is significant but not very large. Further, since for this material ϕ_B is nearly equal to that of Total Internal Reflection, Fig.4.2, from Snell's Law the light rays in the air is at $74.17°$ to the $x-axis$ (if light inside the device travel at the Brewster Angle), which is almost parallel to the $x-axis$ Fig.4.3; from a practical viewpoint this is very inconvenient since it becomes difficult to collect the light at this extremely acute angle to the facet.

4.3 V-Stripe ee-LED Design – Approximate Analysis

In order to make a better polarisation-selective device, it is suggest using the reflected signal. This will require a second stripe contact，which has an Injection Current to generate it, to be at least transparent, then the stripe will be able to maintain the reflected signal. This is the design idea for the approximate analysis of the V-stripe device, which can be used as a polarisation-selective device, simply by placing the stripe at the Brewster angle, as shown geometrically in Fig.4.4.

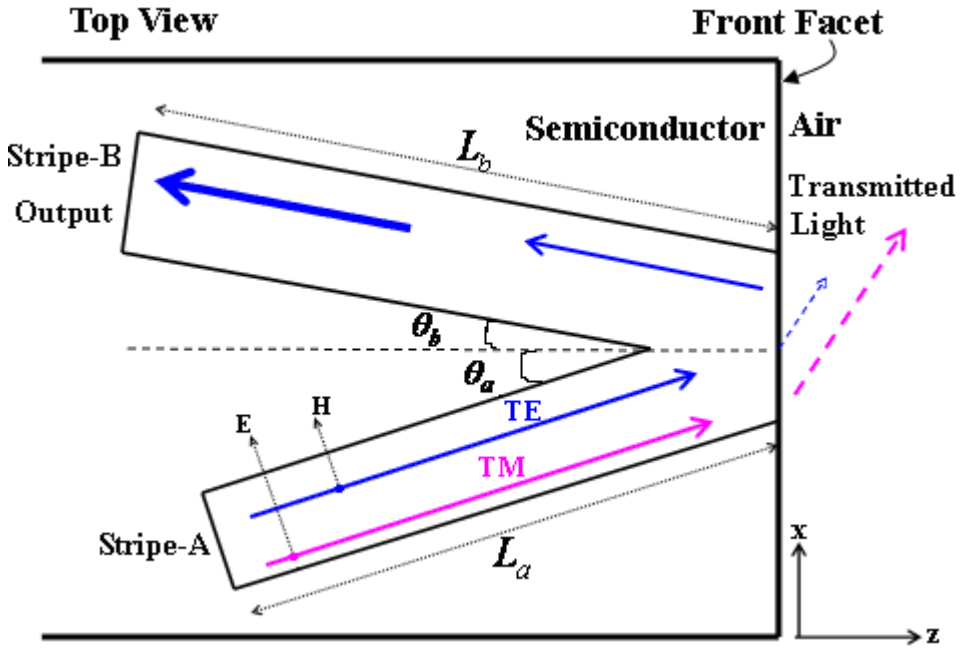

Figure 4.4 Top view of a V-stripe at Brewster angle; all TM polarisations transmitted out of facet. Blues indicate TE polarisation, magentas indicate TM polarisation

Fig.4.4 is the design geometry of a V-stripe, which takes advantage of using the Brewster angle to separate TE and TM polarisations. In the figure the blue arrow represents TE polarisation while the pink arrow represents TM polarisation.

As mentioned earlier in this section, TE and TM polarisation can be separated using only one angled stripe, but it is not effective. One problem is due to the transmitted signal, with a small proportion amount of TE polarised photons on account of the reflectivity index; also, there is another problem, which is the transmitted signal is not parallel to the interface, it has a very narrow angle to the $x-axis$. This causes a big problem when coupling the beam (light), and causes practical problems. Hence, by adding a second stripe to the original angled stripe, it can collect the reflected TE polarised signal very effectively, and as the original reflected TE polarised signal goes through the second stripe, the signal gets amplified. Although the second stripe itself will generate both TE and TM polarisation, because the external input signal is mainly TE, this will enhance the TE polarised photon in the output signal; because the external input signal is amplified as it travels through the second stripe (as can be seen in Fig.4.4, in the second stripe, there is a big TE polarisation arrow and a small TM polarisation arrow).

4.4 V-Stripe ee-LED Model – Approximate Analysis

The approximate analysis model of V-stripe ee-LED is based on the stripe contact model (explained in Chapter-3); by substituting the single stripe contact for a V-stripe, Fig.4.4. The reflected signal from stripe-A will act as an external input signal for stripe-B. Rate Equations for the V-stripe are derived in Appendix-C. A schematic analysis diagram is shown in Fig.4.5.

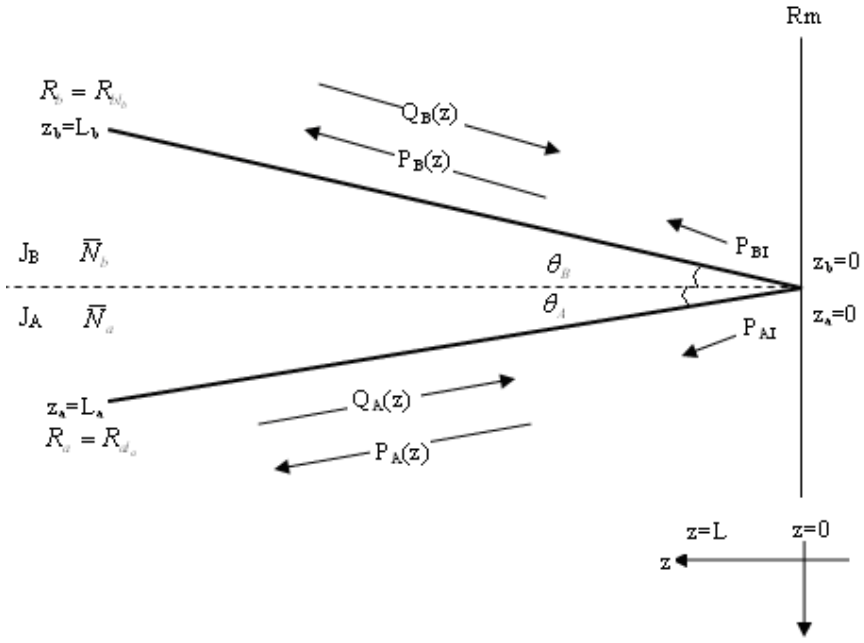

Figure 4.5 Schematic diagram of an optical cavity bound by facet reflectivities R_{aLa} and R_{bLb} for stripes-A and -B. $P_{A,B}(z)$ /$Q_{A,B}(z)$ indicated the photon density travelling direction; P_{AI}/P_{BI} are due to optical inputs at z=0

Using the same photon and carrier 'conservation' requirements as applied in Appendix-A, the polarization decomposed Rate Equations for stripe-A are,

for TE polarized photons:

$$\frac{dP_{Ae}(z_a)}{dz_a} = \overline{g}_{Ae}(\bar{N}_a)P_{Ae}(z_a) + \delta_{fa}\frac{R_{sp}(\bar{N}_a)}{v} \tag{4.1}$$

$$\frac{dQ_{Ae}(z_a)}{dz_a} = -\overline{g}_{Ae}(\bar{N}_a)Q_{Ae}(z_a) + \delta_{ra}\frac{R_{sp}(\bar{N}_a)}{v} \tag{4.2}$$

for TM polarized photons:

$$\frac{dP_{Ah}(z_a)}{dz_a} = \overline{g}_{Ah}(\bar{N}_a)P_{Ah}(z_a) + \delta_{fa}\frac{R_{sp}(\bar{N}_a)}{v} \tag{4.3}$$

$$\frac{dQ_{Ah}(z_a)}{dz_a} = -\overline{g}_{Ah}(\bar{N}_a)Q_{Ah}(z_a) + \delta_{ra}\frac{R_{sp}(\bar{N}_a)}{v} \tag{4.4}$$

and for the carriers:

$$\frac{J_A}{qd_A v} = \overline{g}_{Ae}[P_{Ae}(\bar{N}_a) + Q_{Ae}(\bar{N}_a)] + \overline{g}_{Ah}[P_{Ah}(\bar{N}_a) + Q_{Ah}(\bar{N}_a)] + \frac{B_r(\bar{N}_a + N_d)\bar{N}_a}{v} \tag{4.5}$$

P_{Ae}, P_{Ah} represent the forward-travelling TE and TM polarized photon densities respectively in stripe-A and Q_{Ae}, Q_{Ah} represent the reverse travelling TE and TM polarized photons respectively in stripe-A; g_{Ae}, g_{Ah} are the optical gains for the TE and TM polarized photons in stripe-A; B_r is the bi-molecular recombination; v is the velocity of light in the medium; δ_{fe}, δ_{fh} are the fractions of the total spontaneous emission into the forward travelling TE and TM polarized photons respectively; similarly, δ_{re}, δ_{rh} for the reverse travelling photons.

The polarization decomposed Rate Equations for stripe-B are in exactly the same format as stripe-A, only by substituting the subscript B for A.

4.4.1 The Approximated V-Stripe Model Assumptions

In the approximate analysis of the V-stripe ee-LED model, we have assumed all rays travelling inside the device are plane waves and parallel to the stripe axis. Therefore when the stripe angle is at the Brewster angle, all rays travel at the exact Brewster angle, which means all the TM polarised lights will be transmitted out of facet. Also we have used the weighted average carrier density $\overline{N}$ throughout the calculation, where the value of $\overline{N}_a$ and $\overline{N}_b$ (constant carrier density for stripe-A and –B, respectively) are dependent on the external input source. Namely, $\overline{N}_a$ depends on $\overline{N}_b$, and vice versa (the model will keep tracking the value for $\overline{N}_a$ and $\overline{N}_b$ to satisfy Eq.(4.5) and (4.6)). The fraction of spontaneous emission for the horizontal angle, $\Delta\theta = 0.1°$; the small $\Delta\theta$ allows accurate calculation. Also the current density throughout the rectangular stripe contact region has been assumed to be constant, and remains constant through different layers of the DH structure material.

4.4.2 The Approximated V-Stripe Model Flowchart

The flowchart of Fig.4.6 indicates the numerical procedure of the approximate analysis of the V-stripe model.

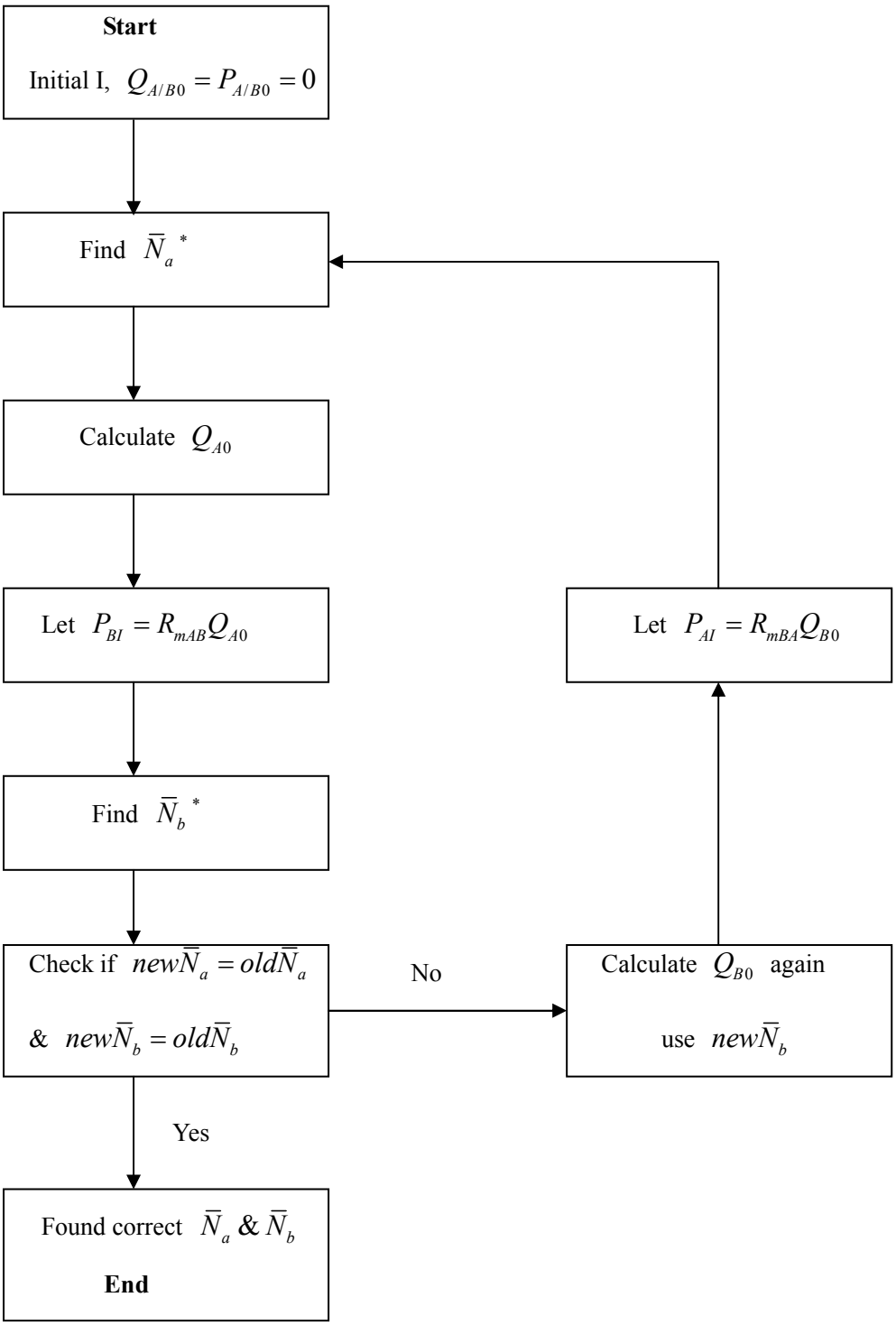

---------- * Variable comes from the Rate Equation calculation in Chapter 3, Sec.3.2.2.

Figure 4.6 Flowchart diagram shows the approximate analysis of the V- stripe, numerical procedure

The carrier density, $\overline{N}_a$ and $\overline{N}_b$ for stripe-A and –B are calculated from the single stripe (the $\overline{N}$ numerical iteration scheme is discussed in Chapter-3). Firstly, with the initial $Q_{A/B0} = P_{A/B0} = 0$, which means $P_{AI} = P_{BI} = 0$, the V-stripe acts as two separate angled stripe, we can calculate the initial value of $Q_{A/B0}, P_{A/B0}$ and P_{BI}, P_{AI}. Secondly, use Q_{A0} to calculate P_{BI}, and check if $new\overline{N}_b = initial\overline{N}_b$; if yes, the correct $\overline{N}_b$ is found; if not, use the $new\overline{N}_b$ (which is now become the $old\overline{N}_b$) to calculate P_{BI}, and obtain another $new\overline{N}_b$ until $new\overline{N}_b = old\overline{N}_b$. The same carrier density tracking procedure is applied in tracking $\overline{N}_a$. Remember in the V-stripe Rate Equation calculation $\overline{N}_b$ depends on P_{BI}, P_{BI} depends on Q_{A0} and Q_{A0} depends on $\overline{N}_a$, that means $\overline{N}_a$ and $\overline{N}_b$ are dependent on each other; by using this self-iterated $\overline{N}_a, \overline{N}_b$ tracking process, an accurate value of $\overline{N}_a, \overline{N}_b$ for the V-stripe can be found.

4.4.3 The Approximated V-Stripe Model Simulation Results

A number of tests have been simulated to study the L-I characteristics and the DOP of V-stripe ee-LED to determine the effect of external input sources to stripe-B (output power from stripe-A reflected into stripe-B) actually enhances the polarisation-selective output. The tests will contain different combinations of stripe parameters to determine the best optimised result. The schematic diagram below explains the notations used in the following tests.

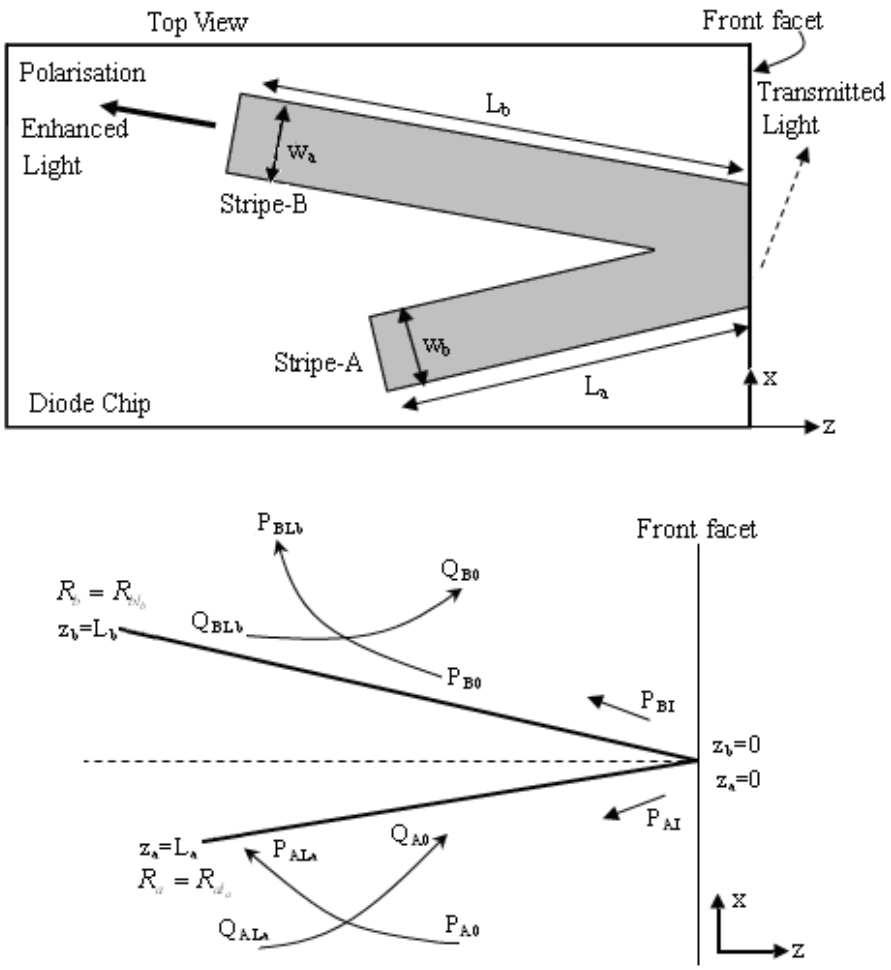

Figure 4.7 Schematic diagram of the V-stripe ee-LED from top view and a top view picture of the photon density analysis schematic diagram for the stripe contact, showing the notations used in this section

Table.4.1 has the parameters used in this approximate analysis of V-stripe ee-LED simulation.

Parameters	Values	Parameters	Values
Speed of light	$c = 3\times10^{10}\,cm/s$	Electron charge	$q = 1.602\times10-19coul$
Refractive index in GaAs	$n_1 = 3.6$	Refractive index in AlGaAs	$n_2 = 3.36$
Wavelength	$\lambda = 850\times10^{-7}\,cm$	Planck's constant	$h = 6.626\times10^{-34}\,J/s$
Material gain coefficient	$A_0 = 1.5\times10^{-16}\,cm^2$	Transparency carrier density	$N_{tr} = 1.55\times10^{18}\,cm^{-3}$

Doping carrier density	$N_d = 1.7\times10^{17} cm^{-3}$	Bimolecular recombination constant	$B_r = 1\times10^{-10} cm^3 / s$
Confinement factor TE	Γ_e various 0.64 Or 0.32	Confinement factor TM	Γ_h various 0.56 or 0.3
Reflectivity at $z = 0$	$R_0 = 0$	Reflectivity at $z = L_a; L_b$	R_{La}, R_{Lb} depends on stripe angle
External input for stripe-A	$P_{IA} = 0$	External input for stripe-B	P_{IB} depends on simulation result
Depth for stripe-A and -B	$d_a = d_b = 0.15\mu m$	Width for stripe-A and -B	$w_a = w_b = 10\mu m$
Length	L_a, L_b various (see test condition)		

Table 4.1 Parameters applied in the approximate V-stripe model

- **Test 1 L-I Characteristics Comparison for Two Segment Stripe and Single Stripe**

The design of the V-stripe ee-LED model has been described earlier in the chapter. In the first test, we will present the comparison with V-stripe and single stripe modelling results. The purpose for this test is to test the validity of the model and verify if the V-stripe model is working reasonably. In order to do so, at the first stage we have assumed both stripes in the V-stripe are parallel to the stripe axis (the V-stripe works as a long stripe contact), where the V-stripe becomes a two segment stripe contact to enable the comparison, as referred to in Fig.4.8. In this test we are using current density instead of current, to make sure both two segment stripe and single stripe have the same current density crossing the whole stripe.

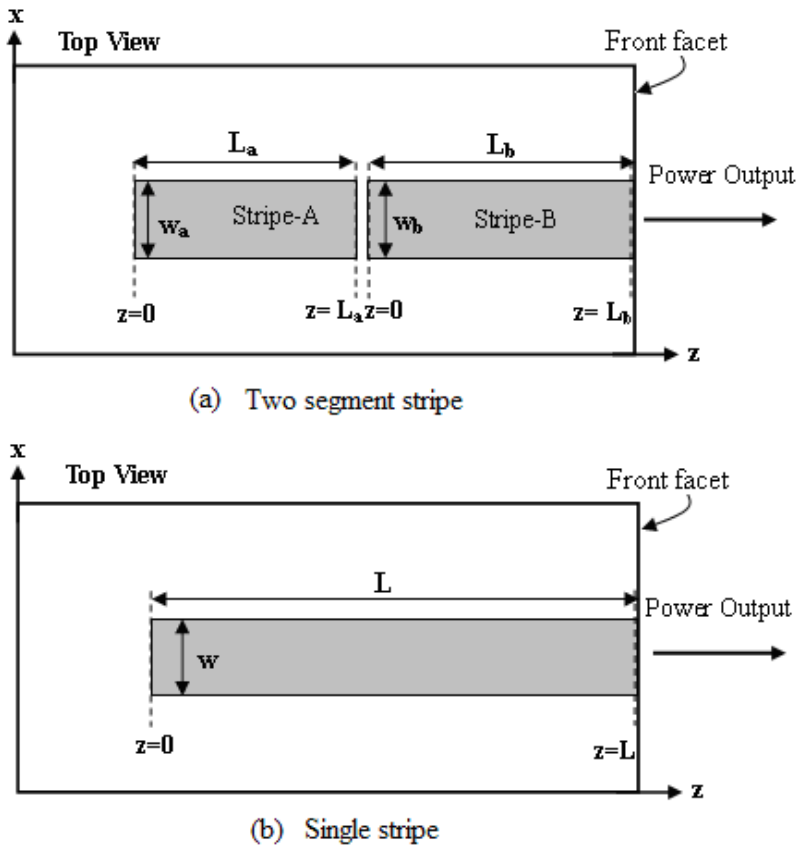

Figure 4.8 Schematic diagram of (a) two segment stripe and (b) single stripe

In this test, we have to use the same carrier density for single and two segment stripe, in order to enable the comparison, because the two segment stripe carrier density calculated by the V-stripe model is different for stripe-A and –B, this will affect the comparison result. Thus, we will use the carrier density from single stripe model in this test.

Parameters used for two segment stripe:

I (A)	$L_a = L_b\,(\mu m)$	$w_a = w_b\,(\mu m)$	$d_a = d_b\,(\mu m)$	Γ_e	Γ_h
0~0.16	400	10	0.15	0.64	0.56

Table 4.2 Device relevant parameters used in Test 1 for two segment stripe

Parameters used for single stripe:

I (A)	L (μm)	w (μm)	d (μm)	Γ_e	Γ_h
0~0.16	800	10	0.15	0.64	0.56

Table 4.3 Device relevant parameters used in Test 1 for single stripe

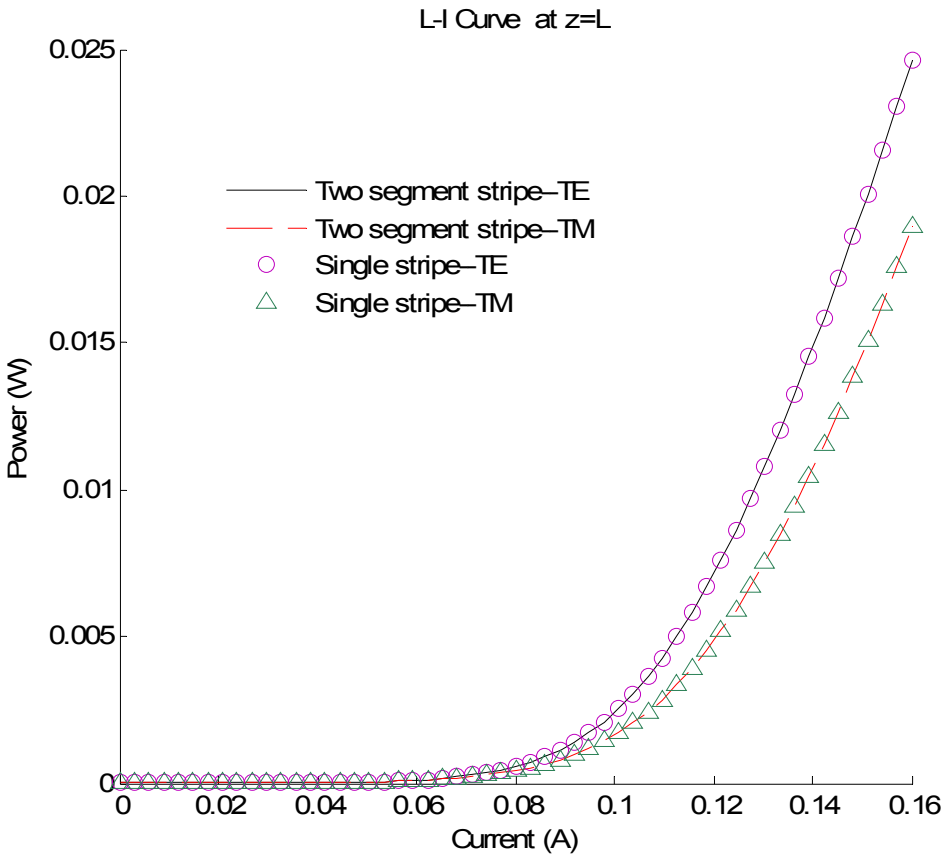

Figure 4.9 Comparison of L-I curve for two segment and single stripe; where black line and red dashed indicate TE and TM polarisation in the two segment stripe; mauve circled and green triangle represents TE and TM polarisation in the single segment stripe

This result illustrated in Fig.4.9 shows that the single segment and the two segment stripe produce the same power output under the same carrier density, with the value of $\bar{N}$ in the range of $0 \sim 2.56 \times 10^{18} cm^{-3}$.

- **Test 2 The L-I Curve**

This test is to simulate the typical L-I characteristic for the approximated V-stripe model, at $z = L_b$, Fig.4.7 (both stripes at the Brewster angle, $15.5°$). In the later tests, we will simulate the approximate analysis of the V-stripe model with different parameter combinations to enhance the polarisation-selective output.

Parameters used:

$I_a = I_b$ (A)	$w_a = w_b$ (μm)	$d_a = d_b$ (μm)	L_a (μm)	L_b (μm)	Γ_e	Γ_h
0~0.16	10	0.15	800	600	0.64	0.56

Table 4.4 Device relevant parameters used in Test 3

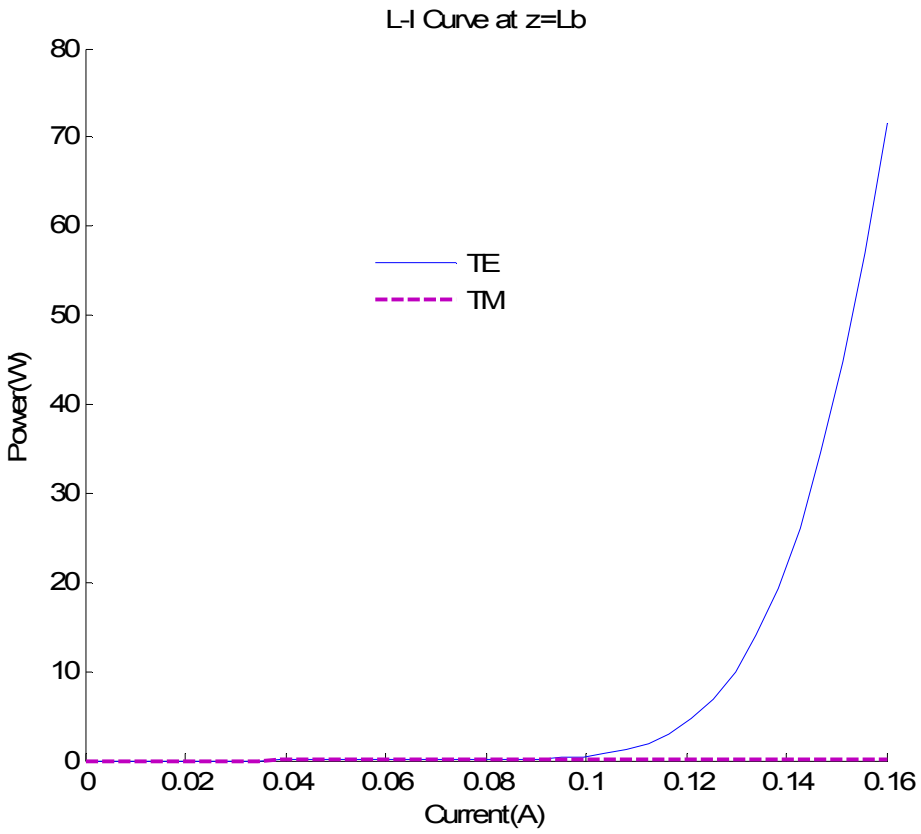

Figure 4.10 L-I curve for the approximate analysis of V-stripe; where blue line is TE polarisation and mauve dashed is TM polarisation

This result illustrated in Fig.4.10 shows that by placing both stripes at the Brewster angle (15.5°), the reflected signal from stripe-A into –B, which is purely TE polarised photons (under the approximate analysis condition), has made a dramatic enhancement to the polarisation-selective output from stripe-B. All TM polarised photons produced in the output are generated in stripe-B.

- **Test 3 DOP Comparison for Stripe-A and-B**

In this test we assume stripe-A and stripe-B are both at the exact Brewster angle, where $\phi_a = \phi_b = \phi_B$. By comparing the DOP with the same Injection Current at $z = L_a$ and $z = L_b$, the enhancement of polarisation-selective result from the V-stripe can be clearly seen. The schematic diagram of the stripe geometry and symbols for this test are shown in Fig.4.11 below;

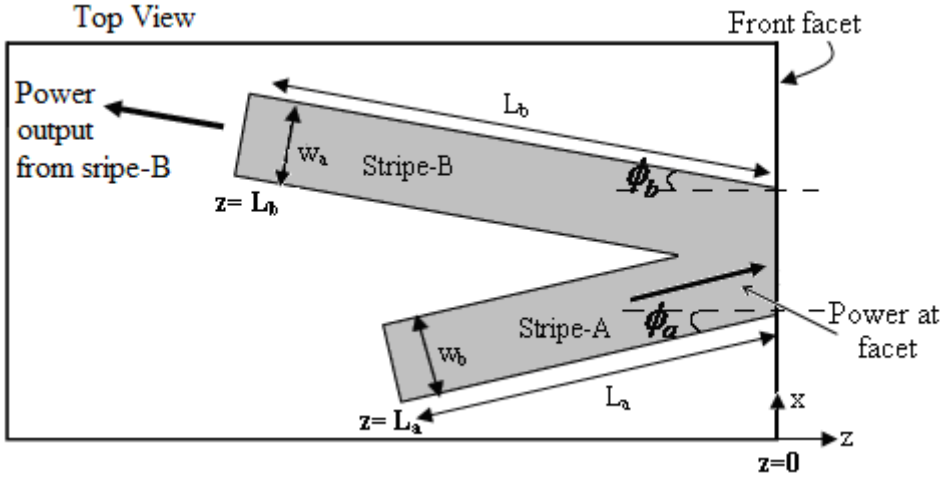

Figure 4.11 Schematic of the simulated point in Test 3 as referred to the "V"-geometric

Parameters used:

$I_a = I_b$ (A)	$w_a = w_b$ (μm)	$d_a = d_b$ (μm)	L_a (μm)	L_b (μm)	Γ_e	Γ_h
0.06~0.16	10	0.15	800	400	0.64	0.56

Table 4.5 Device relevant parameters used in Test 3

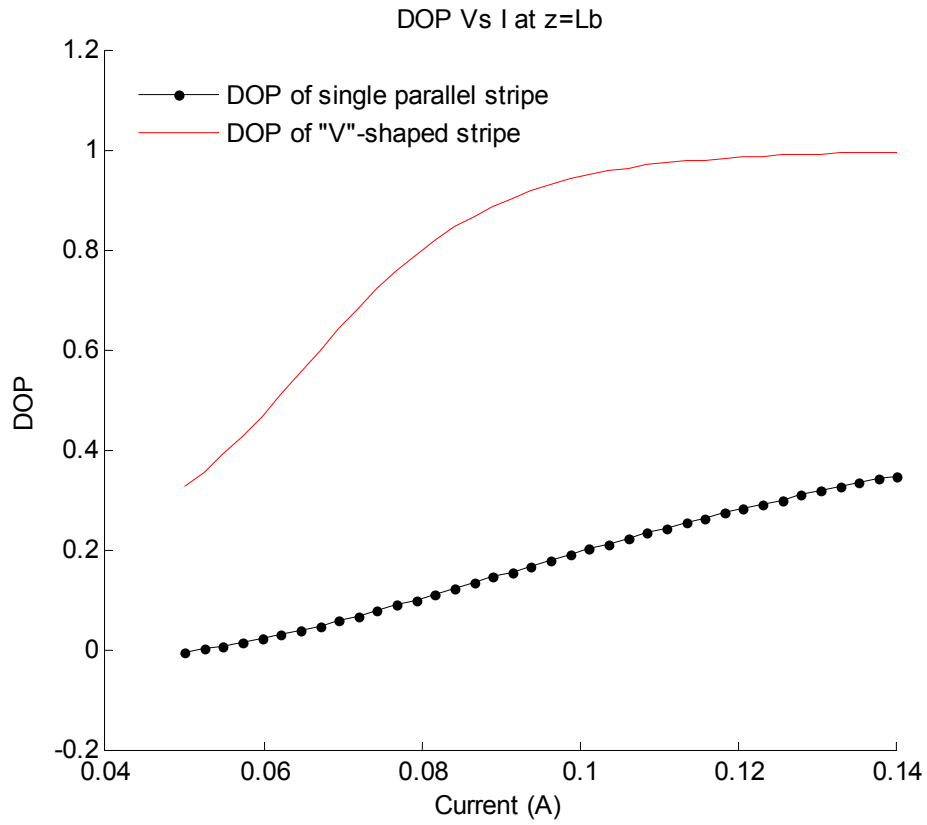

Figure 4.12 Comparison of DOP against I for single stripe and V-stripe, where black circled line indicates DOP of single stripe, and red line indicates V-stripe

where at $I = 0.06A$, $g_e = 10.9cm^{-1}; g_h = 9.3cm^{-1}$. From Fig.4.12, the polarisation-enhanced result from the V-stripe is tremendous; the light output is almost single polarised, when Injection Current is $\geq 0.1A$; the TM polarisation generated in stripe-B by spontaneous emission is so small compared to the large amount of TE polarisation in stripe-B.

- **Test 4 DOP at $z = L_b$**

This test is designed to test the polarisation enhancement that the V-stripe can achieve by different stripe parameters. In the first stage, we will assume the same current injection for stripe-A and -B and we also assumed stripe-A and stripe-B are both at the exact Brewster angle, where $\phi_a = \phi_b = \phi_B$. Test schematic diagram is shown in Fig.4.13.

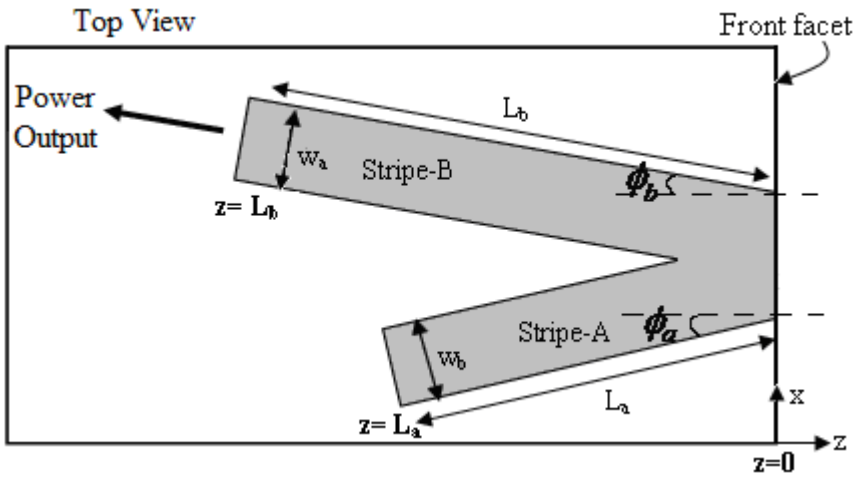

Figure 4.13 Schematic of the simulated point in Test 4 referred to as the "V"-geometry

Parameters used:

I_a (A)	I_b (A)	w_a (μm)	w_b (μm)	d_a (μm)	d_b (μm)
0.06~0.16	0.06~0.16	10	10	0.15	0.15

Table 4.6 Device relevant parameters used in Test 4

Test Conditions	Condition 1	Condition 2	Condition 3	Condition 4	Condition 5	Condition 6
Γ_e	0.64	0.64	0.64	0.32	0.32	0.32
Γ_h	0.56	0.56	0.56	0.3	0.3	0.3
L_a (μm)	800	600	400	800	600	400
L_b (μm)	400	600	800	400	600	800

Table 4.7 Relevant parameters used in Test 4 for conditions 1to 6

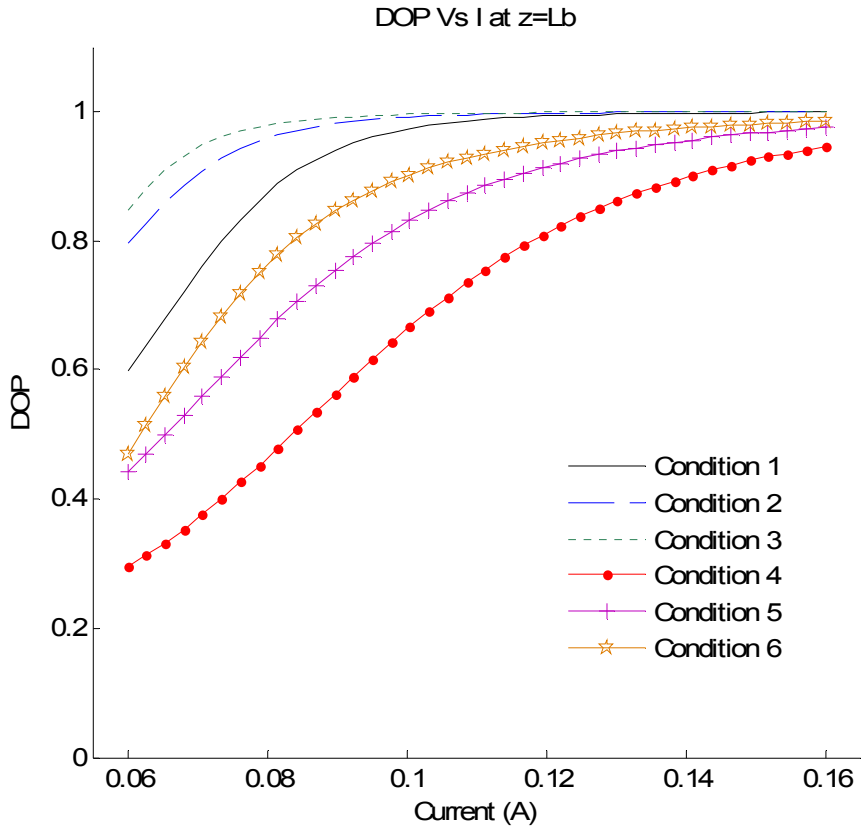

Figure 4.14 Comparison of DOP of different stripe lengths under the Test 4 conditions 1-6; where black line, condition 1; blue dashed, condition 2; green dotted, condition 3; red circled, condition 4; mauve crossed, condition 5, and orange started, condition 6

where at $I = 0.06A$, for $\Gamma_e = 0.64; \Gamma_e = 0.56$, $g_e = 10.9cm^{-1}; g_h = 9.3cm^{-1}$ and for $\Gamma_e = 0.32; \Gamma_e = 0.3$, $g_e = 5.45cm^{-1}; g_h = 5.11cm^{-1}$. This result illustrated in Fig.4.14 shows that with the combination of a shorter stripe-A and a longer stripe-B (as referred to in condition 3 and 6), the V-stripe model produces the best polarisation-selective result. Because there is a large percentage of TE polarisation in the P_{BI}, and this large potion of TE polarisation is getting amplified as it travel through stripe-B, as $P \simeq P_0 e^{gL}$ ($P_0 \approx P_{BI}$ in this case). Therefore, use a longer stripe-B, can increase the percentage of TE polarisation, and lead to a good polarisation-selective result. But we are not suggesting using a very long stripe, because a longer stripe requires more Injection Current to generate, it is not economical and it is beyond the design purpose (which is to design a simple, cheap polarisation-selective device).

Another advantage of the V-stripe model is, it can work with similar confinement factor for TE and TM polarisation (e.g. $\Gamma_e = 0.32; \Gamma_h = 0.3$, see conditions 4 to 6); the model achieved an impressive polarisation enhancement result when using relatively shorter stripe-A and longer stripe-B (see condition 6).

- **Test 5 DOP at $z = L_b$, With $I_a \neq I_b$**

In the previous test, we have tested the V-stripe model with different stripe length combinations, but all under the same current injection. In this test, we will continue to test the polarisation enhancement of the V-stripe design, by injecting different current into the two stripes, to find out the best optimization result. In this test we also assumed stripe-A and stripe-B are both at the exact Brewster angle, where $\phi_a = \phi_b = \phi_B$, Fig.4.15.

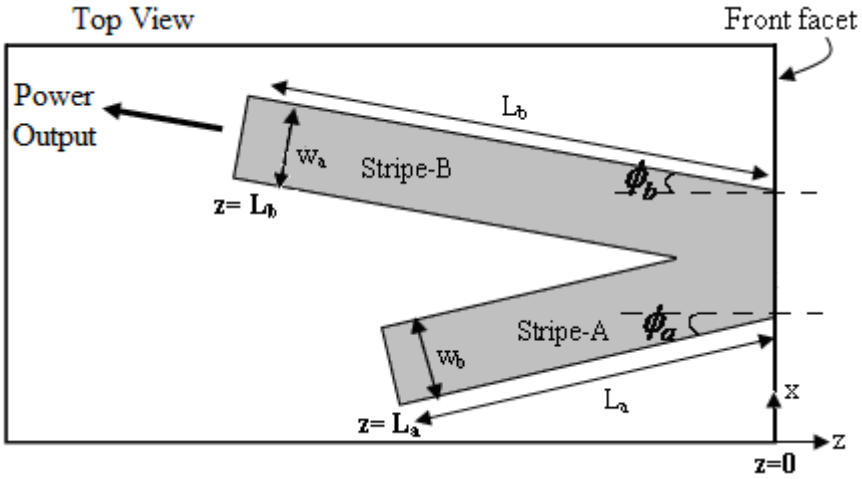

Figure 4.15 Schematic of the simulated point in Test 5 as referred to the "V"-geometry

Parameters used:

Γ_e	Γ_h	$w_a = w_b$ (μm)	$d_a = d_b$ (μm)	L_a (μm)	L_b (μm)
0.64	0.56	10	0.15	400	800

Table 4.8 Device relevant parameters used in Test 5

Test Conditions	Condition 1	Condition 2	Condition 3	Condition 4
I_a (A)	0.06~0.16	0.06~0.16	0.1~0.2	0.1~0.2
I_b (A)	0.06~0.16	0.1~0.2	0.06~0.16	0.1~0.2

Table 4.9 Relevant parameters used in Test 5 for conditions 1to 4

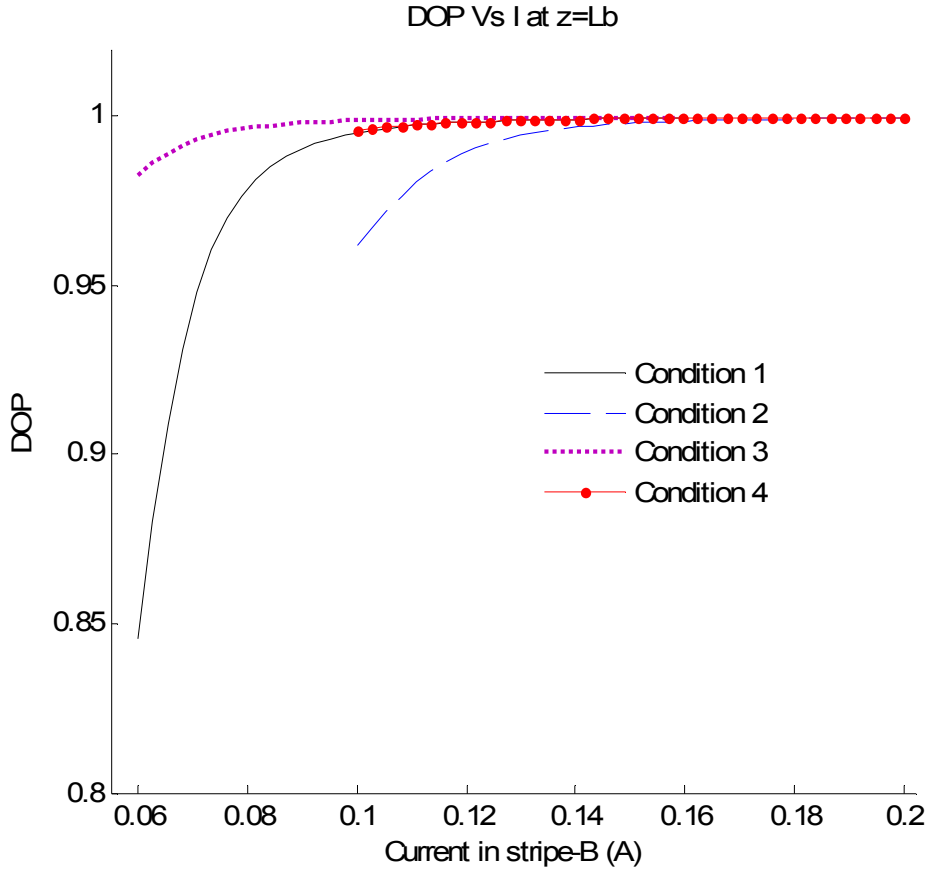

Figure 4.16 Comparison of DOP with different Injection Currents under the Test 5 conditions 1-4; where black line, condition 1; blue dashed, condition 2; dotted mauve, condition 3; and red circled, condition 4

The result of this test illustrated in Fig.4.16 shows with $L_a = 400\mu m, L_b = 800\mu m$, injecting high current into both stripes (as referred to in condition 4) produces the best polarisation-selective result, $DOP = 0.9961$. The number is getting closer to 1 when we used reasonable high current; however Injection Current is not proportional to DOP, as high Injection Current also produces more TM polarisation. As referred to in condition 3, with Injection Current higher for the shorter device and lower for the longer device produces the second best polarisation-selective result, $DOP = 0.9825$.

It is only 0.0142 less in DOP than the best result, thus beyond the energy saving purpose, it is better to have high current injection for the short device and low current injection for the long device, as in condition 3.

- **Test 6 DOP of Transmitted Power at $z = 0$**

If using an the angled stripe, when the light reaches the Brewster angle, the reflected signal will be purely TE polarised photons, but due to high absorption in the "unpumped" region, the reflected signal will soon being absorbed, therefore, it is only possible to consider using the transmitted signal, which will contain mainly TM polarised photons but also with a small portion of TE polarised photons. The aim of this test is to test the DOP of the transmitted signal from stripe-A (treated as the angled stripe) in the V-stripe model. In this test, again, we will assumed stripe-A and stripe-B are both at the exact Brewster angle, where $\phi_a = \phi_b = \phi_B$. The schematic diagram is illustrated in Fig.4.17.

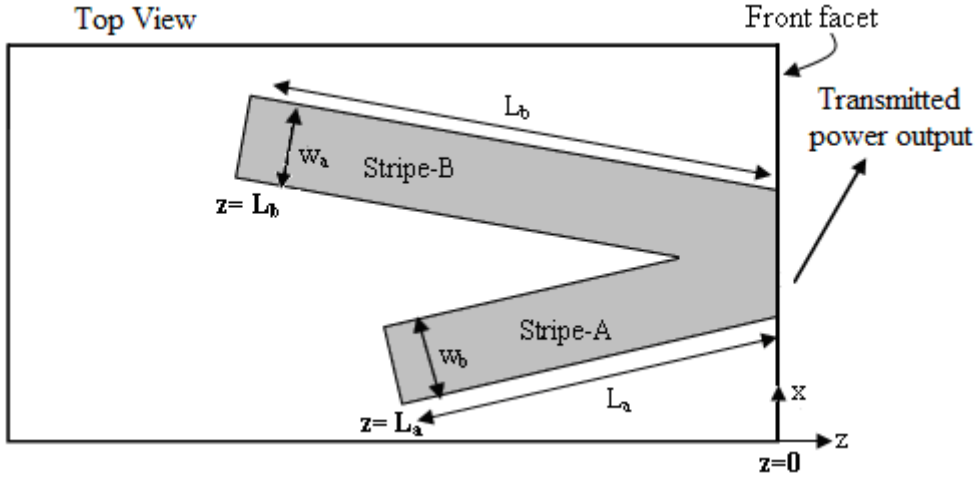

Figure 4.17 Schematic of the simulated point in Test 6 as referred to the "V"-geometry

Parameters used:

I_a (A)	w_a (μm)	d_a (μm)
0.06~0.16	10	0.15

Table 4.10 Relevant stripe parameters for Test 5

Test Conditions	Condition 1	Condition 2	Condition 3	Condition 4	Condition 5	Condition 6
Γ_e	0.32	0.32	0.32	0.64	0.64	0.64
Γ_h	0.3	0.3	0.3	0.56	0.56	0.56
L_a (μm)	400	600	800	400	600	800

Table 4.11 Device relevant parameters used in Test 6 for conditions 1-6

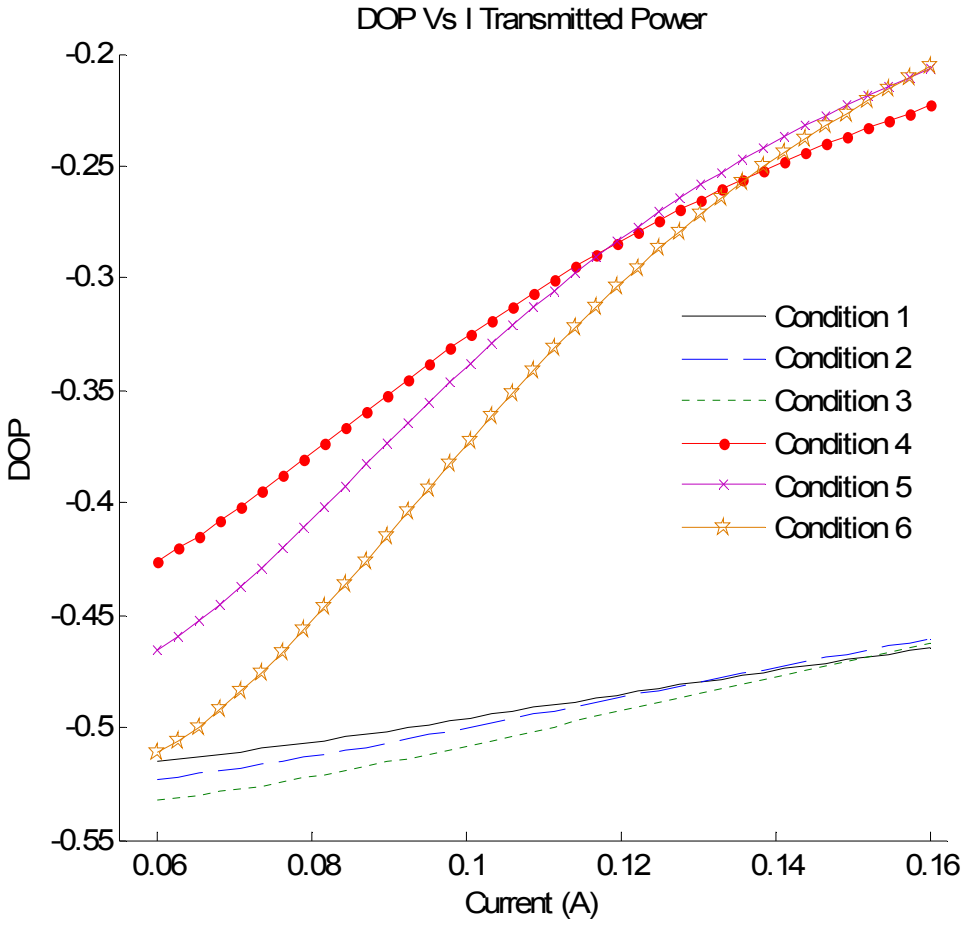

Figure 4.18 Comparison of DOP of transmitted power under the conditions in Test 6; where black line, condition 1; blue dashed, condition 2; green dotted, condition 3; red circled, condition 4; mauve crossed, condition 5; and orange started, condition 6

In this test illustrated in Fig.4.18, there is more TM polarised photons in the transmitted power than TE polarised photons; therefore, the value for DOP approaching -1 is the best polarisation-selective result we are looking for. For conditions 1-3 $\Gamma_e = 0.32; \Gamma_h = 0.3$, and for condition 4-6 $\Gamma_e = 0.64; \Gamma_h = 0.56$; we

can see that in general, with $\Gamma_e = 0.32; \Gamma_h = 0.3$, the transmitted power has a better value in DOP. By comparing this result with the DOP of output power from the V-stripe in Fig.4.14 in Test.4, this DOP of transmitted power from stripe-A is a lot less attractive. Even though at the Brewster angle, all TM polarised photons are transmitted out of the facet, and a small percentage (approximately 30%) of TE polarised photon is transmitted out of facet, that could principally make a relative good polarisation-selective device. However, as the current is increasing, the difference between TE and TM polarised photon (which is cause by confinement factor) becomes more notable (can be referred to in Fig.4.19 and 4.10 in Test.1 and Test.2), this results in the difference for TE and TM polarised photons is decreasing in the transmitted power.

4.5 Summary

In order to enhance the polarisation output from a bulk material ee-LED, a V-stripe has been designed. The design comes from the idea of angle stripe (as discussed in Sec.4.2), that utilised the advantage of the Brewster angle, where theoretically all TM polarised photon will be transmitted. Therefore, by using the reflected signal it will be mainly TE polarization, and it is necessary to add another angled stripe to collect and maintain the reflected signal, otherwise the reflected signal will be absorbed quickly in the high absorption region. Thus a second stripe is necessary, and the V-stripe is explained in Sec.4.3. A computational model has been built and introduced in Sec.4.4, to predict the performance of the V-stripe. This is followed by the step by step tests and simulation results. The results show that the approximate analysis of the V-stripe model works very effectively.

References 4

[1] F. Causa, J. Sarma, 'Realistic Model for the Output Beam Profile of Stripe and Tapered Superluminescent Light-Emitting Diodes', Applied Optics, Vol. 42, No. 21, pp. 4341-4348, July 2003

[2] F. Causa, J. Sarma and S. Yunus, **'Characterization of Angled Tapered Superluminescent LEDs'**, Applied Optics, Vol. 41, No 24, Aug 2002

[3] G. Alphonse et al., **'Superluminescent Diode'**, United States Patent, 4821277 Apr 1989

[4] J. Nieson et al., **'High Power 0.83 .mu.m Angle Stripe Superluminescent Diode'**, Southwest Optics Conference, Feb. 1987

[5] M.J. Adams, **'An Introduction to Optical Waveguides'**, Chichester: Wiley, 1981

Chapter 5:

V-Stripe (Edge-Emitting) Light Emitting Diodes (ee-LEDs) – Refined Analysis

5.1 Introduction

As presented in Chapter-4, a computational model for the approximate analysis of the V-stripe has been developed. In the approximate analysis, it has been assumed that all rays travelling inside the stripe are parallel to the stripe axis and when the stripe is placed at the Brewster angle, all TM polarised rays are transmitted out of facet, which results in the reflected light being purely TE polarised rays. In this chapter, a refined model will be introduced to optimise the polarisation-selective output of ee-LED. The refinement will include the angular distribution of intensities. A computer program has been developed to estimate the angular distribution of the power at the facet from stripe-A. Therefore, a refined analysis of light reflected into the second stripe (stripe-B) can be made, by substituted the angular distribution equations for the Rate Equations to calculate the light emitted in stripe-A; hence to obtain a more comprehensive and realistic model.

5.2 The V-Stripe ee-LED Design -- Refined Analysis

The approximate analysis of the V-stripe ee-LED model is shown in Fig.4.5. The refined analysis of the V-stripe ee-LED model is shown in Fig.5.1; the difference between them is, that in the approximate model, we assumed the reflected power from stripe-A into stripe-B to be purely TE polarised, but in the refined model, as we include the affect of the angular distribution of intensities (which will be explained in the following section), in the reflected power from stripe-A into stripe-B, there is also a small amount of TM polarised photons being reflected.

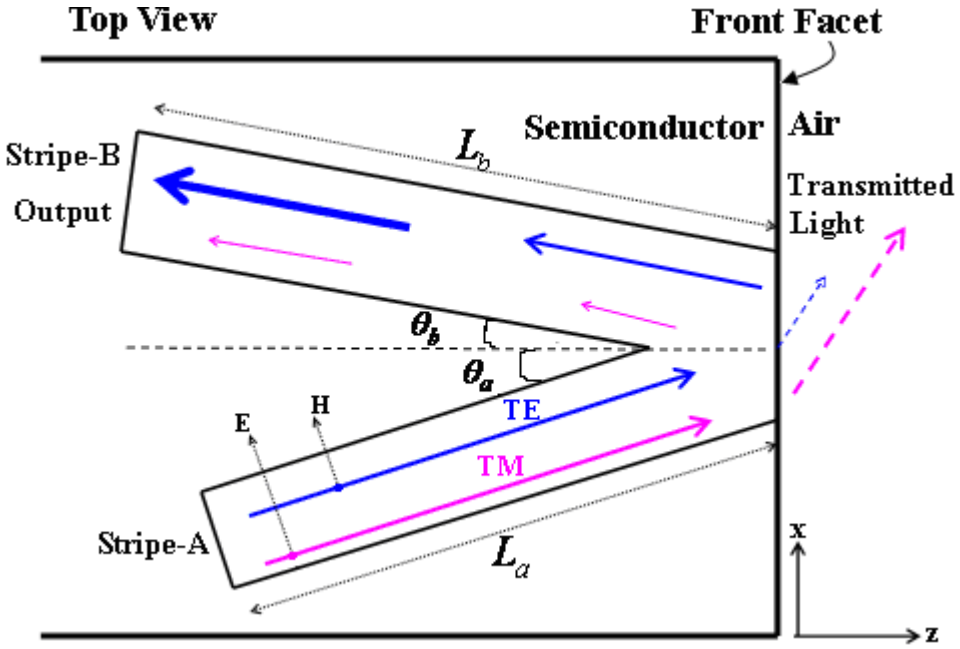

Figure 5.1 Top view of the refined analysis of the V-stripe ee-LED geometry; blues indicate TE polarisation, magentas indicate TM polarisation.

As can be seen from Fig.5.1 assuming that an almost equal amount of TE and TM polarisation are generated in the stripe-A (as mention previously, difference is due to Γ_e, Γ_h), as the rays go through the front facet at the Brewster angle a large amount of TE polarised photons has been reflected, and there is also a small amount of TM polarised photons being reflected. This is due to the angular distribution, where rays travelling inside the stripe are not only parallel to the stripe axis, but rays travel at all different angles, Fig.5.2.

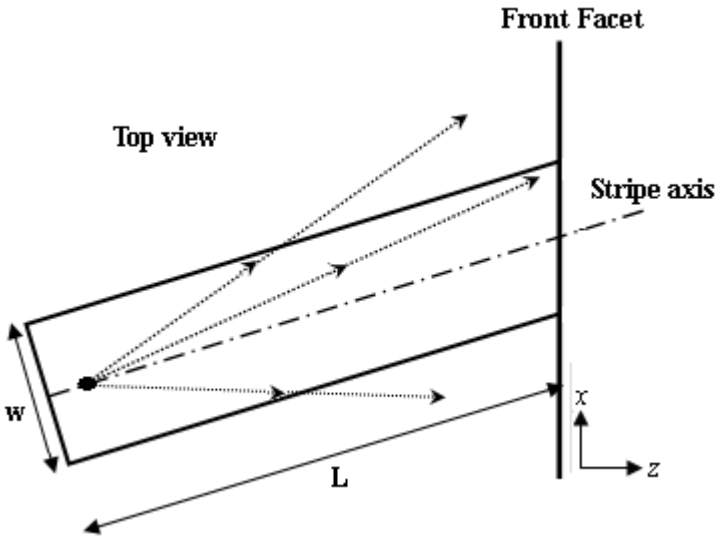

Figure 5.2 Top view of a stripe contact indicating rays travel at different angles; stripe width, w and stripe length, L

Therefore, when the stripe is at the exact Brewster angle, not all the rays will be at the exact Brewster angle, but have a distribution around the angle. Therefore, in the reflected rays, there are no longer purely TE polarised photons, but we also have a small amount of TM polarised photons.

5.3 Angular Distribution of Intensities

In the previous Rate Equation discussion (Chapter-3 and -4), we only considered the rays travelling parallel to the stripe axis. But this is not realistic, because light not only travels parallel to the stripe, but travels at all angles corresponding to the stripe axis. The different angle travelling rays cause an intensity distribution, and this is called intensity angular distribution. The angular distribution of intensities calculations will be explained in Sec.5.3.2. Here, first of all, we define the corresponding angles that we used in the calculation. Fig.5.3 shows the indication of angles used in the intensity angular distribution calculation based on a top view of the angled stripe ee-LED in the *x*-*z* plane

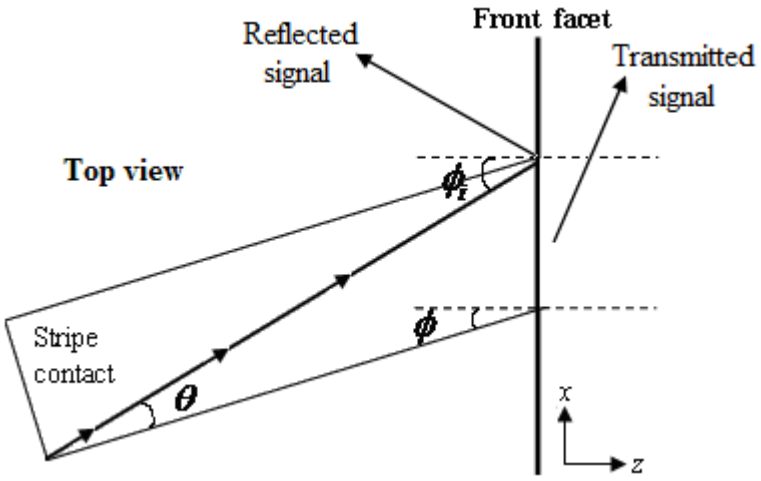

Figure 5.3 Schematic diagram to define the angles that are being used in the calculation

where $\phi_i = \theta + \phi$; θ is the rays travelling angle inside the stripe, the angle is in respective to the stripe axis; ϕ is the stripe angle corresponding to the perpendicular of the front facet; ϕ_i is the rays travelling angle corresponding to the normal to the front facet. Hence, the intensity angular distribution of rays distributed along the $x-axis$ and corresponding to ϕ_i, can be written as, $I_x(\phi_i)$.

Fig.5.4 illustrates how the intensity angular distribution effects the intensity reflectivity from stripe-A into stripe-B, with the corresponding ϕ_i.

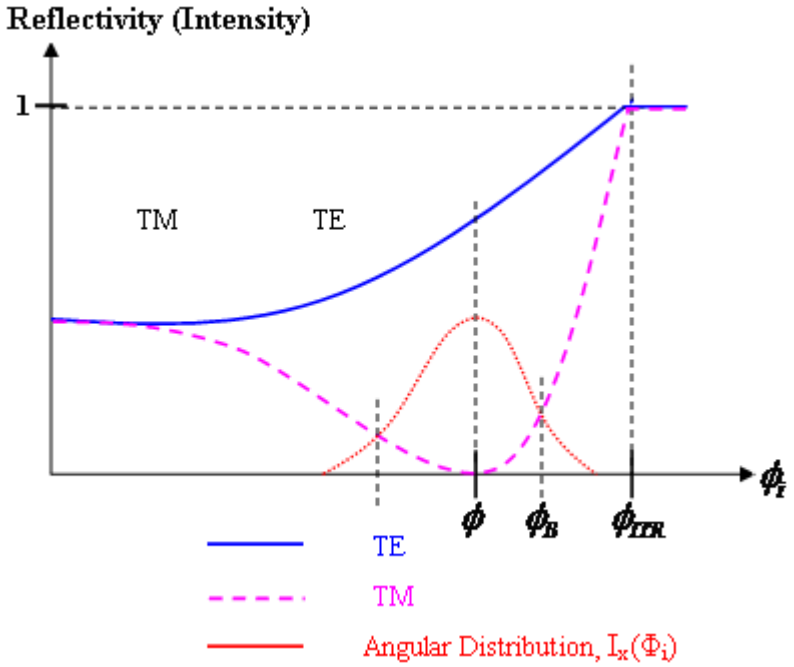

Figure 5.4 The angular distribution of intensities, $I_x(\Phi_i)$ Schematic of the Brewster angle curve

As explained in the previous chapter, the approximate analysis of the V-stripe design is to take the phenomenon of the Brewster angle to separate TE and TM polarisation. In the approximate case all light/rays travel parallel to the stripe axis inside the stripe; then if $\phi = \phi_B$, all TM polarised rays are transmitted out of facet. However, this is not realistic. In the refined analysis, by applying the angular distribution of intensities; when placing the stripe at the exact Brewster angle, there is photon distribution around the Brewster angle, which means not all TM polarised photons are transmitted, some of it is being reflected. Consequently we will need to optimise the stripe angle to obtain the best percentage of Degree of Polarisation (DOP).

5.3.1 Assumptions for Angular Distribution of Intensities

In the formulation of the Angular Distribution of Intensities equation, an approximation used is that rays only at angles $\theta < \theta_M$, $\theta_M = \tan^{-1}(\frac{w}{L})$, are considered. The purpose of setting this maximum angle is to simplify the integration along *x*- and *z*-axis. Although the resulting angular distribution with this limitation of maximum angle is an approximation, but since the main interest is to consider how much light has been reflected into the second stripe, the rays travelling with $\theta > \theta_M$ will not be reflected into the second stripe. The fraction of spontaneous emission for the horizontal angle used is $\Delta\theta = 0.1°$, Fig.5.5; the small $\Delta\theta$ allows accurate calculation. Also current density throughout the rectangular stripe contact region has been assumed to be constant, and remain constant through the different layers of the DH structure material.

5.3.2 Angular Distribution of Intensities Derivation

As explained in Sec.5.3.1, the angular distribution of intensity, ($I_x(\phi_i)$), calculation is based on a restriction of Maximum angle $\theta_M = \tan^{-1}(\frac{w}{L})$. Here is the formulation of the angular distribution equations; the full derivation can be referred to in Appendix-D. Fig.5.5 indicates that a photon travels from a general point $P(x_0, z_0)$ at angle θ along the $s-axis$,

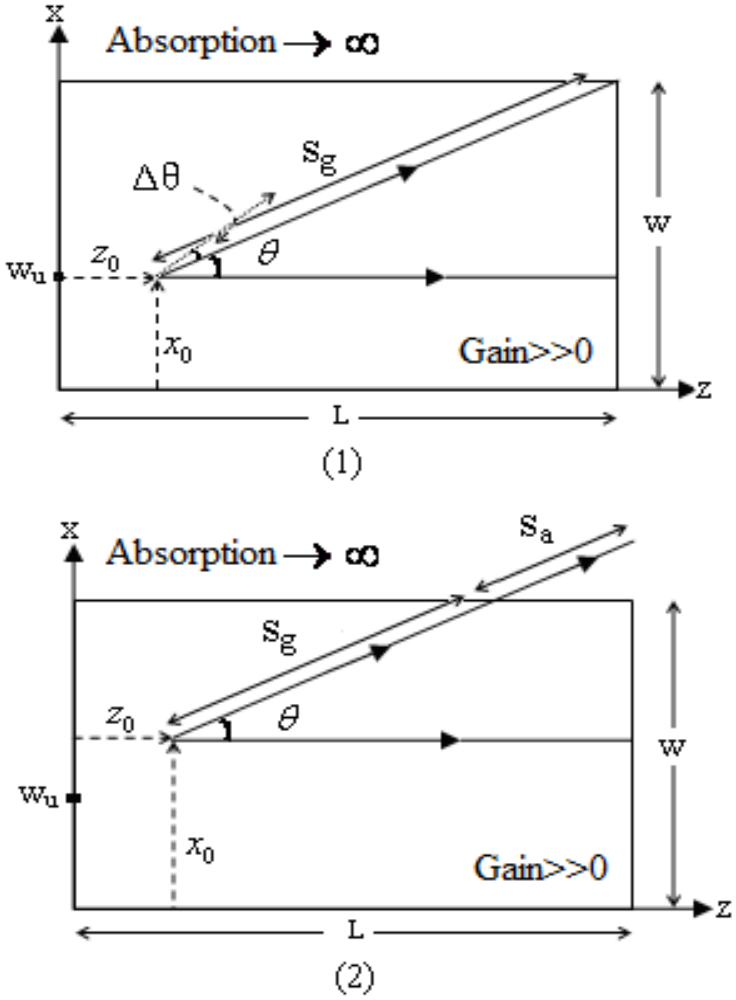

Figure 5.5 Schematic diagram of all rays at angle θ - two categories: (1) Ray entirely in gain region; (2) Ray partly in gain and then in absorption region; w, stripe width; L stripe length

where w_u is the integration limit point. Rays travelling below w_u are in category-1 and rays travelling beyond w_u are in category-2. s_g rays travel in the gain region and s_a rays travel in the absorption region. To avoid confusion, in the following derivations, s_f is used to represent any forward travelling rays in $s-direction$.

From Fig.5.5, for all rays travelling at the same angle θ, we write the forward travelling rays as, $(s_a + s_g) = s_f = \frac{L - z_0}{\cos(\theta)}$; and w_u is defined as,

$$w_u = w - (L - z_0)\tan(\theta) \qquad (5.1)$$

The intensity angular distribution equations are derived from the Rate Equation in Appendix-B-1, Eq.(B1.7). The Rate Equation used to calculate the photon density generated at each general point $P(x_0, z_0)$ for situation (1) is written as,

At z_0, for $x_0 < w_u$; $s_g = s_f$, $s_a = 0$

$$P_1(x_0, z_0, \theta; z = z_L) = P_1(x_0, z_0, \theta; s = s_f) = \overline{P}_{sp}(e^{\overline{g}s_f} - 1) \qquad (5.2)$$

The Rate Equation used to calculate the photon density generated at each general point $P(x_0, z_0)$ for situation (2) is written as,

At z_0, for $x_0 > w_u$; $s_g = \frac{w - x_0}{\sin(\theta)}$,

$$P_2(x_0, z_0, \theta; z = z_L) = P_2(x_0, z_0, \theta; s = s_g) = \overline{P}_{sp}(e^{\overline{g}s_g} - 1)(e^{\alpha(s_f - s_g)}) \qquad (5.3)$$

Note, $(e^{\alpha(s_f - s_g)})$ are the rays travelling outside the gain region, α is the gain in absorption region.

By integrating Eq. 5.2 along the $x-axis$ and $z-axis$, we add up the photon density from each general point. Thus, the intensity angular distribution equation for situation (1) becomes,

$$P_1(\theta) = \overline{P}_{sp}[\frac{w\cos\theta}{\overline{g}}(e^{\overline{g}(\frac{L}{\cos\theta})} - 1) - \frac{L\sin\theta}{\overline{g}}e^{\overline{g}(\frac{L}{\cos\theta})} + \frac{\sin\theta\cos\theta}{\overline{g}^2}(e^{\overline{g}(\frac{L}{\cos\theta})} - 1) + \frac{3}{2}L^2\tan\theta - w.L]$$

(5.4)

By integrating Eq.5.3 along the $x-axis$ and $z-axis$, the intensity angular distribution equation for situation (2) becomes,

$$P_2(\theta) = \overline{P}_{sp}[\frac{\cos\theta}{\alpha}(e^{\alpha(\frac{L}{\cos\theta})} - 1)(\frac{\sin\theta}{\alpha - \overline{g}} + \frac{\sin\theta}{\alpha}) + \frac{\sin\theta}{\alpha - \overline{g}}\frac{\cos\theta}{\overline{g}}(1 - e^{\overline{g}(\frac{L}{\cos\theta})}) - \frac{\sin\theta}{\alpha}L] \quad (5.5)$$

The computer model for intensity angular distribution is based on Eq.5.4 and Eq.5.5, by adding up the value from Eq.5.4 and Eq.5.5, the total photon density generated in the stripe can be known. The polarisation decomposed intensity angular distribution equation are following the same procedure as the polarisation decomposed Rate Equations in Appendix-B2. By using the model gain, $\overline{g}_e, \overline{g}_h$ instead of material gain, $\overline{g}$, and with subscript e, h to represent TE and TM polarisation, respectively.

5.3.3 Angular Distribution of Intensities Simulation Results

In this test, we choose to use a similar value of confinement factor for TE and TM polarisation, where $\Gamma_e = 0.32, \Gamma_h = 0.3$. Using similar values for TE and TM polarisation confinement factor in the V-stripe model enables us to verify the efficiency of the optimised polarisation-selective result. In the angular distribution calculation, the weighted carrier density $\overline{N}$ is obtained from the single stripe Rate Equation calculation (refer Chapter-3). The schematic diagram of the stripe geometry and symbols for this test are shown in Fig.5.6,

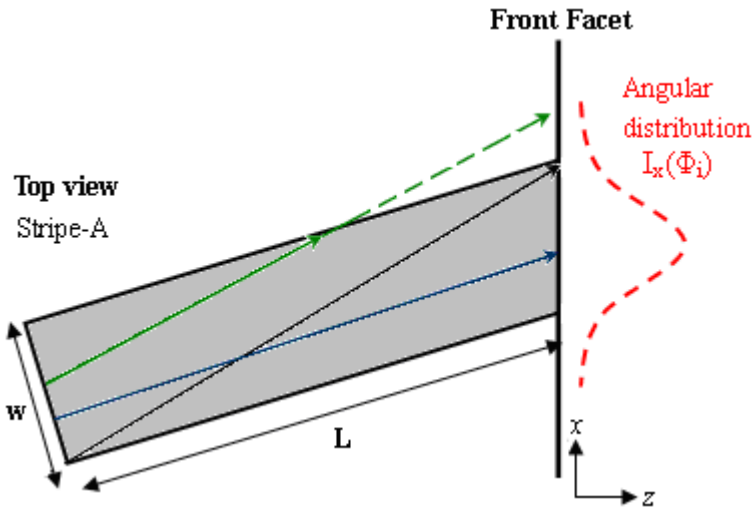

Figure 5.6 Schematic diagram of angular distribution test as referred to the stripe geometry; stripe width w and stripe length, L

- **Angular Distribution of Intensities Test**

Parameters used:

L (μm)	w (μm)	d (μm)	I_a (A)	$\Delta\theta$	Γ_e	Γ_h
400	10	0.15	0.16	0.05	0.32	0.3

Table 5.1 Device relevant parameters used in angular distribution test

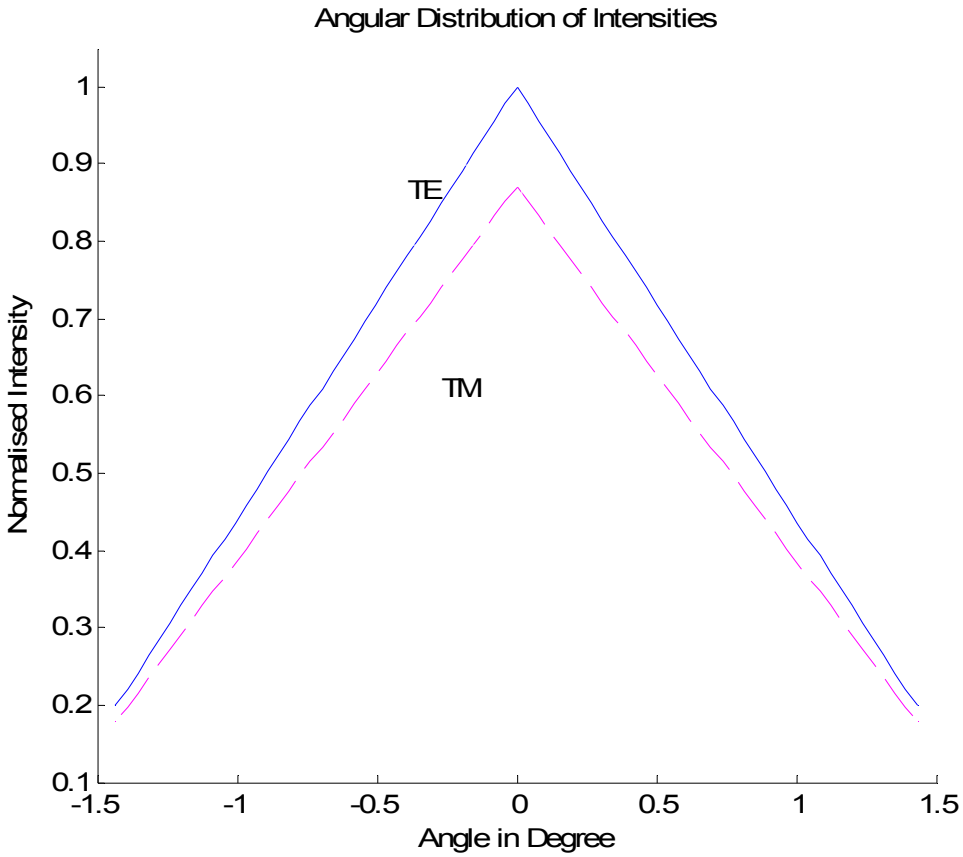

Figure 5.7 Angular distribution of intensities, where blue line indicates TE polarisation and mauve dashed indicates TM polarisation, [1]-[3]

Fig.5.7 shows the angular distribution of intensities with the limitation of maximum angle $|\theta_{\max}|$. For this particular device structure, the angular distribution is $\pm 1.4°$ from zero degree (the peak). The peak of the intensity angular distribution is represented by the rays travel parallel to the stripe axis and the rays travelling at some angle to the stripe axis are represented by the intensity angular distribution decaying from the peak. The difference of intensities between TE and TM polarisation is caused by the confinement factor difference in this case.

5.4 The V-Stripe ee-LED Model -- Refined Analysis

This is the refined model to the approximate analysis of V-stripe model. In this realistic model it has included the rays travelling at different angles, $\phi_i(x)$, inside the device. Hence the intensity angular distribution calculation is applied in the calculation.

5.4.1 The Refined V-Stripe Model Assumptions

In the refined analysis of V-stripe model, constant current is flowing within the stripe, weighted average carrier density $\overline{N}$ is applied throughout the calculation and constant current density is assumed throughout the rectangular stripe contact region and to remain constant throughout the different layer of the D-H structure material; there are no reflectivities at both ends of stripes. The rays that are used for external input to stripe-B (P_{BI}) is an approximation, which comes from stripe-A's angular distribution calculation times the stripe reflectivity at an angle. Also, as mentioned in the previous section, the angular distribution calculation is based on an approximation where the calculation is limited to a maximum angle $\theta_M = \tan^{-1}(\frac{w}{L})$.

This approximation works, because not all the rays generated from stripe-A can be reflected into stripe-B, as some of the rays will be reflected into the absorbing region, this means only a small angle of the light distribution can be effectively input into stripe-B. In the model we have assumed no reverse travelling photons as both ends of stripe have no reflectivity.

5.4.2 The Refined V-Stripe Model Flowchart

The flowchart in Fig.5.8 shows the numerical procedure of the refined analysis of the V-stripe model calculation, where the carrier density, $\bar{N}_a$ for stripe-A is calculated from the single stripe (the $\bar{N}$ numerical iteration scheme is discussed in Chapter-3), and the output/reflected power from stripe-A is calculated based on the angular distribution of intensities equations. The value of $\bar{N}_b$ is calculated depending on the external input signal from stripe-A.

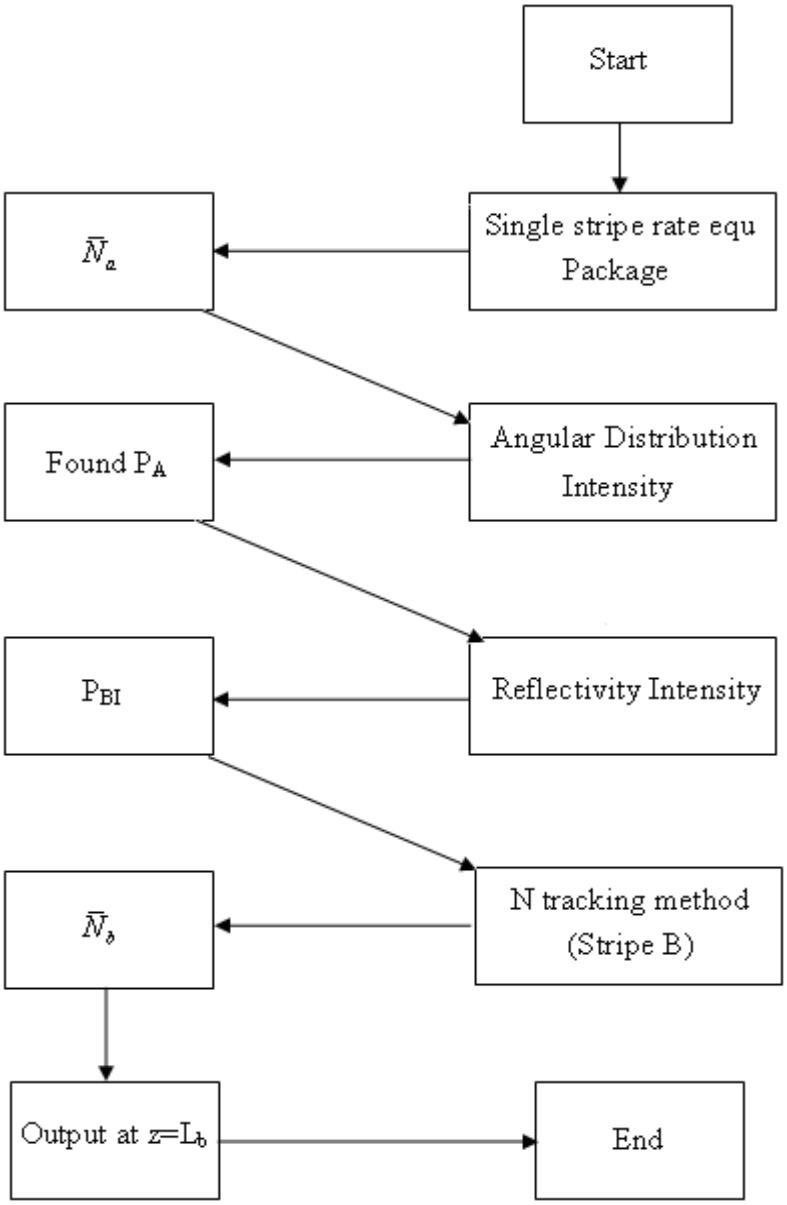

Figure 5.8 Flowchart diagram showing the numerical calculation procedure of the refined analysis of the V-stripe, which has included the angular distribution of intensities calculation

5.4.3 The Refined V-Stripe Model Simulation Results

- **Definition of DOP Used in The Tests**

For Test.1, DOP of power at the front facet, stripe-A, at $z = L_a$, is defined as,

$$DOP\_A = \frac{T_{e\_A} - T_{h\_A}}{T_{e\_A} + T_{h\_A}} \qquad (5.6)$$

where $T_{e\_A} = P_{1e}(\theta) + P_{2e}(\theta)$; $T_{h\_A} = P_{1h}(\theta) + P_{2h}(\theta)$, from Eq.D4 and D7

For Test.2, 3, DOP of reflected power from stripe-A into stripe-B (P_{BI}), is defined as,

$$DOP\_R = \frac{\int_{-\theta_{Max}}^{+\theta_{Max}} T_{e\_A} \times R_e(\theta) - \int_{-\theta_{Max}}^{+\theta_{Max}} T_{h\_A} \times R_h(\theta)}{\int_{-\theta_{Max}}^{+\theta_{Max}} T_{e\_A} \times R_e(\theta) + \int_{-\theta_{Max}}^{+\theta_{Max}} T_{h\_A} \times R_h(\theta)} \qquad (5.7)$$

where $R_e(\theta), R_h(\theta)$ are intensity reflectivities at each corresponding angle to $P_1(\theta), P_2(\theta)$ for TE and TM polarisation, respectively.

For Test.4, DOP of power output from stripe-B, at $z = L_b$, is defined as,

$$DOP\_B = \frac{T_{e\_B} - T_{h\_B}}{T_{e\_B} + T_{h\_B}} \qquad (5.8)$$

where T_{e_B}, T_{h_B} are the generated power outputs from stripe-B for TE and TM polarisation, respectively.

- **Simulation Procedure**

A number of tests have been done to study the DOP of the refined analysis of the V-stripe ee-LED to determine if the refined P_{BI}, (where power generated from stripe-A reflected into stripe-B calculated by the angular distribution of intensities equations) has enhanced the polarisation-selective output. The first thing is to decide the best angle to place stripe-A, which can obtain the maximum DOP_R and then we use different combinations of stripe parameters to determine the best optimised polarisation-selective result. In addition, for the following tests, we also assumed stripe-A and stripe-B are both at the exact Brewster angle, where $\phi_a = \phi_b = \phi_B$. The schematic diagram of Fig.5.9 explaines the notations used in the following tests.

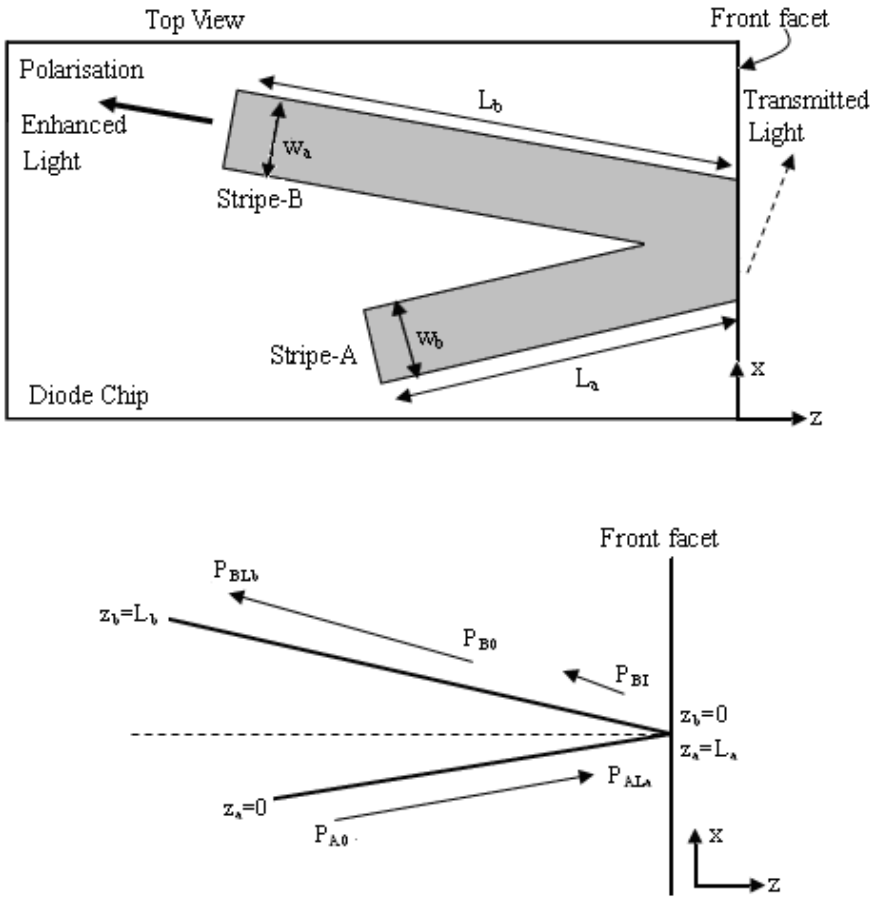

Figure 5.9 Schematic diagram of a V-stripe ee-LED from top view and a top view picture of the photon density analysis schematic diagram for the stripe contact, showing the notations used in this section

Table.5.2 shows the parameters used in this refined V-stripe model simulation.

Parameters	Values	Parameters	Values
Speed of light	$c = 3\times10^{10} cm/s$	Electron charge	$q = 1.602\times10-19coul$
Refractive index in GaAs	$n_1 = 3.6$	Refractive index in AlGaAs	$n_2 = 3.36$
Wavelength	$\lambda = 850\times10^{-7} cm$	Planck's constant	$h = 6.626\times10^{-34} J/s$
Material gain coefficient	$A_0 = 1.5\times10^{-16} cm^2$	Transparency carrier density	$N_{tr} = 1.55\times10^{18} cm^{-3}$
Doping carrier density	$N_d = 1.7\times10^{17} cm^{-3}$	Bimolecular recombination constant	$B_r = 1\times10^{-10} cm^3/s$
Confinement factor TE	$\Gamma_e = 0.32$	Confinement factor TM	$\Gamma_h = 0.3$
Reflectivity at $z = 0$	$R_0 = 0$	Reflectivity at $z = L_a; L_b$	R_{La}, R_{Lb} depends on stripe angle
External input for stripe-A	$P_{IA} = 0$	External input for stripe-B	P_{IB} depends on simulation result
Depth for stripe-A and -B	$d_a = d_b = 0.15\mu m$	Width for stripe-A and -B	$w_a = w_b = 10\mu m$
Length for stripe-A and -B	L_a, L_b various (see test condition)		

Table 5.2 Parameters applied in the refined V-stripe model

- **Test 1 DOP_A**

The power output from stripe-A has include the intensity angular distribution, $I_x(\phi_i)$. The aim of this test is to compare the DOP_A, DOP_R (in Test.3) and DOP_B (in Test.4). From these three step comparison, the polarisation-selective enhancement result of the V-stripe can be clearly seen.

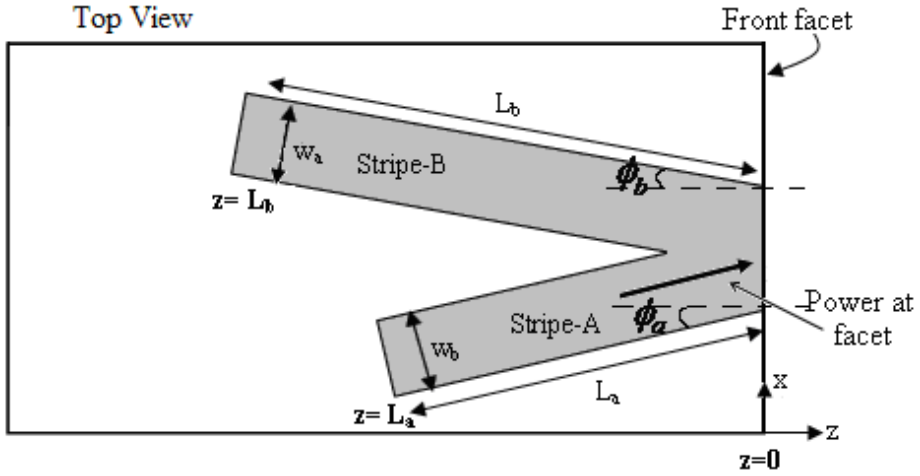

Figure 5.10 Schematic of the simulated point in Test 1 as referred to the "V"-geometry

Parameters used:

I_a (A)	w_a (μm)	d_a (μm)	$\Delta\theta$	Γ_e	Γ_h
0.06~0.16	10	0.15	0.05^o	0.32	0.3

Table 5.3 Relevant stripe parameters for Test 1

Test Conditions	Condition 1	Condition 2	Condition 3
L_a (μm)	400	600	800

Table 5.4 Relevant parameters used in Test 1 for conditions 1-3

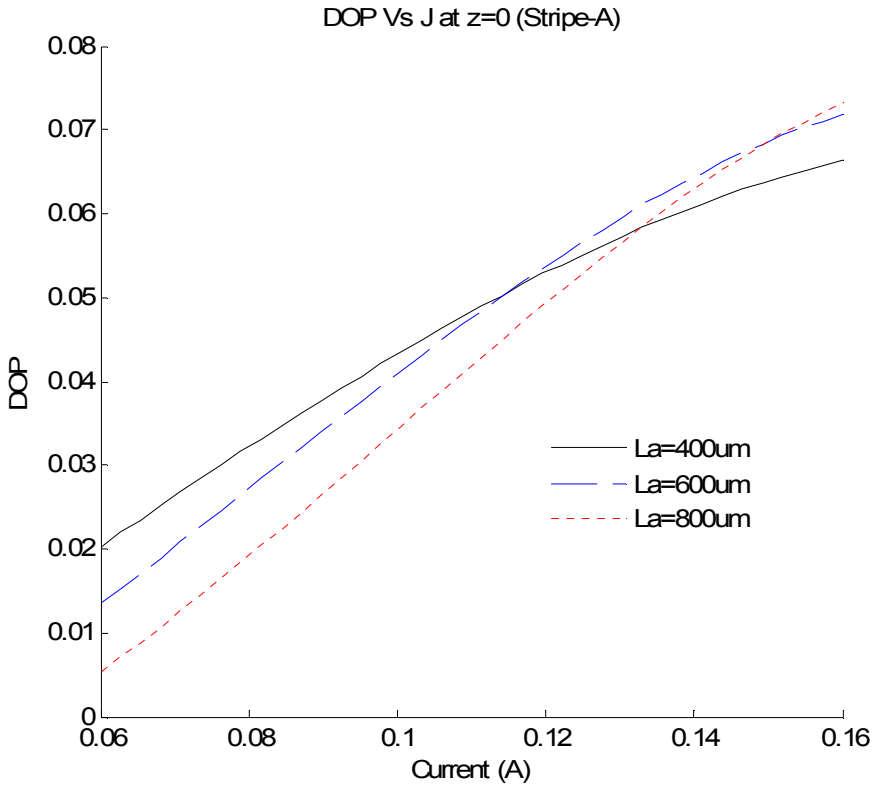

Figure 5.11 DOP of power at facet, stripe-A; where black line, L_a=400μm; blue dashed, L_a=600μm and red dotted, L_a=800μm

The result illustrated in Fig.5.11 shows that the difference between the two polarisations is very small, they are dependent on the confinement factor. As can be seen in the result, even if we have double the length of the stripe, the DOP have just increased 0.01 at $I = 0.16A$. Hence, by comparing this DOP result (before polarisation enhancement) with the DOP result in the later tests (after polarisation enhancement); we can see the achievement of the V-stripe more easily.

- **Test 2 Stripe-A Angle, ϕ Vs DOP_B**

This test is to determine the best angle ϕ to place the stripe to obtain the maximum DOP_R. The DOP_R value is very important, as it is the first stage optimisation to obtain the polarisation-selective output. By having a large proportion of TE polarisation in the external input signal (P_{BI}), as it travels through stripe-B, TE

polarisation is getting amplified significantly. Hence this has made a major improvement to the polarisation-selective outcome. In this test we have compared 6 different angles for stripe-A, with 4 different Injection Currents to investigate at which angle it will generate more TE polarisation with less TM polarisation signal.

Parameters used:

ϕ	I_a (A)	w_a (μm)	d_a (μm)	$\Delta\theta$	Γ_e	Γ_h
11^o ~16^o	0.06	10	0.15	0.05^o	0.32	0.3

Table 5.5 Relevant stripe parameters for optimise the stripe-A angle in Test 2

Test Conditions	Condition 1	Condition 2
L_a (μm)	400	600

Table 5.6 Relevant parameters used in optimise the stripe-A angle in Test 2

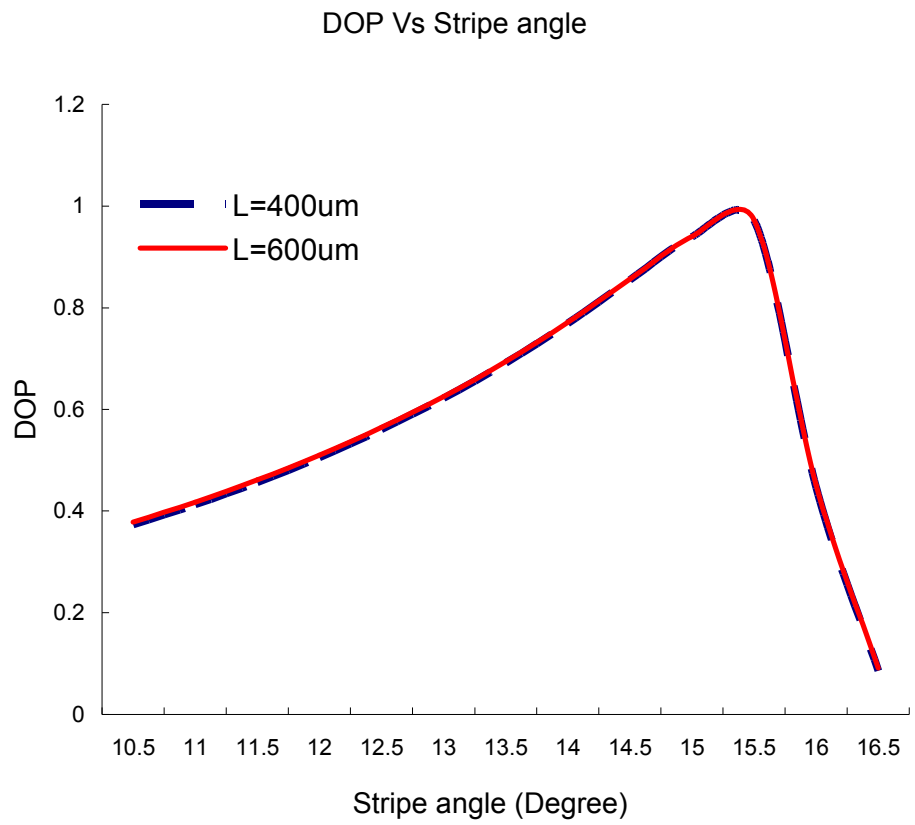

Figure 5.12 Comparison the DOP at stripe-A angles; where black dashed represents L_a=400μm and red line represents L_a=600μm

Fig.5.12 shows that by putting stripe-A at $15.25°$, which is slightly before the Brewster angle; P_{BI} has a large proportion of the TE polarisation. We have also tried different stripe structures (e.g. different stripe lengths and widths) to investigate the best stripe angle for comparison. The result comes out to be almost the same (the maximum output is when stripe at $15.25°$), based on the angular distribution calculation we have used. As a result, the next step of the optimisation is to consider the actual P_{BI}, at this stage, we assume the stripe angle for stripe-A and-B are the same.

Note, the simulation shows that by using $w_a = 20\mu m$, $L_a = 300\mu m$ at $I_a = 0.16A$, the Maximum angle become, $\theta_{Max} = \pm 3.8°$ (refer to Fig.5.9, $\theta_{Max} = \pm 1.4°$). In this case, the peak of Fig.5.14 will shift to $14°$, where the effect of intensity angular distribution become more significant.

- **Test 3 DOP_R**

In this test, stripes have been placed at $15.25°$, as the result in Test.1 shows that stripes at angle $15.25°$, which is exactly at the Brewster angle, produce the highest DOP_R, see Fig.5.13.

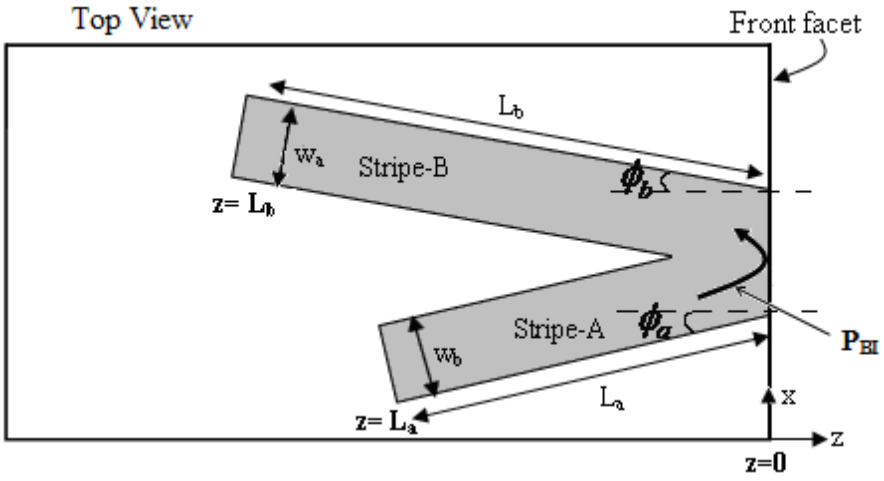

Figure 5.13 Schematic of the simulated point in Test 3 as referred to the "V"-geometry

Parameters used:

I_a (A)	w_a (μm)	d_a (μm)	$\Delta\theta$	ϕ	Γ_e	Γ_h
0.06~0.16	10	0.15	0.05^o	14^o	0.32	0.3

Table 5.7 Relevant stripe parameters for Test 3

Test Conditions	Condition 1	Condition 2	Condition 3
L_a (μm)	400	600	800

Table 5.8 Relevant parameters used in Test 3 for conditions 1-3

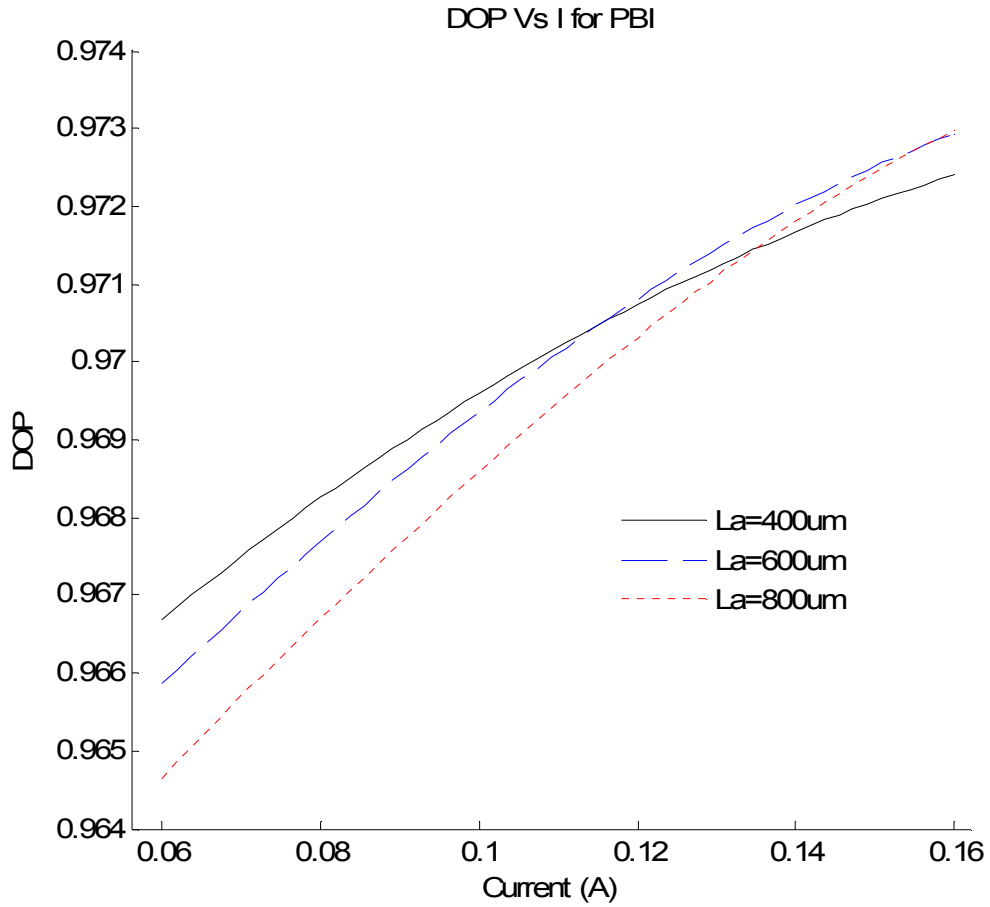

Figure 5.14 DOP of power reflected from stripe-A into stripe-B (P_{BI}); where black line represents L_a=400μm, blue dashed represents L_a=600μm and red dotted line indicates L_a=800μm

This result illustrated in Fig.5.14 shows that when lights travels at 15.25°, a small portion of TM polarised rays has been reflected into stripe-B (unlike in Chapter-4, all TM polarisation has been transmitted at Brewster angle); the amount is still small compared to TE polarisation.

- **Test 4 DOP_B**

This test is the most important test to this project, because this result has showed the impressive enhancement the V-stripe has given to achieve a polarisation-selective result. Fig.5.15 shows the schematic diagram of this test.

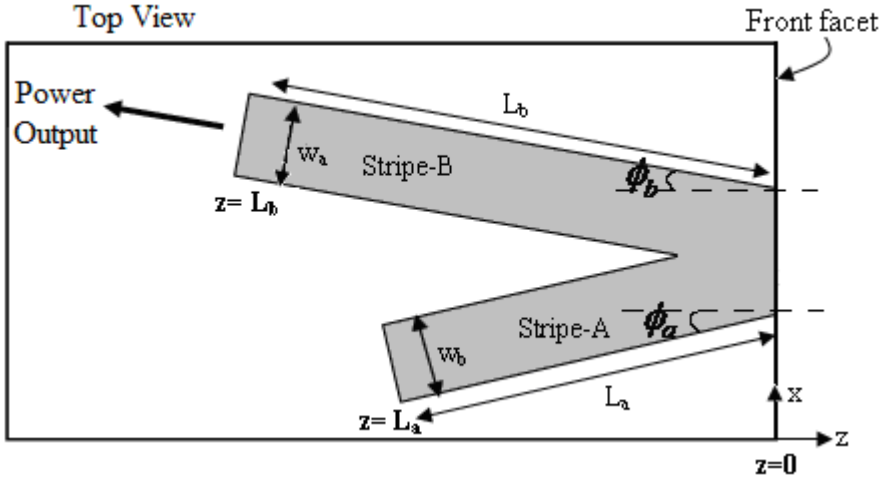

Figure 5.15 Schematic of the simulated point in Test 4 as referred to the "V"-geometry

Parameters used:

I_a (A)	I_b (A)	$w_a = w_b$ (μm)	$d_a = d_b$ (μm)	$\Delta\theta$	ϕ	Γ_e	Γ_h
0.06~0.16	0.06~0.16	10	0.15	0.05^o	14^o	0.32	0.3

Table 5.9 Relevant stripe parameters for Test 4

Test Conditions	Condition 1	Condition 2	Condition 3	Condition 4	Condition 5	Condition 6
L_a (μm)	400	400	400	600	600	600
L_b (μm)	400	600	800	400	600	800

Table 5.10 Relevant parameters used in Test 4 for conditions 1to 6

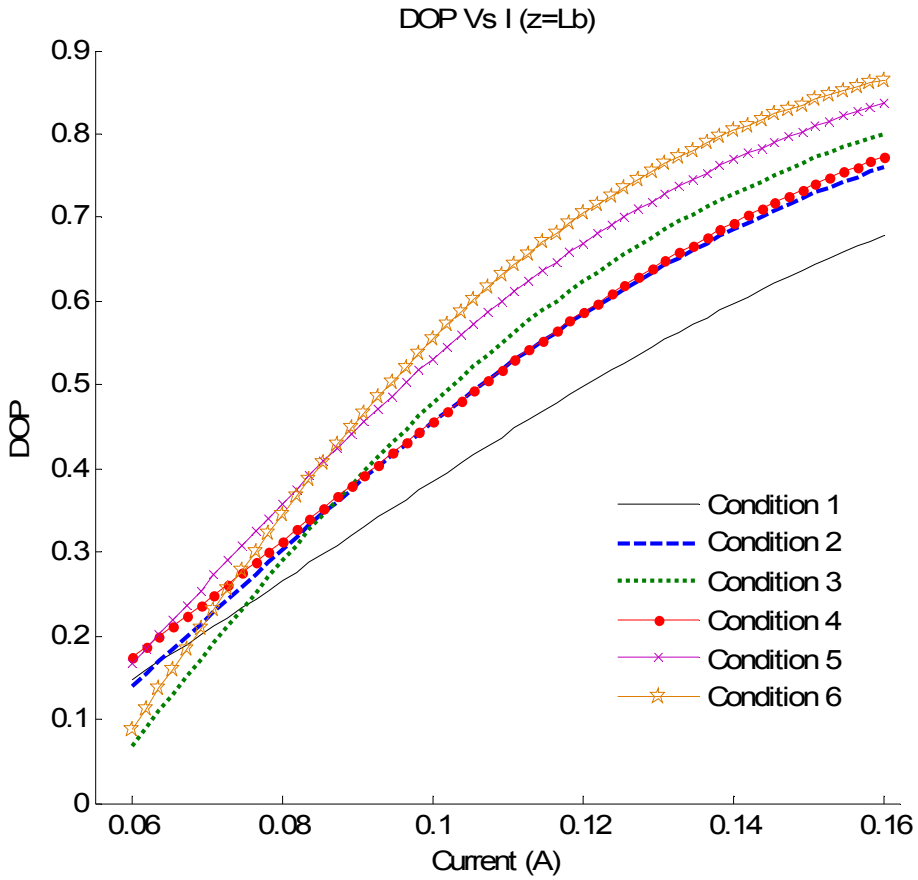

Figure 5.16 Comparison of DOP of different stripe lengths under the Test 4 conditions 1-6; where black line, condition 1; blue dashed, condition 2; green dotted, condition 3; red circled, condition 4; mauve crossed line, condition 5 and orange started, condition 6

In this test result illustrated in Fig.5.16, which under the same Injection Current for both stripe, and with different stripe length combinations under conditions 1-6, we can see that under condition 6, where $L_a = 600\mu m; L_b = 800\mu m$, it is the best DOP at relatively high current injection. Under condition 5, where $L_a = 600\mu m; L_b = 600\mu m$, both stripes have the same length, we have the second best DOP result in relatively high current; however in low current, with both stripes at $600\mu m$ we have the best DOP result, which means, overall with both stripes at $600\mu m$, the refined analysis of the V-stripe model can achieve the best performance in separating TE and TM polarisation, and of course, needs to have the same Injection Current for both stripes.

- **Test 5 DOP_B, with $I_a \neq I_b$**

In the previous test, we have tested the V-stripe model with different stripe length combinations, but all under the same current injection. In this test, we will continue testing the V-stripe to obtain better polarisation enhancement result by injecting different current into the two stripes, to find a better optimization result.

Parameters used:

$w_a = w_b$ (μm)	$d_a = d_b$ (μm)	$\Delta\theta$	ϕ	Γ_e	Γ_h
10	0.15	0.05^o	14^o	0.32	0.3

Table 5.11 Relevant stripe parameters for Test 5

Test Conditions	Condition 1	Condition 2	Condition 3	Condition 4	Condition 5	Condition 6
L_a (μm)	600	600	600	600	600	600
L_b (μm)	600	600	600	800	800	800
I_a (A)	0.06~0.16	0.16~0.26	0.06~0.16	0.06~0.16	0.16~0.26	0.06~0.16
I_b (A)	0.06~0.16	0.06~0.16	0.16~0.26	0.06~0.16	0.06~0.16	0.16~0.26

Table 5.12 Relevant parameters used in Test 5 with conditions 1to 6

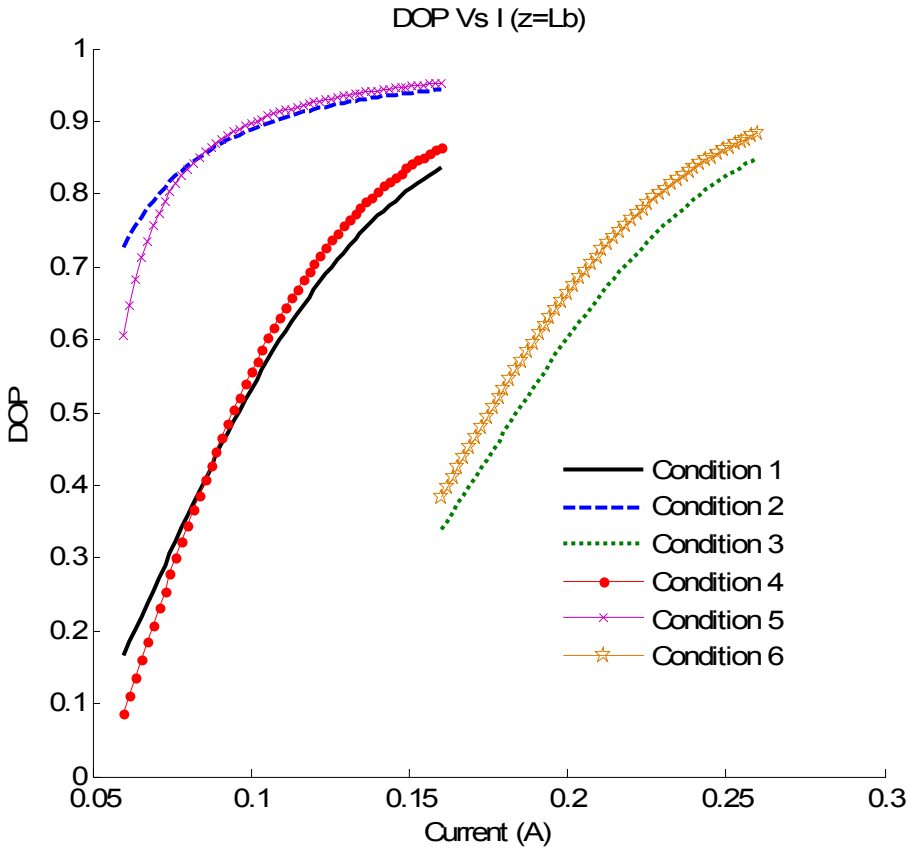

Figure 5.17 Comparison of DOP of different Injection Current under the Test 5 conditions 1-4; where black line is for test condition 1, blue dashed is condition 2 and dotted mauve is condition 3, condition 4 is represents by red circled

The result illustrated in Fig.5.17 shows that higher Injection Current in stripe-A will achieve a better polarisation-selective result as shown in conditions 2 and 5. Although in condition 5 ($L_a = 600\mu m; L_b = 800\mu m$) the DOP is slightly higher than condition 2 ($L_a = 600\mu m; L_b = 600\mu m$) for relatively high Injection Current, however, condition 2 gives an overall best optimisation result.

- **Test 6 DOP of Transmitted Power at $z = 0$**

The idea of considering the transmitted out of facet power is to prove if the V-stripe design can activate two applications at the same time, with one of the applications not requiring highly single polarised light.

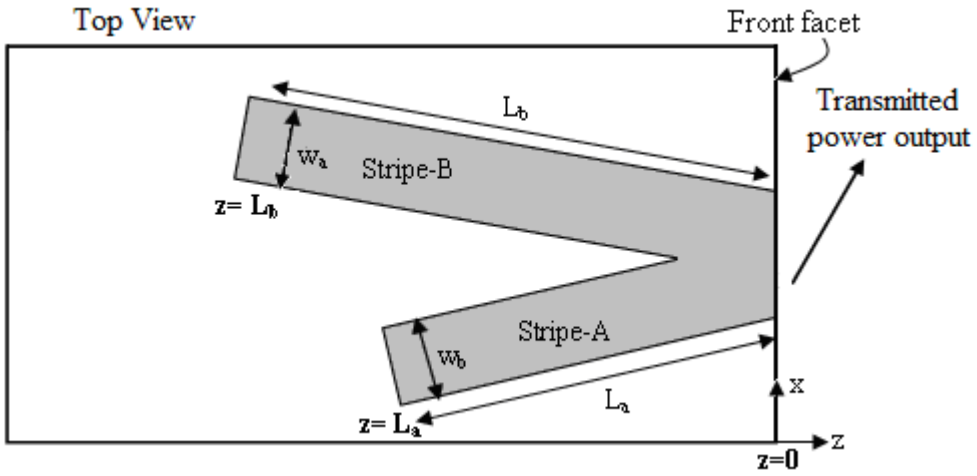

Figure 5.18 Schematic of the simulated point in Test 6 as referred to the "V"-geometry

Parameters used:

I_a (A)	w_a (μm)	d_a (μm)	$\Delta\theta$	ϕ
0.06~0.16	10	0.15	0.05^o	14^o

Table 5.13 Relevant stripe parameters for Test 6

Test Conditions	Condition 1	Condition 2	Condition 3	Condition 4	Condition 5	Condition 6
Γ_e	0.32	0.32	0.32	0.64	0.64	0.64
Γ_h	0.3	0.3	0.3	0.56	0.56	0.56
L_a (μm)	400	600	800	400	600	800

Table 5.14 Device relevant parameters used in Test 6 with conditions 1-6

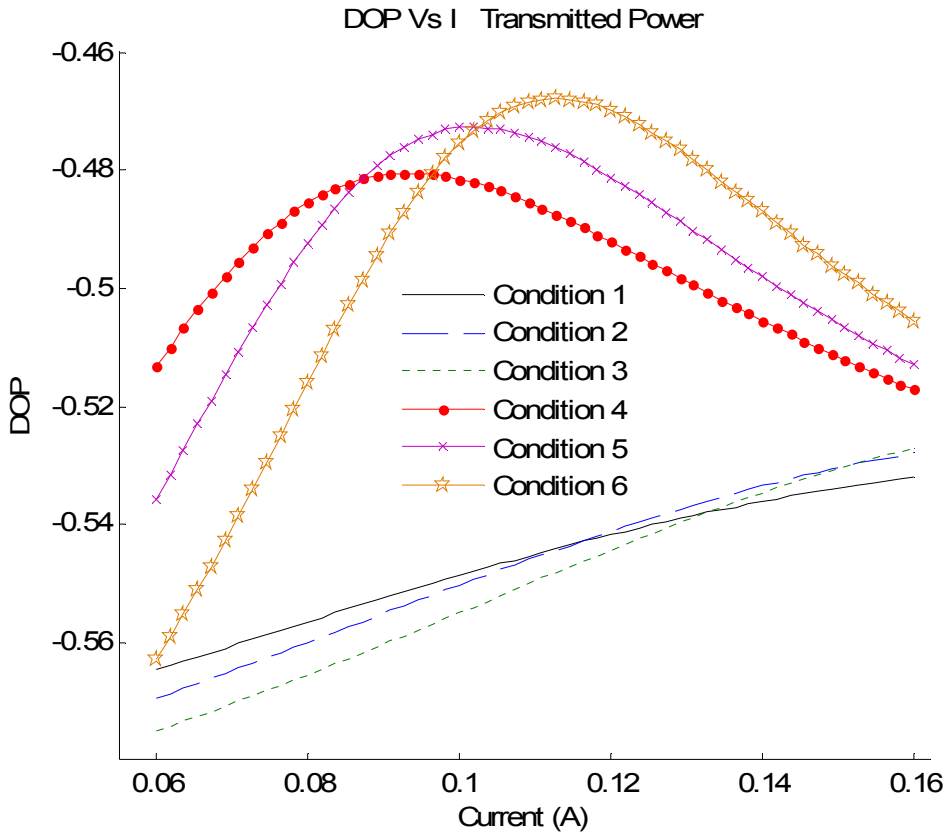

Figure 5.19 Comparison of DOP of transmitted out of facet power under the conditions in Test 6; where black line, condition 1; blue dashed, condition 2; green dotted, condition 3; red circled, condition 4; mauve crossed, condition 5 and orange started, condition 6

In this test illustrated in Fig.5.19 there is more TM polarisation in the transmitted out of facet power than TE polarisation; therefore, the value for DOP approaching -1 is the best polarisation-selective result. For conditions 1-3 $\Gamma_e = 0.32; \Gamma_h = 0.3$, and for condition 4-6 $\Gamma_e = 0.64; \Gamma_h = 0.56$; we can see that in general, with $\Gamma_e = 0.32; \Gamma_h = 0.3$, the transmitted power have better value for DOP. The result shows the transmitted power have relatively good DOP value, and there is a possibility to have some applications, which do not require highly single polarised signal to utilise the transmitted signal and that makes the V-stripe even more attractive, that it can operate two applications at the same time to maximise the resources.

5.5 Summary

The refined analysis of the V-stripe discussed in this chapter is an improved model to the approximate analysis of the V-stripe model. In Sec.5.2, we have discussed that one of the imperfections the V-stripe has is due to intensity angular distribution. The formulation of angular distribution of the intensity equation has been discussed in Sec.5.3, with a computer model to predict the effect of intensity angular distribution influence on the external input source to stripe-B (P_{BI}). The results show that by including the intensity angular distribution, the best stripe angle to place the stripe is at $15.25°$, slightly before the Brewster angle. In Sec.5.4, we presented explanations with the step by step test results of our refined analysis of V-stripe model. We have broken the test into three main steps, which are the DOP of power at facet, stripe-A; the DOP of power reflected into stripe-B (which is P_{BI}) and the DOP of the final optimised output from stripe-B.

Comparing the Test.4 results in this chapter (Fig.5.16), with the Test.4 result in Chapter-4 (Fig.4.15), we can see that, in the approximate analysis (Chapter-4), the best DOP result is with $L_a = 400\mu m; L_b = 800\mu m$, but in the realistic result (Chapter-5), the best DOP result is with both stripes at $600\mu m$. This is because the P_{BI} in Chapter-5 is less than in Chapter-4 (due to angular distribution of intensities affect), and stripe-B will produce it own TE and TM polarisation, so with less P_{BI} (in Chapter-5), it is better to use a relatively shorter stripe-B to achieve the best optimisation of a polarisation-selective result.

References 5

[1] F. Causa, J. Sarma, 'Realistic Model for the Output Bean Profile of Stripe and Tapered Superluminescent Light-Emitting Diodes', Applied Optics, Vol. 42, No. 21, pp. 4341-4348, July 2003

[2] F. Causa, J. Sarma and S. Yunus, **'Characterization of Angled Tapered Superluminescent LEDs'**, Applied Optics, Vol. 41, No 24, Aug 2002

[3] T. Kambayashi and J. Sarma, **'Spontaneous Emission Noise Distribution from a Gain-Guide Multimode Waveguide'**, IEEE J. Quantum Electron. QE-19, 1084-1091, 1983

Chapter 6:

Conclusions and Future Work

6.1 Conclusions

A compact model for polarisation-selective edge-emitting LED (ee-LED) has been developed, which is called the V-stripe ee-LED. Firstly, the single stripe contact ee-LED has been analysed, by using a numerical self consistent iteration scheme based on the weighted average constant carrier density $\bar{N}$ method. This numerical procedure is used to find the self-consistent value for the assumed constant carrier density. By use of this method, which is keeping constant $\bar{N}$ along z-direction, resulted in simplification in mathematical terms and the model providing highly accurate value of $\bar{N}$ in a short computational time. This model has been used to simulate the carrier density and also the forward and reverse travelling photon density within the device. From the single stripe model, it was observed that with the same Injection Current into the stripe, the shorter the stripe, the larger the output power is being generated. Moreover, the difference between TE and TM polarisation purely depends on the confinement factor difference.

Secondly, the single stripe contact model has been extended to apply in the V-stripe calculations. The V-stripe design has utilized the advantage of the Brewster angle, to separate the TE and TM polarisations in stripe-A, and use the stripe-B to maintain and amplify the reflected signal from stripe-A. The simulation results from the approximate analysis of the V-stripe model showed that the DOP of the power output from the V-stripe has a significant polarisation-enhancement than the angled stripe.

The result also showed that when using the same Injection Current for both stripes, with the stripe lengths $L_a = 400\mu m, L_b = 800\mu m$, the DOP of the output power from the V-stripe was the best, which was almost equal to 1, this means the V-stripe was performing as a single polarised stripe. From the simulation results, we also suggest that with a relatively higher current injected into stripe-A and a relatively lower current injected into stripe-B, it gave a better polarisation-selective result to the V-stripe.

Furthermore, the approximate analysis of the V-stripe model has been extended to include the angular distribution of intensity affect from stripe-A, to obtain a more realistic result. Thus, the external input signal for stripe-B was less than we predicted in the approximate analysis and the best angle to place the stripe is at $15.25°$, slightly before the Brewster angle. However, the simulation results proved that, even with a relatively small amount of single polarised external signal input (to stripe-B), we are still able to obtain a good polarisation-selective output. It was shown in the refined analysis of the V-stripe model simulation, with the same current injected into both stripes, and with both stripe lengths at $600\mu m$, it gives the best DOP of the output power, the value of DOP is in the region of 0.72 to 0.95 depending on the Injection Current. It is also suggested that with a relatively higher Injection Current to stripe-A and a relatively lower current injected into stripe-B, the polarisation-selective result can be enhanced.

6.2 Future Work

The work contained in this thesis has shown the optimization of the polarisation-selective output from a bulk material active layer semiconductor ee-LED. In Chapter-2, the research work has also made an assumption on using an effective relative permittivity and an effective refractive index to calculate the vertical mode in the multilayer media, hence, simplifying the mode as a PW propagating in a homogeneous media. In order to work on a more realistic case, a realistic vertical mode shape can be obtained; by using the actual number of different relative permittivities (for different layer of the multilayer) and refractive index.

Also in Chapter-2, in the modal gain calculation, we have omitted the effect of free carrier absorption, α_{fc}, in the cladding layer, since it is typically small compared to the material gain. It is suggested that for calculation accuracy, it is useful to put the free carrier absorption back into the model gain equation.

In Chapter-3, it was discussed that a weighted average constant carrier density ($\bar{N}$) is used in all Rate Equation related calculations to simplify the computational scheme in the whole research. However it is possible to obtain the variable carrier distribution $N(z)$ to refine the calculation by use the z-dependent Rate Equation solutions at the end of the iteration process. Hence put back the functions $P(z)$ and $Q(z)$ into Equation (4.3) to finally derive a z-dependent carrier density profile, [1].

Moreover, in Chapter-5, the formulation of angular distribution of intensities, an approximation of Maximum angle ($\theta_{Max} = \tan^{-1}(\frac{w}{L})$) has been used, in order to integrate the photon density along the z-axis. A problem occurred when stripe length increases, θ_{Max} becomes a very small angle if the stripe is narrow and long,

$\theta_{Max} \approx \frac{w}{L}$. Therefore, rays travelling inside the stripe are almost at the same angle. We suggest improving this imperfection, firstly, it is necessary to obtain a realistic intensity angular distribution, [3], [4]. Secondly, we need to consider the effective reflected light, which is the actual amount of light being reflected into stripe-B. By combining the realistic angular distribution of intensities and the effective reflected light, the V-stripe model can be enhanced.

Furthermore, it is worth and necessary to take the current spreading and carrier diffusion into account to complete the V-shaped model. Because in a typical ee-LED device, the Injection Current is mainly flowing in the centre region. But once the current comes out from the stripe, it spreads laterally in the cladding layer, [4], [5]. This results in current density distribution. But in the calculations throughout this project, it is assumed that current injected into the stripe are flowing only along the $y-axis$, current spreading has been ignored. The spreading of current also causes carrier diffusion, and together, they will cost light spreading and influence the consideration of choosing correct thickness of an active layer.

Reference 6

[1] C.F. HO, 'Integrated Optical Control of Semiconductor Optical Source', MPhil Thesis, University of Bath, 2006

[2] T. Kambayashi and J. Sarma, **'Spontaneous Emission Noise Distribution from a Gain-Guide Multimode Waveguide'**, IEEE J. Quantum Electron. QE-19, 1084-1091, 1983

[3] F. Causa, J. Sarma and S. Yunus, **'Characterization of Angled Tapered Superluminescent LEDs'**, Applied Optics, Vol. 41, No 24, Aug 2002

[4] S. Yunus, **'Development and Study of High Power tapered Geometry Superluminescent Diodes'**, PHD Thesis, University of Bath, 2002

[5] J. Sarma, F. Causa, N.S. Brooks, S. Yunus, T. Ryan, and I. Middlemast, **'Characteristics of Material for Optoelectronics Device Applications'**, Poster presentation at 1999 Users Workshop-Industrial Liason Meeting, Engineering and Physical Sciences Research Council, Sheffield Central Facility for Ⅲ-Ⅴ Semiconductors, July 1999

Appendix A

Photon and Current Density Conservation

A.1 Photon Conservation

---Spontaneous emission

Firstly, by considering an optically active media (active layer) in which there is optical absorption or gain (when sufficient inversion population density exist), illustrated in Fig.A.1. Within the derivation uniformity along x and y direction is assumed and only variation in the z direction is considered, photon either travelling in the positive or negative z direction.

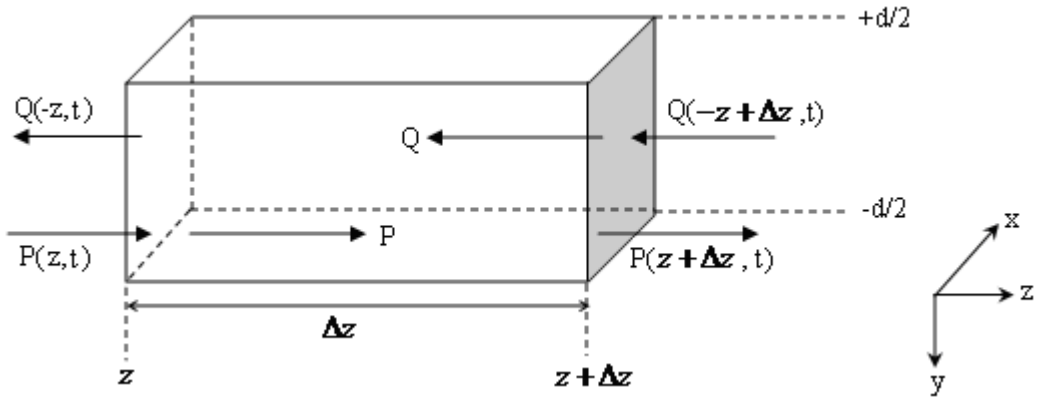

Figure A.1 A diagram illustrating photons passing through a volume element of length Δz and unit cross sectional area.

Let the photon density per unit effective volume of forward travelling photons, which is travelling in positive z direction in this active medium, be P , and the reverse travelling photons, be Q. As referred to Fig.A.1, the increase in the net number of forward travelling photons in this volume at the given time Δt is:

$$[P(z,t+\Delta t)-P(z,t)]\Delta V \qquad \text{(A1)}$$

Where ΔV is the volume of the active media and $\Delta V = \Delta x.\Delta y.\Delta z$. Consider a density

of photons, P, of unit cross sectional area passing through the active media with a uniform velocity v in the positive z direction. The number of photons entering and leaving this volume ΔV after a time Δt can be written as,

Entering $$P(z,t).\Delta x.\Delta y.v.\Delta t \qquad \text{(A2)}$$

Leaving $$P(z+\Delta z,t).\Delta x.\Delta y.v.\Delta t \qquad \text{(A3)}$$

The change in net number of photons in the volume at a time Δt is:

$$[P(z+\Delta z,t)-P(z,t)].\Delta x.\Delta y.v.\Delta t \qquad \text{(A4)}$$

Hence, the net number of photons in the active media after a time Δt is equal to the change in the net number of photons in the media plus the number of photons which have been generated. In the active layer, photons are generated via two processes: spontaneous emission and stimulated emission (which has been discussed in Chapter-2, Sec.2.1).

---The Spontaneous Emission Contribution

Spontaneous emission occurs at random and therefore gives incoherent radiation, it also emits in all directions (isotropic radiation), in many wavelengths, phase and polarisation. Fraction of spontaneous emission assuming spontaneous emission isotropic radiation over solid angle 4π, as shown in Fig.A.2, $(\Delta\Omega)_f$ is considered to contribute to P, [1].

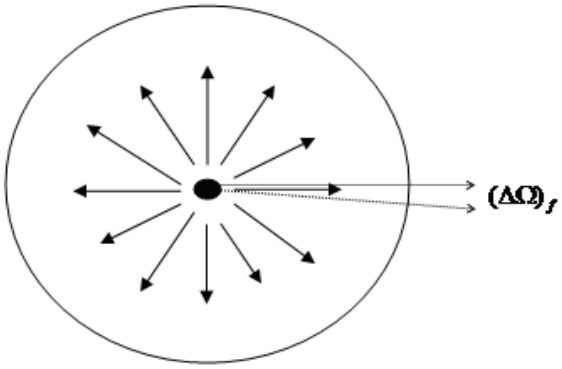

Figure A.2 Spontaneous emission isotropic radiations over full solid angle 4π .

Therefore, the fraction of the isotropic radiation is contributes to the forward travelling photons becomes,

$$\delta_f = (\Delta\Omega)_f / 4\pi \qquad \text{(A5)}$$

vice versa for the considered to contribute to Q that $\delta_r = (\Delta\Omega)_r / 4\pi$

Here for simplicity polarisation and wavelength dependencies are ignored. Also since only the forward travelling photons are considered, only a fraction of the isotropic radiation actually contributes to the forward travelling photons. Therefore contribution from spontaneous emission in the volume at a time Δt can be written as:

$$\delta_f . \frac{N}{\tau_{sp}} . \Delta V . \Delta t \qquad \text{(A6)}$$

where N is the carrier density and τ_{sp} is the spontaneous emission recombination lifetime; and $\tau_{sp} = \dfrac{1}{B_r (N + N_d)}$, where B_r $(cm^3 / s)$is bimolecular recombination constant, and N_d is doping carrier density, which is very small compare to N, and sometimes can be neglected.

---Stimulated Emission

Contrary to spontaneous emission, stimulated emission gives coherent radiation due to all photons released have identical wavelength, phase, polarisation and direction. In this case, within the active layer, photons add in a constructive manner providing amplification. The net number of stimulated emission in the volume at a time Δt is:

$$\tilde{g}(N).P(z,t).\Delta t.\Delta V \qquad \text{(A7)}$$

where $\tilde{g}$ is the material gain in unit time^{-1}

Hence, by using equation (A4), (A6) and (A7), the net number of forward travelling photon densities in the media after a time Δt is:

$$\begin{aligned} &P((z,t+\Delta t)-P(z,t)).\Delta x.\Delta y.\Delta z = (P(z,t)-P(z+\Delta z,t)).\Delta x.\Delta y.v.\Delta t + \\ &[\tilde{g}(N).P(z,t)+\delta_f.B_r(N+N_d)N].\Delta x.\Delta y.\Delta z.\Delta t \end{aligned} \qquad \text{(A8)}$$

where δ_f represent the fraction of spontaneous emission in the forward direction

Dividing equation (A8) through by $\Delta x, \Delta y, \Delta z, \Delta t$ and taking the limit of Δz tends to zero and Δt tends to zero give the differential Photon Rate Equation for the forward travelling photon density, which represented by the notation $P(z,t)$ is:

$$\frac{\partial P}{\partial t} = -v\frac{\partial P}{\partial z} + \tilde{g}(N)P + \delta_f B_r(N+N_d)N \qquad \text{(A9)}$$

The Photon Rate Equation for the reverse travelling photon density, which represented by the notation $Q(z,t)$, can be derived as:

$$\frac{\partial Q}{\partial t} = v\frac{\partial Q}{\partial z} + \tilde{g}(N)Q + \delta_r B_r(N+N_d)N \qquad \text{(A10)}$$

Where δ_r represents the fraction of spontaneous emission in the reverse direction

For solutions with no time variation $\frac{\partial}{\partial t} = 0$ (i.e. steady state solution) [2], the photon Rate Equations for forward and reverse travelling photon densities, $P(z), Q(z)$, are:

$$\frac{dP}{dz} = g(N)P + \delta_f \frac{B_r(N+N_d)N}{v} \qquad \text{(A11)}$$

$$\frac{dQ}{dz} = -g(N)Q + \delta_r \frac{B_r(N+N_d)N}{v} \qquad \text{(A12)}$$

Where $g(N) = \dfrac{\tilde{g}(N)}{v}$ is the material gain in unit volume^{-1}

Note, in the derivation of the Photon Rate Equation phase effects were not been considered since in the case of LEDs a spread of wavelengths exists.

A.2 Current density conservation

The current density conservation equation derivation gives the relationship between carrier density (N) and current density (J). Consider the device structure below:

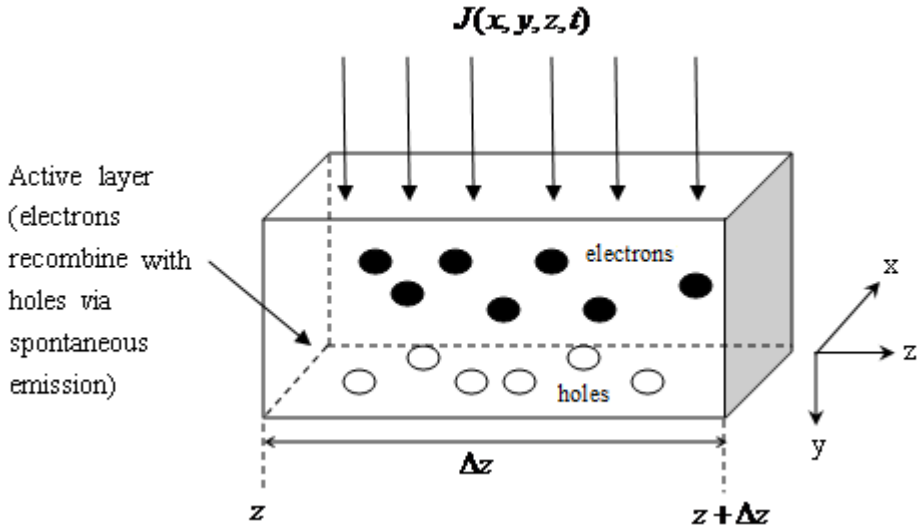

Figure A.3 A diagram illustrating the flow of current into the device active layer and the recombination of elections and holes within the device active layer.

In the derivation, current density is assumed to be constant throughout the rectangular striped region, which has neglected the current spreading and carrier diffusion. It has also assumed that current density is evenly distributed throughout the active layer thickness that $J = J_0$. The number of particles entering and leaving in this volume $\Delta V = \Delta x.\Delta y.\Delta z$ at the given time Δt is:

Entering $$\frac{J(x,y,z,t)}{q}.\Delta x.\Delta z.\Delta t.v \qquad \text{(A13)}$$

Leaving $$\frac{J(x,y-\Delta y,z,t)}{q}.\Delta x.\Delta z.\Delta t.v \qquad \text{(A14)}$$

where q is the electron charge.

Therefore, the increased net number of particles in the volume ΔV at time Δt is:

$$\frac{1}{q}[J(x,y,z,t)-J(x,y-\Delta y,z,t)].\Delta x.\Delta z.\Delta t.v \qquad \text{(A15)}$$

The increased carriers in the volume ΔV at time Δt by definition are:

$$[N(x,y,z,t+\Delta t)-N(x,y,z,t)].\Delta x.\Delta y.\Delta z \qquad \text{(A16)}$$

Nevertheless, the depletion of carriers which causes by the recombination due to spontaneous emission and stimulated emission must be taken into account.

The total number of particles recombining in the time Δt during spontaneous emission and stimulated emission are:

Spontaneous Emission $$B_r(N+N_d)N.\Delta x.\Delta y.\Delta z.\Delta t \qquad \text{(A17)}$$

Stimulated Emission $$g(N)[P+Q].\Delta x.\Delta y.\Delta z.\Delta t \qquad \text{(A18)}$$

where g is the material gain in units of volume^{-1}, P and Q are representing the forward and reverse travelling photon density respectively.

Hence, the increased carriers in the active layer after a time Δt is equal to the increased net number of particles in the volume ΔV minus the total number of particles recombining via spontaneous emission and stimulated emission. This can be written as:

$$[N(x,y,z,t+\Delta t)-N(x,y,z,t)].\Delta x.\Delta y.\Delta z=\frac{1}{q}[J(x,y,z,t)-J(x,y-\Delta y,z,t)].\Delta x.\Delta z.\Delta t.v - [g(N)(P+Q)+B_r(N+N_d)N].\Delta x.\Delta y.\Delta z.\Delta t \qquad \text{(A19)}$$

Dividing equation (A19) through by $\Delta x, \Delta y, \Delta z, \Delta t$ and taking the limit of Δy tends to zero and Δt tends to zero give the differential current density conservation equation, which is:

$$\frac{\partial N}{\partial t} = \frac{1}{qv}\frac{\partial J_0}{\partial y} - [g(N)(P+Q) + \frac{B_r(N+N_d)N}{v}] \qquad \text{(A20)}$$

The steady state solution to above equation is:

$$\frac{J_0}{qdv} = g(N)(P+Q) + \frac{B_r(N+N_d)N}{v} \qquad \text{(A21)}$$

References Appendix A

[1] J. Sarma, **'Optical Devices and Systems'**, EE40130, Lecture Notes

[2] J. Wilson and J.F.B. Hawkes, **'Optoelectronics An Introduction'**, Second Edition, 1989

Appendix B-1

Photon Conservation Rate Equation

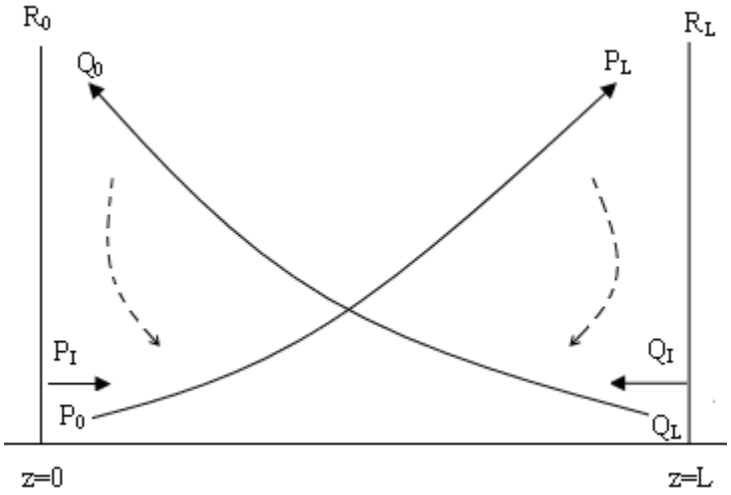

Figure B1.1 Schematic diagram of an optical cavity bound by parallel facets with reflectivity R_0 and R_L. *P(z), Q(z)* are the travelling direction of photon densities; P_I, Q_I are the external input sources.

$$Let \quad \overline{p}_{sp} = \frac{\delta_f B_r (\overline{N} + N_d)\overline{N}}{\overline{g}v} \qquad \text{(B1.1)} \quad , \quad Let \quad \overline{q}_{sp} = \frac{\delta_r B_r (\overline{N} + N_d)\overline{N}}{\overline{g}v} \qquad \text{(B1.2)}$$

Where $\overline{N}$ is the constant carrier density (cm^{-3}); N_d is the doping carrier density; $\overline{g}$ is the material gains (m^{-1}), B_r is the bi-modular recombination constant (cm $second^{-1}$), v is the velocity of light in the medium (cm $second^{-1}$) and $\delta_{f,r}$ represents the fraction of spontaneous emission in the forward and reverse direction.

$$\frac{dP(z)}{dz} = \overline{g}[P(z) + \overline{p}_{sp}] \qquad \text{(B1.3)}$$

$$\frac{dQ(z)}{dz} = -\overline{g}[Q(z) + \overline{q}_{sp}] \qquad \text{(B1.4)}$$

$\overline{q}_{sp}, \overline{p}_{sp}, \overline{N}, g(\overline{N})$ are constants

$$\hat{P}(z) = P(z) + \overline{p}_{sp} \qquad \text{(B1.5)}$$

$$\hat{Q}(z) = Q(z) + \overline{q}_{sp} \qquad \text{(B1.6)}$$

Substituting (B1.6) into (B1.4)

$$\frac{dP(z)}{dz} = \bar{g}\hat{P}(z) \qquad \text{(B1.7)}$$

Substituting (B1.7) into (B1.5)

$$\frac{dQ(z)}{dz} = \bar{g}\hat{Q}(z) \qquad \text{(B1.8)}$$

$$\hat{P}(z) = \hat{P}_o e^{\bar{g}z} \qquad \text{(B1.9)}$$

$$\hat{Q}(z) = \hat{Q}_o e^{-\bar{g}z} \qquad \text{(B1.10)}$$

Substituting (B1.6) into (B1.10)

$$P(z) = P_o e^{\bar{g}z} + \bar{p}_{sp}[e^{\bar{g}z} - 1] \qquad \text{(B1.11)}$$

Substituting (B1.7) into (B1.11)

$$Q(z) = Q_o e^{-\bar{g}z} + \bar{q}_{sp}[e^{-\bar{g}z} - 1] \qquad \text{(B1.12)}$$

At z=L,

$$P_L = P_o e^{\bar{g}L} + (e^{\bar{g}L} - 1)\bar{p}_{sp} \qquad \text{(B1.13)}$$

$$Q_L = e^{-\bar{g}L}[Q_o - (e^{\bar{g}L} - 1)\bar{q}_{sp}] \qquad \text{(B1.14)}$$

Apply Boundary conditions

$$P_o = P_I + R_o Q_o \qquad \text{(B1.15)}$$

$$Q_L = R_L P_L \qquad \text{(B1.16)}$$

Substituting (B1.14) & (B1.15) into (B1.17)

$$Q_o = R_L e^{2\bar{g}L} P_o + R_L e^{\bar{g}L}(e^{\bar{g}L} - 1)\bar{p}_{sp} + (e^{\bar{g}L} - 1)\bar{q}_{sp} \qquad \text{(B1.17)}$$

Now use $P_o = P_I + R_o Q_o$, For Boundary Condition

$$P_o = \frac{P_I + R_o R_L e^{\bar{g}L}(e^{\bar{g}L} - 1)\bar{p}_{sp} + R_o(e^{\bar{g}L} - 1)\bar{q}_{sp}}{1 - R_o R_L e^{2\bar{g}L}} \tag{B1.18}$$

Forward travelling photon at output, $P_L = P(z = L)$

$$P_L = \frac{P_I e^{\bar{g}L} + (e^{\bar{g}L} - 1)(\bar{p}_{sp} + R_o e^{\bar{g}L}\bar{q}_{sp})}{1 - R_o R_L e^{2\bar{g}L}} \tag{B1.19}$$

For Boundary condition $Q_L = R_L P_L$,

$$Q_L = \frac{R_L P_I e^{\bar{g}L} + R_L(e^{\bar{g}L} - 1)(\bar{p}_{sp} + R_o e^{\bar{g}L}\bar{q}_{sp})}{1 - R_o R_L e^{2\bar{g}L}} \tag{B1.20}$$

Expressions for forward and reverse photon densities in $\bar{N}$ -dependent

$$P(\bar{N}) = \frac{1}{L}[\frac{P_0}{\bar{g}}(e^{\bar{g}L} - 1) + \frac{\bar{P}_{sp}}{\bar{g}}(e^{\bar{g}L} - 1) - \bar{P}_{sp}L] \tag{B1.21}$$

$$Q(\bar{N}) = -\frac{1}{L}[\frac{Q_0}{\bar{g}}(e^{-\bar{g}L} - 1) + \frac{\bar{q}_{sp}}{\bar{g}}(e^{-\bar{g}L} - 1) + \bar{q}_{sp}L] \tag{B1.22}$$

For Carrier Density Equation:

$$\frac{J}{qdv} = \bar{g}[P(\bar{N}) + Q(\bar{N})] + \frac{B_r(\bar{N} + N_d)\bar{N}}{v} \tag{B1.23}$$

where J is current density (A/cm^2), q is Electron charge (1.602×10^{-19} C), d is the thickness of optical active layer (μm)

Appendix B-2

Polarisation Decomposed Photon Conservation Rate Equation

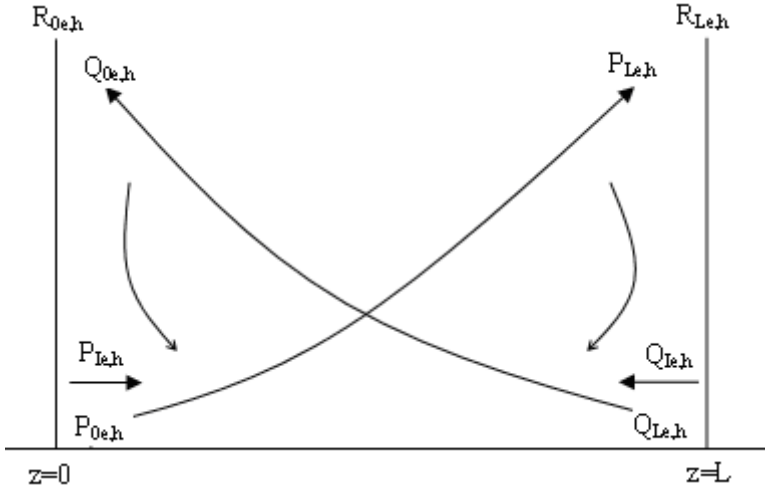

Figure B2.1 Schematic of an optical cavity formed by parallel facets with TE and TM polarisation reflectivities $R_{0e,h}$ and $R_{Le,h}$. $P_{e,h}$, $Q_{e,h}$ are the travelling direction of photon densities; $P_{Ie,h}$, $Q_{Ie,h}$ are the external input sources.

Equations for TE (e) polarised photon:

Optical Gain (g)

$$\overline{g} = A_0 \times (\overline{N} - N_{tr}) \qquad \text{(B2.1)}; \qquad \overline{g}_e = \Gamma_e \times \overline{g} \qquad \text{(B2.2)}$$

Spontaneous Emission

$$\overline{P}_{spe} = \frac{\delta_f B_r (\overline{N} + N_d)\overline{N}}{\overline{g}_e v} \qquad \text{(B2.3)}$$

$$\overline{Q}_{spe} = \frac{\delta_r B_r (\overline{N} + N_d)\overline{N}}{\overline{g}_e v} \qquad \text{(B2.4)}$$

Where A_0 is material constant (cm^{-3}); $\overline{N}$ is the constant carrier density (cm^{-3}); N_{tr} is the transparency carrier density; N_d is the doping carrier density; $\overline{g}_{e,h}$ are the

material gains for TE and TM polarisation (m^{-1}), B_r is the bi-modular recombination constant (cm $second^{-1}$), v is the velocity of light in the medium (cm $second^{-1}$) and $\delta_{f,r}$ represents the fraction of spontaneous emission in the forward and reverse direction.

Let $P_{oe} = P_e(z=0)$; $P_{Le} = P_e(z=L)$; $Q_{oe} = Q_e(z=0)$; $Q_{Le} = Q_e(z=L)$

Photon density changes with z in the active layer. The solution to $\frac{dP(z)}{dz}$ and $\frac{dQ(z)}{dz}$ gives the expression for the forward and reverse travelling photon densities for TE polarisation.

$$\because P_e(z) = P_{0e}e^{\bar{g}z\Gamma_e} + \bar{p}_{spe}(e^{\bar{g}z\Gamma_e} - 1) \quad \text{(B2.5)}$$

$$Q_e(z) = Q_{0e}e^{-\bar{g}z\Gamma_e} + \bar{q}_{spe}(e^{-\bar{g}z\Gamma_e} - 1) \quad \text{(B2.6)}$$

Apply Boundary Conditions

$$P_{0e} = P_{Ie} + R_{0e}Q_{0e} \quad \text{(B2.7)}; \qquad Q_{Le} = Q_{Ie} + R_{Le}P_{Le} \quad \text{(B2.8)}$$

Therefore,

$$P_{0e} = \frac{P_{Ie} + R_{0e}Q_{Ie}e^{\bar{g}_e L} + (e^{\bar{g}_e L} - 1)(R_{0e}R_{Le}e^{\bar{g}_e L}\bar{p}_{spe} + R_{0e}\bar{q}_{spe})}{1 - R_{0e}R_{Le}e^{2\bar{g}_e L}} \quad \text{(B2.9)}$$

$$P_{Le} = \frac{P_{Ie}e^{\bar{g}_e L} + R_{0e}Q_{Ie}e^{2\bar{g}_e L} + (e^{\bar{g}_e L} - 1)(R_{0e}e^{\bar{g}_e L}\bar{q}_{spe} + \bar{p}_{spe})}{1 - R_{0e}R_{Le}e^{2\bar{g}_e L}} \quad \text{(B2.10)}$$

$$Q_{0e} = Q_{Ie}e^{\bar{g}_e L} + R_{Le}e^{2\bar{g}_e L}P_{0e} + R_{Le}e^{\bar{g}_e L}(e^{\bar{g}_e L} - 1)\bar{p}_{spe} + (e^{\bar{g}_e L} - 1)\bar{q}_{spe} \quad \text{(B2.11)}$$

$$Q_{Le} = Q_{Ie} + \frac{P_{Ie}e^{\bar{g}_e L}R_{Le} + R_{0e}Q_{Ie}e^{2\bar{g}_e L}R_{Le} + (e^{\bar{g}_e L} - 1)(R_{0e}e^{\bar{g}_e L}\bar{q}_{spe} + \bar{p}_{spe})R_{Le}}{1 - R_0 R_L e^{2\bar{g}_e L}} \quad \text{(B2.12)}$$

Expressions for forward and reverse photon densities in $\overline{N}$ -dependent

$$P_e(\overline{N}) = \frac{1}{L}[\frac{P_{0e}}{\overline{g}_e}(e^{\overline{g}_e L} - 1) + \frac{\overline{P}_{spe}}{\overline{g}_e}(e^{\overline{g}_e L} - 1) - \overline{P}_{spe} L] \qquad \text{(B2.13)}$$

$$Q_e(\overline{N}) = -\frac{1}{L}[\frac{Q_{0e}}{\overline{g}_e}(e^{-\overline{g}_e L} - 1) + \frac{\overline{q}_{spe}}{\overline{g}_e}(e^{-\overline{g}_e L} - 1) + \overline{q}_{spe} L] \qquad \text{(B2.14)}$$

Equations for TM (h) polarised photon:

The Rate Equations for TM(h) polarisation is in the exact format as TE(e) polarisation, except the optical gain for TM polarisation is depends on the TM confinement factor, where $g_h = g \times \Gamma_h$.

Carrier Density Equation:

$$\frac{J}{qdv} = \overline{g}_e[P_e(\overline{N}) + Q_e(\overline{N})] + \overline{g}_h[P_h(\overline{N}) + Q_h(\overline{N})] + \frac{B_r(\overline{N} + N_d)\overline{N}}{v} \qquad \text{(B2.15)}$$

where J is current density (A/cm^2), q is Electron charge (1.602×10^{-19} Coul), d is the thickness of optical active layer (μm).

Appendix C

Polarisation Decomposed Carrier Conservation Rate Equation for the V-Stripe

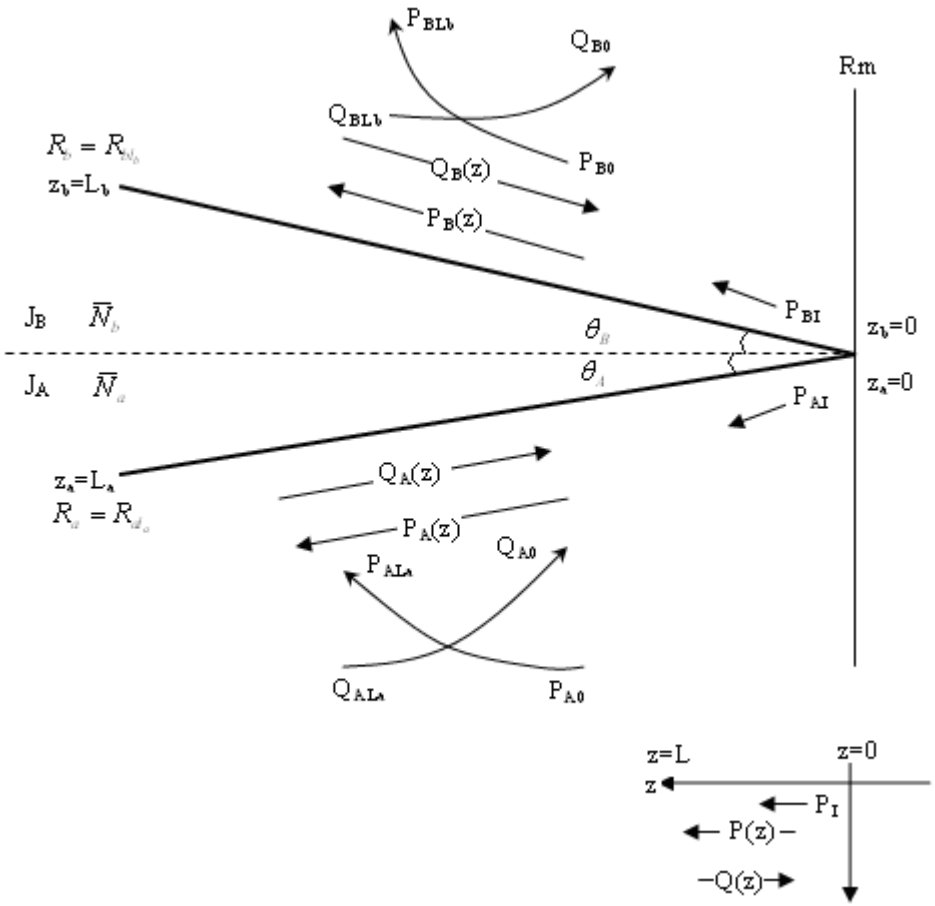

Figure C.1 Schematic diagram of an optical cavity bound by facet reflectivities R_{aLa} and R_{bLb} for stripes-A and -B. $P_{A,B}(z)$ /$Q_{A,B}(z)$ indicated the photon density travelling direction; P_{AI}/P_{BI} are due to optical inputs at z=0

For TE (e) polarised photon

let $R_{me}(\theta_A) = R_{meA}$; $R_{me}(\theta_B) = R_{meB}$

$R_{me}(\theta_A)$ in which the photon reflected back into Region A = R_{meAA}

$R_{me}(\theta_A)$ in which the photon transmitted into Region B = R_{meAB}

In Region A

Then forward and reverse photon density is represent by $P_{Ae}(z_a)$ and $Q_{Ae}(z_a)$

$$P_{A0e} = P_{Ae}(z_a = 0); \qquad Q_{A0e} = Q_{Ae}(z_a = 0)$$

$$P_{AL_ae} = P_{Ae}(z_a = L_a); \qquad Q_{AL_ae} = Q_{Ae}(z_a = L_a)$$

Spontaneous emission

$$\overline{P}_{spAe} = \frac{\delta_{fA} B_r (\overline{N}_a + N_d)\overline{N}_a}{\overline{g}_{Ae} v} \quad \text{(C1)}; \qquad v = \frac{c}{n_1} \quad \text{(C2)}$$

$$\overline{Q}_{spAe} = \frac{\delta_{rA} B_r (\overline{N}_a + N_d)\overline{N}_a}{\overline{g}_{Ae} v} \quad \text{(C3)}$$

$$\delta_{fa} = \delta_{ra} \frac{w_a \times a\cos\left(\frac{n_1}{n_2}\right)}{2 \times 3.14 \times L_a} \quad \text{(C4)}$$

$$\overline{g}_A = A_0 \times (\overline{N}_a - N_{tr}); \quad \text{(C5)} \qquad \overline{g}_{Ae} = \overline{g}_A \times \Gamma_e \quad \text{(C6)}$$

where A_0 is material constant (cm^{-3}); $\overline{N}_a$ is the constant carrier density in stripe-A (cm^{-3}); N_{tr} is the transparency carrier density; N_d is the doping carrier density; $\overline{g}_{e,h}$ are the material gains for TE and TM polarisation (m^{-1}); Γ_e is the confinement factor for TE polarisation; B_r is the bi-modular recombination constant (cm second^{-1}); v is the velocity of light in the medium (cm second^{-1}) and $\delta_{f,r}$ represents the fraction of spontaneous emission in the forward and reverse direction.

Applying Boundary Condition

$$P_{A0e} = P_{AIe} + R_{meAA}Q_{A0e}\text{, where } P_{AIe} = R_{meBA}Q_{B0e} \qquad \text{(C7)}$$

$$Q_{AL_ae} = R_{aLe}P_{AL_ae} \qquad \text{(C8)}$$

$$Q_{A0e} = R_{aL_ae}e^{2\bar{g}_{Ae}L_a}P_{A0e} + R_{aL_ae}e^{\bar{g}_{Ae}L_a}(e^{\bar{g}_{Ae}L_a}-1)\bar{p}_{spAe} + (e^{\bar{g}_{Ae}L_a}-1)\bar{q}_{spAe} \qquad \text{(C9)}$$

$$P_{A0e} = \frac{P_{AIe} + R_{meAA}(e^{\bar{g}_{Ae}L_A}-1)(R_{aL_ae}e^{\bar{g}_{Ae}L_a}\bar{p}_{spAe} + \bar{q}_{spAe})}{1 - R_{meAA}R_{aL_ae}e^{2\bar{g}_{Ae}L_a}} \qquad \text{(C10)}$$

$$P_{AL_ae} = \frac{P_{AIe}e^{\bar{g}_{Ae}L_a} + (e^{\bar{g}_{Ae}L_a}-1)(R_{meAA}e^{\bar{g}_{Ae}L_a}\bar{q}_{spAe} + \bar{p}_{spAe})}{1 - R_{meAA}R_{aL_ae}e^{2\bar{g}_{Ae}L_a}} \qquad \text{(C11)}$$

$$Q_{AL_ae} = \frac{P_{AIe}e^{\bar{g}_{Ae}L_a}R_{aL_ae} + R_{aL_ae}(e^{\bar{g}_{Ae}L_a}-1)(R_{meAA}e^{\bar{g}_{Ae}L_a}\bar{q}_{spAe} + \bar{p}_{spAe})}{1 - R_{meAA}R_{aL_ae}e^{2\bar{g}_{Ae}L_a}} \qquad \text{(C12)}$$

where $P_{AIe} = R_{mBAe}[R_{bL_be}e^{2\bar{g}_{Be}L_b}P_{B0e} + R_{bL_be}e^{\bar{g}_{Be}L_b}(e^{\bar{g}_{Be}L_b}-1)\bar{p}_{spBe} + (e^{\bar{g}_{Be}L_b}-1)\bar{q}_{spBe}]$

Expressions for forward and reverse photon densities in $\bar{N}$ -dependent

$$P_{Ae}(\bar{N}_a) = \frac{1}{L_a}[\frac{P_{A0e}}{\bar{g}_{Ae}}(e^{\bar{g}_{Ae}L_a}-1) + \frac{\bar{P}_{spAe}}{\bar{g}_{Ae}}(e^{\bar{g}_{Ae}L_a}-1) - \bar{P}_{spAe}L_a] \qquad \text{(C13)}$$

$$Q_{Ae}(\bar{N}_a) = -\frac{1}{L_a}[\frac{Q_{A0e}}{\bar{g}_{Ae}}(e^{-\bar{g}_{Ae}L_a}-1) + \frac{\bar{q}_{spAe}}{\bar{g}_{Ae}}(e^{-\bar{g}_{Ae}L_a}-1) + \bar{q}_{spAe}L_a] \qquad \text{(C14)}$$

Equations for TM (h) polarised photon:

The Rate Equations for TM(h) polarisation is in the exact format as TE(e) polarisation, except the optical gain for TM polarisation is depends on the TM confinement factor, where $g_h = g \times \Gamma_h$.

For Carrier Density Equation:

$$\frac{J_A}{qd_A v} = \overline{g}_{Ae}[P_{Ae}(\overline{N}_a) + Q_{Ae}(\overline{N}_a)] + \overline{g}_{Ah}[P_{Ah}(\overline{N}_a) + Q_{Ah}(\overline{N}_a)] + \frac{B_r(\overline{N}_a + N_d)\overline{N}_a}{v} \qquad \text{(C15)}$$

where J is current density (A/cm^2), q is Electron charge (1.602×10^{-19} Coul), d is the thickness of optical active layer (μm)

In region B

The Rate Equations for region B are in the exact format as in region A, only by substituting the subscript B for A, as illustrated in Fig.C.1, two stripes are symmetric, this is a simple method to derive the Rate Equations, as when a set of equations for one stripe is derived, the equations for the other stripe is identical. We have built a computer model based on these equations to predict the performance of the V-stripe as a polarisation-enhanced stripe. Although equations for both stripe are identical, but as we have given them different names, the model can support all kinds of different parameters combinations.

Appendix D

Angular Distribution of Intensities Equations

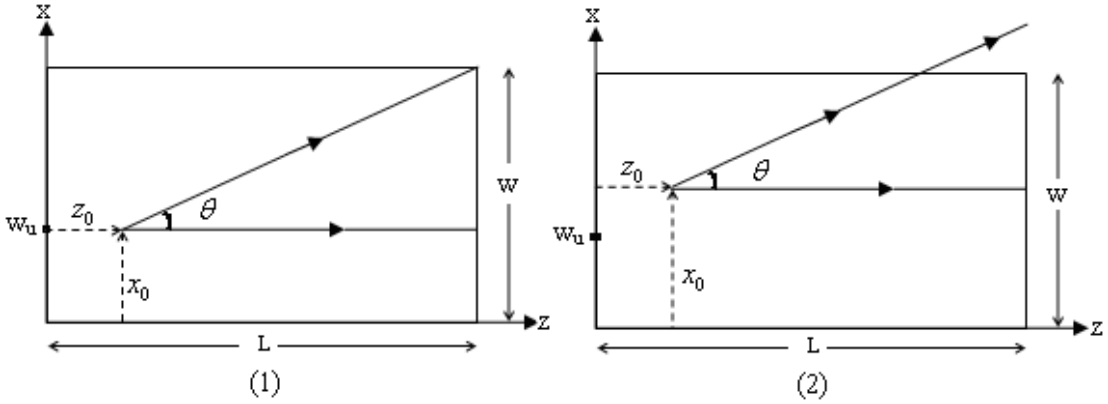

Figure D.1 Schematic diagram of Angular Distribution derive analysis (Top view of a LED device active layer). (1) is the situation where all the rays are travel with in the active layer; (2) is the situation, which all rays travel through the active layer.

Analysis condition: $\theta < \theta_M$; $\theta_M = \tan^{-1}(\frac{w}{L})$

For all rays travel at the same angle θ

$$(s_a + s_g) = s_f = \frac{L - z_0}{\cos(\theta)}$$

$$\frac{w - w_u}{L - z_0} = \tan(\theta); \qquad w_u = w - (L - z_0)\tan(\theta) \qquad \text{(D1)}$$

At z_0, for $x_0 < w_u$ (situation 1), $s_g = s_f$, $s_a = 0$

At z_0, for $x_0 > w_u$ (situation 2), $s_g = \frac{w - x_0}{\sin(\theta)}$,

Situation (1)

At z_0, for $x_0 < w_u$

$$P_1(x_0, z_0, \theta; z = z_L) = P_1(x_0, z_0, \theta; s = s_f) = \overline{P}_{sp}(e^{\overline{g}s_f} - 1) \tag{D2}$$

Note: $P = \overline{P}_{sp}(e^{\overline{g}s_f} - 1)$ comes from the basic Rate Equation derivation in Appendix-B-1, Eq.(B1.7).

$$\begin{aligned} &\int_0^{w_u} P_1(x_0, z_0, \theta; s = s_f)dx_0 = \int_0^{w_u} \overline{P}_{sp}(e^{\overline{g}(\frac{L-z_0}{\cos\theta})} - 1)dx_0 \\ &= w_u \overline{P}_{sp}(e^{\overline{g}(\frac{L-z_0}{\cos\theta})} - 1) \end{aligned} \tag{D3}$$

$$\begin{aligned} &\int_0^{L} P_1(z_0, \theta; s = s_f)dz_0 = \int_0^{L} w_u \overline{P}_{sp}(e^{\overline{g}(\frac{L-z_0}{\cos\theta})} - 1)dz_0 \\ &= \overline{P}_{sp}[\frac{w\cos\theta}{\overline{g}}(e^{\overline{g}(\frac{L}{\cos\theta})} - 1) - \frac{L\sin\theta}{\overline{g}}e^{\overline{g}(\frac{L}{\cos\theta})} + \frac{\sin\theta\cos\theta}{\overline{g}^2}(e^{\overline{g}(\frac{L}{\cos\theta})} - 1) \\ &+ \frac{3}{2}L^2\tan\theta - w.L] \end{aligned} \tag{D4}$$

Situation (2)

At z_0, for $x_0 > w_u$

$$P_2(x_0, z_0, \theta; z = z_L) = P_2(x_0, z_0, \theta; s = s_g) = \overline{P}_{sp}(e^{\overline{g}s_g} - 1)(e^{\alpha(s_f - s_g)}) \tag{D5}$$

$$\begin{aligned} &\int_{w_u}^{w} P_2(x_0, z_0, \theta; s = s_g)dx_0 = \int_{w_u}^{w} \overline{P}_{sp}(e^{\overline{g}(\frac{w-x_0}{\sin\theta})} - 1)(e^{\alpha(\frac{L-z_0}{\cos\theta} - \frac{w-x_0}{\sin\theta})})dx_0 \\ &= \overline{P}_{sp}e^{\alpha(\frac{L-z_0}{\cos\theta})}[\frac{\sin\theta}{\overline{g}-\alpha}(e^{(\overline{g}-\alpha)(\frac{L-z_0}{\cos\theta})} - 1) - \frac{\sin\theta}{\alpha}(1 - e^{\alpha(\frac{L-z_0}{\cos\theta})})] \end{aligned} \tag{D6}$$

$$\begin{aligned} &\int_0^{L} P_2(z_0, \theta; s = s_g)dz_0 \\ &= \int_0^{L} \overline{P}_{sp}e^{\alpha(\frac{L-z_0}{\cos\theta})}[\frac{\sin\theta}{\overline{g}-\alpha}(e^{(\overline{g}-\alpha)(\frac{L-z_0}{\cos\theta})} - 1) - \frac{\sin\theta}{\alpha}(1 - e^{\alpha(\frac{L-z_0}{\cos\theta})})]dz_0 \\ &= \overline{P}_{sp}[\frac{\cos\theta}{\alpha}(e^{\alpha(\frac{L}{\cos\theta})} - 1)(\frac{\sin\theta}{\alpha - \overline{g}} + \frac{\sin\theta}{\alpha}) + \frac{\sin\theta}{\alpha - \overline{g}}\frac{\cos\theta}{\overline{g}}(1 - e^{\overline{g}(\frac{L}{\cos\theta})}) - \frac{\sin\theta}{\alpha}L] \end{aligned} \tag{C7}$$